

中文摘要

本篇論文將解析發展沉埋基礎之扭轉、垂直、水平、翻轉與耦合阻抗矩陣分析程式。在分析沉埋基礎之阻抗矩陣時，所分析層狀土壤可分成內域與外域兩部分，內域與外域的土壤可分別以未知模態係數表示，未知模態係數將透過變分技巧及利用內外域之間位移與應力的連續性來求得，土層的形狀函數亦可用求得的模態係數來表示。

分析整體的層狀土壤形狀函數時，土壤可分成內域與外域兩部分，內域的解析解為特解加上齊性解，而外域部份僅存在齊性解。內外域的超越函數齊性解將透過數值方法發展出一套程式可求得複數彈性波數值。層狀土壤的阻抗矩陣可藉由彈性波數的值求得來建立，完成後進行沉埋基礎數值的阻抗矩陣程式開發，並發展出一套沉埋基礎之扭轉、垂直、水平、翻轉與耦合阻抗矩陣分析程式。

在分析半無限域中沉埋基礎之阻抗矩陣時，係利用有限域解析沉埋基礎的阻抗矩陣並調整土層之深度來近似，為了求得半無限域中沉埋基礎的阻抗矩陣，在有限域的沉埋基礎之阻抗矩陣中，增加最下層土層之厚度來近似半無限域沉埋基礎的阻抗矩陣，但增加下層土壤的厚度會發生數值不穩定現象，此時可透過所提出的數值方法解決數值不穩定現象，最後發展出一套半無限域沉埋基礎之扭轉、垂直、水平、翻轉與耦合阻抗矩陣分析程式。

關鍵詞：超越函數、阻抗矩陣、土壤與結構物的互制

Abstract

A computer program is developed in the thesis for calculating torsional, vertical, horizontal, coupling and rocking impedances in frequency domain for axial-symmetric foundations embedded in layered medium. In this process of formulating the impedances, the soil medium is divided into interior and exterior domains. The analytical solutions are formed separately with unknown coefficients for both domains. In order to find the unknown coefficients for both domains, the variational principle is employed using the continuity conditions (both displacements and stresses) at the interfaces between interior and exterior domains, interior domain and foundation, and exterior domain and foundation to find impedance functions.

To solve those problems, the analytic solution for the interior domain is the combination of a homogeneous solution and a particular solution, the exterior domain is described by a homogeneous solution only. To obtain the homogeneous solution, one has to solve the complex root of the transcendental equations. A numerical scheme has been proposed. The wave numbers of transcendental equations have been employed for finding impedance matrices. Some numerical results of torsional, vertical, horizontal, coupling and rocking impedances with different embedded depths will be presented in layered medium and comments on the numerical scheme will be given.

The impedance matrices of axial-symmetric foundations embedded in an elastic half-space medium approximated using analytical solutions in layer. To approximate the situation of half-space medium, the thickness of one layer medium gradually increased to see if the impedance function is approaching those for the case of half-space medium. However, as the thickness increases the numerical instability problem will be arisen. To overcome this numerical problem, a new numerical technique will be developed. Some numerical results of torsional, vertical, horizontal, coupling and rocking impedances with different embedded depths will be presented in an elastic half-space medium and comments on the numerical scheme will be given.

Key words : transcendental equations, impedance matrix, soil-structure interaction.

誌謝

在這六年的博士生涯中首先要感謝指導教授 劉俊秀老師，這六年來對本人之悉心教導與鼓勵，才能將研究工作中從光明正確的方向走出，先後完成國科會三年計劃案，並發表一篇期刊 SCI 論文已刊登，另一篇 SCI 論文已投稿和一篇國際會議論文，這些成果的點點滴滴都是恩師嚴謹的治學態度並帶給與本人受益匪淺一段深刻之學習經驗，使我能順利完成博士班的學業，在此致上最深的謝意。

在論文口試期間，承蒙國立台灣大學土木系 陳正興教授、國立宜蘭大學土木系 李洋傑教授與本校 黃炯憲教授、洪士林教授、鄭復平教授對本文提供寶貴的意見與指教，使得本論文更加完備，在此致上最誠摯之感謝。

在交大這段日子，感謝系上老師的教導與梁立中學長的碩士論文點亮我一盞光明前進的燈，同時在這段學習的過程中謝謝學弟 曹治本、李宗穎、林暉盛、黃天宇在口試期間的幫忙與協助。

最後，謹將本論文獻給我最摯愛的父母、家人與親戚，謝謝他們的關心與鼓勵支持才能完成本論文，願與大家分享這項榮耀。



Contents

中文摘要.....	i
Abstract.....	ii
誌謝	iii
Contents.....	iv
Table captions.....	vi
Figure captions.....	vii

Chapter 1 Introduction

	page
1.1 Motivation of the research.....	1
1.2 Scope of the thesis.....	2



Chapter 2 Impedance matrices for circular foundation embedded in layered medium

Summary.....	6
2.1 Derivations for 3D wave propagation problem.....	7
2.2 Formulation of impedance matrix.....	17
2.3 Numerical investigations.....	22
2.4 Concluding remarks.....	25

Chapter 3 Solving of the transcendental equations for the analysis of
transient wave propagation in layered media

Summary.....40

3.1 Analytical derivations for three-dimensional wave propagation
problems..... 40

3.2 Root searching scheme for transcendental equations.....41

3.3 Numerical investigations.....42

3.4 Concluding remarks.....43

Chapter 4 Impedance matrices for axial symmetric foundation
embedded in half-space medium by layered
approximation

Summary.....62

4.1 Derivations of the approximate model shapes functions for exterior
and interior domains.....62

4.2 Numerical investigations.....68

4.3 Concluding remarks.....70

Chapter 5 Conclusions and further research

5.1 Conclusions.....92

5.2 Further research.....93

References.....94

Appendix A.....96

Table captions

Table 2-1 Non-dimensionalized torsional Impedance $\frac{K_{TT}}{Ga_0^3}$ for $\frac{d}{a_0} = 0, \frac{L}{a_0} = 2$	
and $\frac{\omega a_0}{\text{Re}(C_s)} = 0.01$	26
Table 2-2 Non-dimensionalized vertical Impedance $\frac{K_{TT}}{Ga_0^3}$ for $\frac{d}{a_0} = 0, \frac{L}{a_0} = 2$	
and $\frac{\omega a_0}{\text{Re}(C_s)} = 0.01$	26
Table 2-3 Non-dimensionalized horizontal Impedance $\frac{K_{TT}}{Ga_0^3}$ for $\frac{d}{a_0} = 0, \frac{L}{a_0} = 2$	
and $\frac{\omega a_0}{\text{Re}(C_s)} = 0.01$	26
Table 2-4 Non-dimensionalized coupling Impedance $\frac{K_{TT}}{Ga_0^3}$ for $\frac{d}{a_0} = 0, \frac{L}{a_0} = 2$	
and $\frac{\omega a_0}{\text{Re}(C_s)} = 0.01$	27
Table 2-5 Non-dimensionalized rocking Impedance $\frac{K_{TT}}{Ga_0^3}$ for $\frac{d}{a_0} = 0, \frac{L}{a_0} = 2$	
and $\frac{\omega a_0}{\text{Re}(C_s)} = 0.01$	27

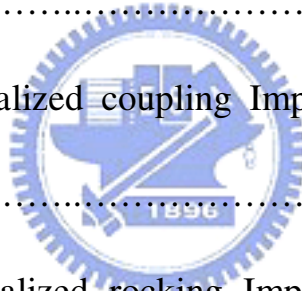


Figure captions

Fig. 1-1 The organization of the thesis.....	5
Fig. 2-1 Total soil system with prescribed.....	28
Fig. 2-2 Solutions at interfaces.....	29
Fig. 2-3 Comparison of non-dimensionalized torsional impedance with Liou's results for $\frac{L}{a_0} = 2$	30
Fig. 2-4 Comparison of non-dimensionalized vertical impedance with Liou's results for $\frac{L}{a_0} = 2$	31
Fig. 2-5 Comparison of non-dimensionalized horizontal impedance with Liou's results for $\frac{L}{a_0} = 2$	32
Fig. 2-6 Comparison of non-dimensionalized coupling impedance with Liou's results for $\frac{L}{a_0} = 2$	33
Fig. 2-7 Comparison of non-dimensionalized rocking impedance with Liou's results for $\frac{L}{a_0} = 2$	34
Fig. 2-8 Non-dimensionalized torsional impedance with different depths for $\frac{L}{a_0} = 2$	35
Fig. 2-9 Non-dimensionalized vertical impedance with different depths for $\frac{L}{a_0} = 2$	36
Fig. 2-10 Non-dimensionalized horizontal impedance with different depths for $\frac{L}{a_0} = 2$	37
Fig. 2-11 Non-dimensionalized coupling impedance with different depths for $\frac{L}{a_0} = 2$	38
Fig. 2-12 Non-dimensionalized rocking impedance with different depths for $\frac{L}{a_0} = 2$	39



Fig. 3-1 Mesh of the region $-a \leq x \leq a$ and $-b \leq y \leq b$ on complex plane	44
Fig. 3-2 Typical grid patterns.....	45
Fig. 3-3 Soil profile of example.....	46
Fig. 3-4 Analytical wave number values of undamping system.....	47
Fig. 3-5 Analytical wave number values of undamping system.....	48
Fig. 3-6 Analytical wave number values of undamping system.....	49
Fig. 3-7 Analytical wave number values of damping system.....	50
Fig. 3-8 Analytical wave number values of damping system.....	51
Fig. 3-9 Analytical wave number values of damping system.....	52
Fig. 3-10 Numerical wave number values of undamping system.....	53
Fig. 3-11 Numerical wave number values of undamping system.....	54
Fig. 3-12 Numerical wave number values of undamping system.....	55
Fig. 3-13 Numerical wave number values of damping system.....	56
Fig. 3-14 Numerical wave number values of damping system.....	57
Fig. 3-15 Numerical wave number values of damping system.....	58
Fig. 3-16 Numerical wave number values of damping system.....	59
Fig. 3-17 Numerical wave number values of damping system.....	60
Fig. 3-18 Numerical wave number values of damping system.....	61
Fig. 4-1 Comparison of non-dimensionalized torsional impedance with Liou's results for $\frac{d}{a_0} = 0$	72
Fig. 4-2 Comparison of non-dimensionalized vertical impedance with Liou's results for $\frac{d}{a_0} = 0$	73
Fig. 4-3 Comparison of non-dimensionalized horizontal impedance with Liou's results for $\frac{d}{a_0} = 0$	74
Fig. 4-4 Comparison of non-dimensionalized coupling impedance with Liou's results for $\frac{d}{a_0} = 0$	75

Fig. 4-5 Comparison of non-dimensionalized rocking impedance with Liou's results for $\frac{d}{a_0} = 0$	76
Fig. 4-6 Comparison of non-dimensionalized torsional impedance with Liou's results for $\frac{d}{a_0} = 0$	77
Fig. 4-7 Comparison of non-dimensionalized vertical impedance with Liou's results for $\frac{d}{a_0} = 0$	78
Fig. 4-8 Comparison of non-dimensionalized horizontal impedance with Liou's results for $\frac{d}{a_0} = 0$	79
Fig. 4-9 Comparison of non-dimensionalized coupling impedance with Liou's results for $\frac{d}{a_0} = 0$	80
Fig. 4-10 Comparison of non-dimensionalized rocking impedance with Liou's results for $\frac{d}{a_0} = 0$	81
Fig. 4-11 Torsional impedance for $\frac{d}{a_0} = 0$ with damp ratio $\xi = 0.02$	82
Fig. 4-12 Vertical impedance for $\frac{d}{a_0} = 0$ with damp ratio $\xi = 0.02$	83
Fig. 4-13 Horizontal impedance for $\frac{d}{a_0} = 0$ with damp ratio $\xi = 0.02$	84
Fig. 4-14 Coupling impedance for $\frac{d}{a_0} = 0$ with damp ratio $\xi = 0.02$	85
Fig. 4-15 Rocking impedance for $\frac{d}{a_0} = 0$ with damp ratio $\xi = 0.02$	86
Fig. 4-16 Non-dimensionalized torsional impedance with different depths ..	87
Fig. 4-17 Non-dimensionalized vertical impedance with different depths....	88
Fig. 4-18 Non-dimensionalized horizontal impedance with different depths.	89
Fig. 4-19 Non-dimensionalized coupling impedance with different depths...	90
Fig. 4-20 Non-dimensionalized rocking impedance with different depths....	91

Chapter 1

Introduction

1.1 Motivation of the research

Soil-structure interaction effect plays important roles in the seismic analysis of heavy and stiff structures. Many approaches may be considered to deal with the soil-structure interaction analysis problems. Along with the substructure method, hybrid modelling of soil domain can be employed to investigate soil-structure interaction effects. In hybrid modelling, the far-field of a semi-infinite soil domain is represented by an impedance matrix at the interface of the far-field and the near-field. Finite element method is used for the near-field [1]. Also, several modelling techniques have been developed for infinite soil medium. These included viscous boundary [2,3], transmitting boundary [4], boundary element method [5], and infinite element methods [6]. Among the above mentioned modelling, boundary element method requires boundary discretization which can reduce some computational cost while compared to that of finite element method. In boundary element method, Green function is used as a fundamental solution to generate the impedance functions at the assumed boundary of structure [7]. However, using Green function in the formulation, one has to deal with the singularity problem. To avoid this situation, the analytical solutions for the layered medium with prescribed harmonic displacement time history on the surface are derived by Liou [8].

To obtain the impedance matrix for the surface foundation, some analytic approaches are available [9-12]. In these analytical approaches, the interaction tractions at the interface of foundation and soil medium are assumed to be piecewise linear or piecewise constant.

Regarding analytical or semi-analytical approaches for embedded foundation, Aviles and Perez [13] solved the problem of torsional impedance for foundation embedded in layered medium, Tassoulas and Kansel [14] used layer elements to obtain torsional, vertical, horizontal, and rocking impedance functions, and Wolf and Preisig [15] employed cone model to calculate

impedance functions. Also, cone model was developed to calculate approximately the dynamic response of a disk on the surface of a soil layer resting on flexible rock subjected to harmonic excitations [16]. Furthermore, the concept of cone model was extended to calculate the dynamic stiffness of a foundation embedded in a multiple-layered half-space [15,17].

Sezawa [18] has developed a procedure to separate the dilatational and the rotational waves to solve the wave equation in cylindrical coordinates for the half-space medium. Tzong and Penzien [1] extended this solution to find impedance matrix of a single-layer half-space system. Regards of analytical solution technique, Liou has developed a technique to decompose the boundary conditions to fit the general solutions of wave equations in cylindrical coordinates for the cases of layered media. The technique has been successfully applied to find the impedance functions for foundations on layered half-space medium [10] and axial symmetric foundation embedded in layered medium [11,19].



1.2 Scope of the thesis

The organization of the thesis is shown in Fig. 1-1. In chapter 2, a numerical scheme is developed to generate complete impedance functions for foundation embedded in layered medium. The impedance functions will be frequency dependent functions. To obtain the impedances, the analytical solutions of three dimensional wave equations in cylindrical coordinates in layered medium with satisfying the necessary boundary conditions are employed [8]. In the process of formulating the impedances, the soil medium is divided into interior and exterior domains. The analytical solutions are formed separately with unknown coefficients for both domains. And the interaction stresses at the interface between foundation and surrounding soil are assumed to be piecewise linear in z direction or r direction of the cylindrical coordinates. Then, the continuity conditions of stresses and displacements at the interface between both domains and the interface between the foundation and surrounding soil are applied to generate the impedance functions. In the process of applying the continuity

conditions and generating the impedance functions, variational principle and reciprocal theorem are employed.

Some numerical aspects will be investigated in order to show the effectiveness and efficiency of the presented scheme. And the results for torsional, vertical, horizontal, coupling and rocking impedances of a cylindrical foundation embedded with different depths will also be presented to show the importance of embedment effect.

In chapter 3, we will employ the analytic solution for soil-structure interaction in layered media to develop a general-purpose program of the transcendental equations. In developing the program, the transient wave propagation problems in layered media should be calculated and the wave numbers for the soil-structure interaction in layered media will be analytically predicted. In this chapter, the wave numbers of transcendental equations for soil-structure interaction in layered media will be derived analytically and numerically.

In Chapter 4, the cases of foundation embedded in layered half-space medium, one can employ the technique by increasing the thickness of layered medium to simulate the half-space medium. However, some numerical problem arises as the thickness of layer increases. This is due to upward propagation waves which vary along z -direction with $e^{v'z}$ or e^{vz} and downward propagation waves which vary along z -direction with $e^{-v'z}$ or e^{-vz} in magnitude. The v and v' are the vertically apparent wave numbers for shear and compressional waves respectively. The magnitude difference between $e^{v'z}$ and $e^{-v'z}$ (or e^{vz} or e^{-vz}) becomes enormously huge for the modes with large real part of vz and $v'z$. This phenomenon will make the contribution of upward propagation wave cover up the contribution of downward propagation wave of this mode. However, in the real situation for the modes with large real part of vz or $v'z$, the contribution of downward wave should be much more important than that of upward wave if the thickness of the layered medium is very

large, since the driving force to cause wave propagation is located at the place near free surface.

To remedy the numerical problem stated above, the upward propagating wave for the modes with large real part of $\nu'L$, in which L is the thickness of large should be suppressed or neglected. The chapter 4 is devoted to deal with this problem. Therefore, the procedure developed in chapter 2 for layered medium will be employed as basis and modified in order to simulate the cases of layered half-space medium. To simulate half-space, the thickness of layered is gradually increased. As the real part of $\nu'L$ for some modes is greater than 25, the upward propagating waves for these modes are suppressed. Thus, the expressive for displacements and tractions at the interfaces between interior and exterior domains, interior domain and foundation and exterior domain and foundation will be derived by considering downward propagating wave only. The numerical results show that considering only downward propagation waves for the modes with large real part of $\nu'L$ is satisfactory. Also, the thicknesses of large needed to simulate half-space medium will be shown for different damping ratios of medium. Finally, the conclusions of this work as well as the further researches are summarized in chapter 5.

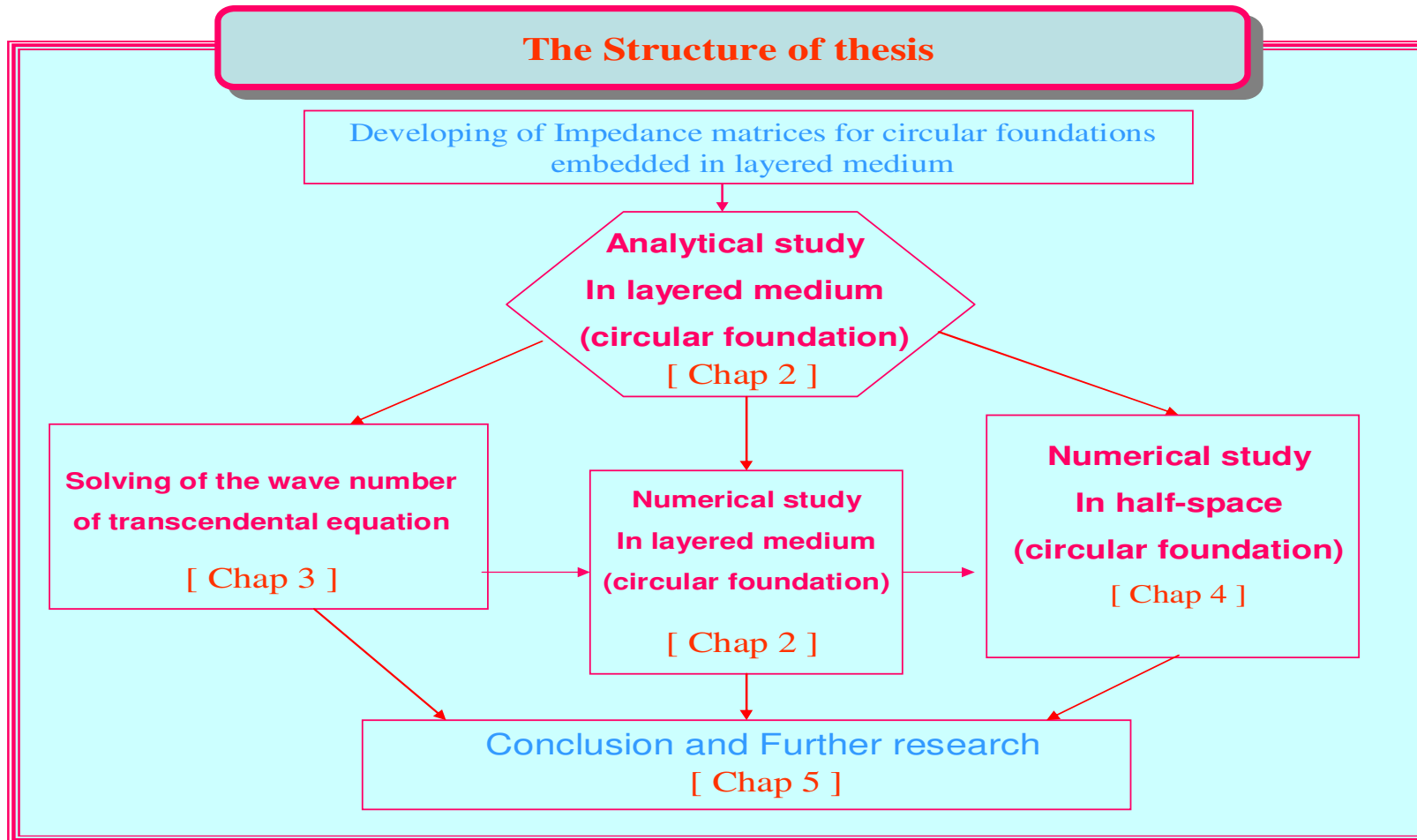


Fig. 1-1 The organization of the thesis

Chapter 2

Impedance matrices for circular foundation embedded in layered medium

Summary

A numerical scheme is developed in the chapter for calculating torsional, vertical, horizontal, coupling and rocking impedances in frequency domain for axial-symmetric foundations embedded in layered media. In the scheme, the whole soil domain is divided into interior and exterior domains. For the exterior domain, the analytic solutions with unknown coefficients are obtained by solving three dimensional wave equations in cylindrical coordinates satisfying homogeneous boundary conditions. For the interior domain, the analytical solutions are also obtained by solving the same three dimensional wave equations satisfying the homogeneous boundary conditions and the prescribed boundary conditions. The prescribed conditions are the interaction tractions at the interfaces between embedded foundation and surrounding soil. The interaction tractions are assumed to be piecewise linear. The piecewise linear tractions at the bottom surface of foundation will be decomposed into a series of Bessel functions which can be easily fitted into the general solutions of wave equations in cylindrical coordinates. After all the analytic solutions with unknown coefficients for both interior and exterior domains are found, the variational principle is employed using the continuity conditions (both displacements and stresses) at the interfaces between interior and exterior domains, interior domain and foundation, and exterior domain and foundation to find impedance functions. Some numerical results of torsional, vertical, horizontal, coupling and rocking impedances with different embedded depths will be presented and comments on the numerical scheme will be given.

2.1 Derivations for 3D wave propagation problems

The total soil system with prescribed tractions $t_{b1}e^{i\alpha x}$ and $t_{b2}e^{i\alpha x}$ having time harmonic variations at the sidewall and the bottom of the cylindrical cavity respectively is shown in Fig. 2-1 The prescribed tractions can be expressed in terms of Fourier components with respect to the azimuth as follows:

$$t_{b1}(\theta, z) = \sum_{n=0}^{\infty} F(\theta)t_{b1}^n(z) = \sum_{n=0}^{\infty} \begin{bmatrix} \sigma_{rr}^n(z) \begin{Bmatrix} \cos(n\theta) \\ \sin(n\theta) \end{Bmatrix} \\ \tau_{rz}^n(z) \begin{Bmatrix} \cos(n\theta) \\ \sin(n\theta) \end{Bmatrix} \\ \tau_{r\theta}^n(z) \begin{Bmatrix} -\sin(n\theta) \\ \cos(n\theta) \end{Bmatrix} \end{bmatrix} \quad r = a_0 \quad \text{and} \quad 0 \leq z \leq d \quad (2-1)$$

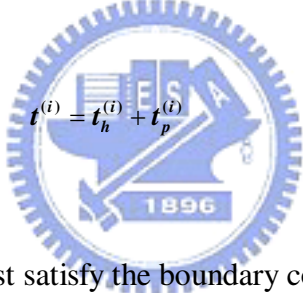
and

$$t_{b2}(\theta, r) = \sum_{n=0}^{\infty} F(\theta)t_{b2}^n(r) = \sum_{n=0}^{\infty} \begin{bmatrix} \tau_{rz}^n(r) \begin{Bmatrix} \cos(n\theta) \\ \sin(n\theta) \end{Bmatrix} \\ \sigma_{zz}^n(r) \begin{Bmatrix} \cos(n\theta) \\ \sin(n\theta) \end{Bmatrix} \\ \tau_{\theta z}^n(r) \begin{Bmatrix} -\sin(n\theta) \\ \cos(n\theta) \end{Bmatrix} \end{bmatrix} \quad z = d \quad \text{and} \quad 0 \leq r \leq a_0 \quad (2-2)$$

where $\sigma_{rr}^n(z)$, $\tau_{rz}^n(z)$, $\tau_{r\theta}^n(z)$, $\tau_{rz}^n(r)$, $\sigma_{zz}^n(r)$, $\tau_{\theta z}^n(r)$ are the stress amplitudes of the n^{th} Fourier component (either a symmetric component or an anti-symmetric component). To solve the wave propagation problem with the prescribed tractions of Eqs. (2-1) and (2-2) as shown in Fig. 2-1, Liou [8] has proposed a technique to decompose each Fourier component of the prescribed boundary condition at S_2 surface. This decomposed boundary condition can be easily fitted into the general solutions of 3D wave equations in cylindrical coordinates. By following the procedure of the technique, the solutions in interior domain

consist of particular solutions which satisfy the boundary conditions of prescribed traction in Eq. (2-2) and rigid base $z = L$ in Fig. 2-1, and homogeneous solutions which satisfy the homogeneous boundaries at free surface (Traction free) $z = d$ and rigid base $z = L$. The solutions for exterior domain contain only homogeneous solutions which satisfy the homogeneous boundaries at free surface $z = 0$ and rigid base $z = L$. Since the solving process is the same for all the Fourier components, the superscript n in Eqs. (2-1) and (2-2) will be omitted in the following derivations of homogeneous solutions and particular solutions.

The solution (e.g. traction) for interior domain in Fig. 2-1 is the combination of homogeneous and particular solutions as follows :

$$\mathbf{t}^{(i)} = \mathbf{t}_h^{(i)} + \mathbf{t}_p^{(i)} \quad (2-3)$$


The particular solution $\mathbf{t}_p^{(i)}$ must satisfy the boundary conditions of Eq. (2-2) and rigid base condition $z = L$ (zero displacement), and the homogeneous solution $\mathbf{t}_h^{(i)}$ satisfies the boundary conditions of rigid base and the free surface (zero traction).


From the general solutions of 3D wave equations, the stress and the displacement fields in a layer can be expressed in terms of the displacements and tractions on the upper boundary of the layer [8]. By employing the continuity conditions of displacements and tractions consecutively at the horizontal interface between two layers, one obtains

$$\mathbf{Y}_m^{(i)} = \bar{\mathbf{J}} \mathbf{a}_m \mathbf{a}_{m-1} \cdots \mathbf{a}_1 \bar{\mathbf{J}}^{-1} \mathbf{Y}_0^{(i)} = \bar{\mathbf{J}} \mathbf{T}^{(i)} \bar{\mathbf{J}}^{-1} \mathbf{Y}_0^{(i)} \quad (2-4)$$

where $\mathbf{Y}_m^{(i)} = (u_r^{(i)} \quad u_z^{(i)} \quad \tau_{rz}^{(i)} \quad \sigma_{zz}^{(i)} \quad u_\theta^{(i)} \quad \tau_{\theta z}^{(i)})_m^T$ is the displacement-stress vector on the m^{th} horizontal interface in Fig. 2-1, $\bar{\mathbf{J}}$ is the Bessel function matrix and the \mathbf{a}_j 's are the transfer matrices given by Eqs. (A1), (A2), (A3) and (A4) in the Appendix. Using Eqs. (A2)-(A4) for the matrices \mathbf{a}_j 's, $\mathbf{T}^{(i)}$ can be written as

$$\mathbf{T}^{(i)} = \begin{bmatrix} t_{11}^{(i)} & t_{12}^{(i)} & t_{13}^{(i)} & t_{14}^{(i)} & 0 & 0 \\ t_{21}^{(i)} & t_{22}^{(i)} & t_{23}^{(i)} & t_{24}^{(i)} & 0 & 0 \\ t_{31}^{(i)} & t_{32}^{(i)} & t_{33}^{(i)} & t_{34}^{(i)} & 0 & 0 \\ t_{41}^{(i)} & t_{42}^{(i)} & t_{43}^{(i)} & t_{44}^{(i)} & & \\ 0 & 0 & 0 & 0 & t_{55}^{(i)} & t_{56}^{(i)} \\ 0 & 0 & 0 & 0 & t_{65}^{(i)} & t_{66}^{(i)} \end{bmatrix} \quad (2-5)$$

By applying the homogeneous boundary conditions of rigid base at $z = L$ and free surface at $z = d$, one obtains



$$\begin{bmatrix} 0 \\ 0 \\ 0 \end{bmatrix} = \mathbf{J} \begin{bmatrix} t_{11}^{(i)} & t_{12}^{(i)} & 0 \\ t_{21}^{(i)} & t_{22}^{(i)} & 0 \\ 0 & 0 & t_{55}^{(i)} \end{bmatrix} \mathbf{J}^{-1} \begin{bmatrix} u_r \\ u_z \\ u_\theta \end{bmatrix}_0 \quad (2-6)$$

where

$$\mathbf{J} = \begin{bmatrix} J'_n(kr) & 0 & \frac{n}{r} J_n(kr) \\ 0 & kJ_n(kr) & 0 \\ \frac{n}{r} J_n(kr) & 0 & J'_n(kr) \end{bmatrix} \quad (2-7)$$

The Eq. (2-6) gives the transcendental equations

$$t_{11}^{(i)} t_{22}^{(i)} - t_{12}^{(i)} t_{21}^{(i)} = 0 \quad (2-8)$$

for the wave numbers representing Rayleigh modes, and

$$t_{55}^{(i)} = 0 \quad (2-9)$$

for the wave numbers representing Loves modes. For each wave number k , a root of Eq. (2-8) or (2-9), the tractions at depth z on the vertical interface (s_3 in Fig. 2-1) between the exterior and the interior domains can be expressed in terms of the displacement-stress vector on the free surface as follows :

$$\mathbf{t}_j^{(i)}(z) = (\mathbf{J}_1 \mathbf{F}_1 + \mathbf{J}_2 \mathbf{F}_2) \mathbf{e}_j(z - h_{j-1}) \mathbf{E}_j^{-1} \mathbf{a}_{j-1} \cdots \mathbf{a}_1 \bar{\mathbf{J}}^{-1} \mathbf{Y}_0^{(i)} \quad (2-10)$$

where $\mathbf{t}_j^{(i)}(z) = (\sigma_{rr}^{(i)} \quad \tau_{rz}^{(i)} \quad \tau_{\alpha z}^{(i)})^T|_{r=d_0}$ in the j^{th} layer, and the matrices \mathbf{J}_1 , \mathbf{J}_2 , $\mathbf{F}_1 \mathbf{e}_j(z - h_{j-1}) \mathbf{E}_j^{-1}$ and $\mathbf{F}_2 \mathbf{e}_j(z - h_{j-1}) \mathbf{E}_j^{-1}$ are given by Eqs. (A5)-(A8) in the Appendix.

Substituting the root of Eq. (2-8) into Eq. (2-4) and making use of the free surface conditions, one can easily show that $\bar{\mathbf{J}}^{-1} \mathbf{Y}_0^{(i)}$ in Eqs. (2-4) and (2-10) can be written as

$$\bar{\mathbf{J}}^{-1} \mathbf{Y}_0^{(i)} = (1 \quad \xi_i \quad 0 \quad 0 \quad 0 \quad 0)^T \alpha_i^{(i)} \quad (2-11)$$

for the i^{th} Rayleigh mode, in which $\xi_i = -\frac{t_{11}^{(i)}}{t_{12}^{(i)}} = -\frac{t_{21}^{(i)}}{t_{22}^{(i)}}$ and $\alpha_i^{(i)}$ is the unknown modal participation factor. Similarly, substituting the root of Eq. (2-9) into Eq. (2-4), one can obtain

$$\bar{\mathbf{J}}^{-1} \mathbf{Y}_0^{(i)} = (0 \quad 0 \quad 0 \quad 0 \quad 1 \quad 0)^T \alpha_j^{(i)} \quad (2-12)$$

for the j^{th} Love mode, in which $\alpha_j^{(i)}$ is the unknown modal participation factor. Because Eqs. (2-8) and (2-9) have an infinite number of roots, the displacement and stress fields in the interior domain can be approximated by a finite number of lower modes. Substituting Eqs. (2-11) and (2-12) into Eqs. (2-4) and (2-10), the displacement and stress vectors at the vertical interface (vertical surface s_3 in Fig. 2-1) due to homogeneous solutions can be implicitly expressed by the combination of these modes with unknown participation factors as follows :

$$\mathbf{u}_{h,s_3}^{(i)}(z) = \mathbf{N}_{h,s_3}^{(i)}(z)\boldsymbol{\alpha}^{(i)} \quad , \quad r = a_0 \quad (2-13)$$

and

$$\mathbf{t}_{h,s_3}^{(i)}(z) = \mathbf{G}_{h,s_3}^{(i)}(z)\boldsymbol{\alpha}^{(i)} \quad , \quad r = a_0 \quad (2-14)$$

where $\mathbf{N}^{(i)}(z)$ and $\mathbf{G}^{(i)}(z)$ are the matrices of modal displacements and stresses respectively, and $\boldsymbol{\alpha}^{(i)}$ is the vector of unknown modal participation factors. By use of Eqs. (2-11), (2-12) and (2-4), one can express the displacement and traction vectors at the surface s_2 of interior domain due to the homogeneous solutions in terms of the vector $\boldsymbol{\alpha}^{(i)}$ as follows :

$$\mathbf{u}_{h,s_2}^{(i)}(r) = \mathbf{N}_{h,s_2}^{(i)}(r)\boldsymbol{\alpha}^{(i)} \quad , \quad z = d \quad (2-15)$$

and

$$\mathbf{t}_{h,s_2}^{(i)}(r) = 0 \quad , \quad z = d \quad (2-16)$$

To obtain the particular solutions for interior domain, the n^{th} Fourier component of the prescribed traction in Eq. (2-2) can be expressed in a form compatible to finite element model of foundation structure. The variation of $t_{b_2}^n(r)$ in Eq. (2-2) is assumed to be piecewise linear in r direction. Also, by the same reason, the variation of $t_{b_1}^n(z)$ in Eq. (2-1) is assumed to be piecewise linear in z direction for generating impedance functions. For Eq. (2-1), the depth of embedded foundation d is divided into m_1 subintervals with equal width $b = \frac{d}{m_1}$. Then $t_{b_1}^n(z)$ in Eq. (2-1) can be approximated as

$$\begin{aligned}\sigma_{rr}^n(z) &= \sum_{j=1}^{m_1-1} h_j(z)q_j + h_0(z)q_0 + h_{m_1}(z)q_{m_1} \\ \tau_{rz}^n(z) &= \sum_{j=1}^{m_1-1} h_j(z)p_j + h_0(z)p_0 + h_{m_1}(z)p_{m_1} \\ \tau_{r\theta}^n(z) &= \sum_{j=1}^{m_1-1} h_j(z)s_j + h_0(z)s_0 + h_{m_1}(z)s_{m_1}\end{aligned}\quad (2-17)$$

or

$$t_{b_1}^n(z) = \mathbf{H}_1^T \mathbf{P}_1 \quad (2-18)$$

where

$$h_j(z) = \begin{cases} 1 + \frac{z-jb}{b}, & \text{if } (j-1)b \leq z \leq jb \quad \text{and} \quad 1 \leq j \leq m_1 \\ 1 - \frac{z-jb}{b}, & \text{if } jb \leq z \leq (j+1)b \quad \text{and} \quad 0 \leq j \leq m_1 - 1 \\ 0, & \text{otherwise,} \end{cases} \quad (2-19)$$

matrix $\mathbf{H}_1^T = \text{diag}[\mathbf{h}^T, \mathbf{h}^T, \mathbf{h}^T]$ in which \mathbf{h}^T is the vector contains element $h_j(z)$ in Eqs. (2-19), vector $\mathbf{P}_1^T = (\mathbf{q}^T, \mathbf{p}^T, \mathbf{s}^T)$ in which vectors $\mathbf{q}^T, \mathbf{p}^T$ and \mathbf{s}^T contains the elements q_j, p_j and s_j respectively in Eqs. (2-17), and q_j, p_j and s_j are the intensities of traction at

node j for $\sigma_{rr}^n(z)$, $\tau_{rz}^n(z)$ and $\tau_{r\theta}^n(z)$ in Eqs. (2-17) respectively.

Similarly, the foundation radius a_0 can be divided into m_2 subintervals and the traction $\mathbf{t}_{b2}^n(\mathbf{r})$ of each Fourier component in Eq. (2-2) can also be approximated by

$$\mathbf{t}_{b2}^n(\mathbf{r}) = \mathbf{H}_2^T \mathbf{P}_2 \quad (2-20)$$

where matrix $\mathbf{H}_2^T = \text{diag}[\bar{\mathbf{h}}^T, \bar{\mathbf{h}}^T, \bar{\mathbf{h}}^T]$ with vector $\bar{\mathbf{h}}$ being similar to vector \mathbf{h} defined in Eqs. (2-19) except the piecewise linear variable z is replaced by r , vector $\mathbf{P}_2^T = (\bar{\mathbf{q}}^T, \bar{\mathbf{p}}^T, \bar{\mathbf{s}}^T)$ and \bar{q}_j , \bar{p}_j and \bar{s}_j are the intensities of traction at node j for $\tau_{rz}^n(r)$, $\sigma_{zz}^n(r)$ and $\tau_{\theta z}^n(r)$ respectively. It should be noted that \mathbf{H}_1^T and \mathbf{H}_2^T are $3 \times 3(m_1+1)$ and $3 \times 3(m_2+1)$ matrices respectively. Because the traction $\mathbf{t}_{b2}^n(\mathbf{r})$ must be fitted in the general solutions of 3D wave equations in cylindrical coordinates for interior domain, the traction $\mathbf{t}_{b2}^n(\mathbf{r})$ can be decomposed as follows [8] :

$$\mathbf{t}_{b2}^n(\mathbf{r}) = \begin{bmatrix} \tau_{rz}^n(r) \\ \sigma_{zz}^n(r) \\ \tau_{\theta z}^n(r) \end{bmatrix} = \begin{bmatrix} 1 \\ 0 \\ -1 \end{bmatrix} \left(\frac{\tau_{rz}^n - \tau_{\theta z}^n}{2} \right) + \begin{bmatrix} 0 \\ 1 \\ 0 \end{bmatrix} (\sigma_{zz}^n) + \begin{bmatrix} 1 \\ 0 \\ 1 \end{bmatrix} \left(\frac{\tau_{rz}^n + \tau_{\theta z}^n}{2} \right) \quad (2-21)$$

and

$$\begin{aligned} \frac{\tau_{rz}^n(r) - \tau_{\theta z}^n(r)}{2} &= \sum_{i=1}^{\infty} k_i^{(1)} J_{n+1}(k_i^{(1)} r) A_i + k_0^{(1)} J_{n+1}(k_0^{(1)} r) A_0 \\ \sigma_{zz}^n(r) &= \sum_{j=1}^{\infty} k_j^{(2)} J_n(k_j^{(2)} r) B_j + k_0^{(2)} J_n(k_0^{(2)} r) B_0 \\ \frac{\tau_{rz}^n(r) + \tau_{\theta z}^n(r)}{2} &= \sum_{l=1}^{\infty} k_l^{(3)} J_{n-1}(k_l^{(3)} r) C_l + k_0^{(3)} J_{n-1}(k_0^{(3)} r) C_0 \end{aligned} \quad (2-22)$$

where the $k_i^{(1)}$'s, $k_j^{(2)}$'s and $k_l^{(3)}$'s are the roots of $J_{n+1}(k_i^{(1)}a_0)=0$, $J_n(k_j^{(2)}a_0)=0$ and $J_{n-1}(k_l^{(3)}a_0)=0$ respectively, for $i, j, l=1, 2, \dots, \infty$, and choosing $k_0^{(1)}=0.5k_1^{(1)}$, $k_0^{(2)}=0.5k_1^{(2)}$ and $k_0^{(3)}=0.5k_1^{(3)}$ in order to satisfy the boundary condition at $r=a_0$ and $z=d$. The Bessel functions in Eqs. (2-22), except the first term, are orthogonal to each other with respect to the weighting function $w(r)=r$ in the interval $(0, a_0)$. The A_i 's, B_j 's and C_l 's can be determined from the orthogonal property as follows :

$$A_0 = \frac{\tau_{rz}^n(a_0) - \tau_{\theta z}^n(a_0)}{2k_0^{(1)}J_{n+1}(k_0^{(1)}a_0)} \quad (2-23)$$

$$A_i = \frac{\int_0^{a_0} r \left(\frac{\tau_{rz}^n - \tau_{\theta z}^n}{2} \right) J_{n+1}(k_i^{(1)}r) dr - k_0^{(1)} A_0 \int_0^{a_0} J_{n+1}(k_0^{(1)}r) J_{n+1}(k_i^{(1)}r) r dr}{k_i^{(1)} \int_0^{a_0} J_{n+1}^2(k_i^{(1)}r) r dr} \quad (2-24)$$

$$B_0 = \frac{\sigma_{zz}^n(a_0)}{k_0^{(2)}J_n(k_0^{(2)}a_0)} \quad (2-25)$$

$$B_j = \frac{\int_0^{a_0} r (\sigma_{zz}^n) J_n(k_j^{(2)}r) dr - k_0^{(2)} B_0 \int_0^{a_0} J_n(k_0^{(2)}r) J_n(k_j^{(2)}r) r dr}{k_j^{(2)} \int_0^{a_0} J_n^2(k_j^{(2)}r) r dr} \quad (2-26)$$

$$C_0 = \frac{\tau_{rz}^n(a_0) + \tau_{\theta z}^n(a_0)}{2k_0^{(3)}J_{n-1}(k_0^{(3)}a_0)} \quad (2-27)$$

$$C_l = \frac{\int_0^{a_0} r \left(\frac{\tau_{rz}^n + \tau_{\theta z}^n}{2} \right) J_{n-1}(k_l^{(3)}r) dr - k_0^{(3)} C_0 \int_0^{a_0} J_{n-1}(k_0^{(3)}r) J_{n-1}(k_l^{(3)}r) r dr}{k_l^{(3)} \int_0^{a_0} J_{n-1}^2(k_l^{(3)}r) r dr} \quad (2-28)$$

In Eqs. (2-22), the A_i 's, B_j 's and C_l 's are defined as the modal participation factors with respect to the wave numbers $k_i^{(1)}$'s, $k_j^{(2)}$'s and $k_l^{(3)}$'s respectively. Since vectors $[1, 0, -1]^T$, $[0, 1, 0]^T$, $[1, 0, 1]^T$ are the eigenvectors of J in Eq. (2-7) with respective

eigenvalues $k_i J_{n+1}(k_i r)$, $k_j J_n(k_j r)$, and $k_l J_{n-1}(k_l r)$, one can substitute Eq. (2-20) into Eq.

(2-21) and make use of Eqs. (2-22)-(2-28) to obtain

$$\begin{aligned}
 \mathbf{t}^n_{b2}(\mathbf{r}) &= \begin{bmatrix} \tau_{rz}^n(\mathbf{r}) \\ \sigma_{zz}^n(\mathbf{r}) \\ \tau_{\theta z}^n(\mathbf{r}) \end{bmatrix} = \begin{bmatrix} 1 \\ 0 \\ -1 \end{bmatrix} \left(\frac{\tau_{rz}^n - \tau_{\theta z}^n}{2} \right) + \begin{bmatrix} 0 \\ 1 \\ 0 \end{bmatrix} (\sigma_{zz}^n) + \begin{bmatrix} 1 \\ 0 \\ 1 \end{bmatrix} \left(\frac{\tau_{rz}^n + \tau_{\theta z}^n}{2} \right) \\
 &= \left(\sum_{i=0}^{\infty} \mathbf{J}_n^{(1)} \begin{bmatrix} \mathbf{D}_i^{n+1} & 0 & -\mathbf{D}_i^{n+1} \\ 0 & 0 & 0 \\ -\mathbf{D}_i^{n+1} & 0 & \mathbf{D}_i^{n+1} \end{bmatrix} + \sum_{j=0}^{\infty} \mathbf{J}_n^{(2)} \begin{bmatrix} 0 & 0 & 0 \\ 0 & \mathbf{D}_j^n & 0 \\ 0 & 0 & 0 \end{bmatrix} + \sum_{l=0}^{\infty} \mathbf{J}_n^{(3)} \begin{bmatrix} \mathbf{D}_l^{n-1} & 0 & \mathbf{D}_l^{n-1} \\ 0 & 0 & 0 \\ \mathbf{D}_l^{n-1} & 0 & \mathbf{D}_l^{n-1} \end{bmatrix} \right) \mathbf{P}_2 \quad (2-29) \\
 &= \left(\sum_{i=0}^{\infty} \mathbf{J}_n^{(1)} \bar{\mathbf{D}}_i^{n+1} + \sum_{j=0}^{\infty} \mathbf{J}_n^{(2)} \bar{\mathbf{D}}_j^n + \sum_{l=0}^{\infty} \mathbf{J}_n^{(3)} \bar{\mathbf{D}}_l^{n-1} \right) \mathbf{P}_2 = \mathbf{G}_{p,S_2}^{(i)}(\mathbf{r}) \mathbf{P}_2
 \end{aligned}$$

where

$$\mathbf{D}_i^{n+1} = \frac{1}{2} \int_0^{a_0} \bar{\mathbf{h}} J_{n+1}(k_i^{(1)} r) r dr + \frac{1}{2} [1] \int_0^{a_0} \frac{J_{n+1}(k_0^{(1)} r) J_{n+1}(k_i^{(1)} r) r dr}{k_0^{(1)} J_{n+1}^2(k_0^{(1)} r)} \quad (2-30)$$

$$\mathbf{D}_j^n = \frac{1}{2} \int_0^{a_0} \bar{\mathbf{h}} J_n(k_j^{(2)} r) r dr + \frac{1}{2} [1] \int_0^{a_0} \frac{J_n(k_0^{(2)} r) J_n(k_j^{(2)} r) r dr}{k_0^{(2)} J_n^2(k_0^{(2)} r)} \quad (2-31)$$

$$\mathbf{D}_l^{n-1} = \frac{1}{2} \int_0^{a_0} \bar{\mathbf{h}} J_{n-1}(k_l^{(3)} r) r dr + \frac{1}{2} [1] \int_0^{a_0} \frac{J_{n-1}(k_0^{(3)} r) J_{n-1}(k_l^{(3)} r) r dr}{k_0^{(3)} J_{n-1}^2(k_0^{(3)} r)} \quad (2-32)$$

where vector $\bar{\mathbf{h}}$ is defined in Eq. (2-20), all the elements in vector [1], except the last element is equal to 1, are 0, and $\mathbf{J}_n^{(1)}$, $\mathbf{J}_n^{(2)}$ and $\mathbf{J}_n^{(3)}$ are the matrix \mathbf{J} in Eq. (2-7) with wave numbers $k_i^{(1)}$, $k_j^{(2)}$ and $k_l^{(3)}$ respectively. Substituting each mode in Eq. (2-29) into the general solutions of Eq. (2-4) and making use of rigid base condition $z=L$, one can obtain the displacement field at the surface S_2 of interior domain due to particular solutions as follows :

$$\mathbf{u}_{p,S_2}^{(i)}(\mathbf{r}) = \left(\sum_{i=0}^{\infty} \mathbf{J}_n^{(1)} \mathbf{Q}_n^{(1)} \bar{\mathbf{D}}_i^{n+1} + \sum_{j=0}^{\infty} \mathbf{J}_n^{(2)} \mathbf{Q}_n^{(2)} \bar{\mathbf{D}}_j^n + \sum_{l=0}^{\infty} \mathbf{J}_n^{(3)} \mathbf{Q}_n^{(3)} \bar{\mathbf{D}}_l^{n-1} \right) \mathbf{P}_2 = \mathbf{N}_{p,S_2}^{(i)}(\mathbf{r}) \mathbf{P}_2 \quad (2-33)$$

where $\mathcal{Q}_n^{(1)}$, $\mathcal{Q}_n^{(2)}$ and $\mathcal{Q}_n^{(3)}$ can be obtained using Eqs. (2-4) and (2-5) with wave numbers $k_i^{(1)}$, $k_j^{(2)}$, and $k_l^{(3)}$ respectively as follows :

$$\mathcal{Q}_n = - \begin{bmatrix} t_{11}^{(i)} & t_{12}^{(i)} & 0 \\ t_{21}^{(i)} & t_{22}^{(i)} & 0 \\ 0 & 0 & t_{55}^{(i)} \end{bmatrix}^{-1} \begin{bmatrix} t_{13}^{(i)} & t_{14}^{(i)} & 0 \\ t_{23}^{(i)} & t_{24}^{(i)} & 0 \\ 0 & 0 & t_{56}^{(i)} \end{bmatrix} \quad (2-34)$$

and elements $t_{ij}^{(i)}$ in Eq. (2-34) are defined in Eq. (2-5). From the derivations above, $\mathbf{t}_{p,s_2}^{(i)}(\mathbf{r})$ is equal to $\mathbf{t}_{b_2}^n$ in Eqs (2-20) or (2-29). For each mode in Eqs. (2-33) and (2-29), vectors $\mathbf{J}^{-1}\mathbf{u}_{p,s_2}^{(i)}$ and $\mathbf{J}^{-1}\mathbf{t}_{p,s_2}^{(i)}$ can be combined into the vectors $\bar{\mathbf{J}}_n^{-1}\mathbf{Y}_0^{(i)}$ in Eq. (2-10). Therefore, if one truncates high modes in Eqs. (2-33) and (2-29), the displacement and traction fields due to the prescribed traction $\mathbf{t}_{b_2}^n(\mathbf{r})$ in Eq. (2-20) at the vertical interface s_3 between interior domain and exterior domains can have similar expressions to Eqs. (2-13) and (2-14) respectively.

$$\mathbf{u}_{p,s_3}^{(i)}(\mathbf{z}) = \mathbf{N}_{p,s_3}^{(i)}(\mathbf{z})\mathbf{P}_2 \quad , \quad r = a_0 \quad (2-35)$$

and

$$\mathbf{t}_{p,s_3}^{(i)}(\mathbf{z}) = \mathbf{G}_{p,s_3}^{(i)}(\mathbf{z})\mathbf{P}_2 \quad , \quad r = a_0 \quad (2-36)$$

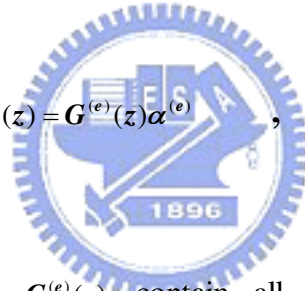
For the exterior domain in Fig. 2-1, only homogeneous solutions are involved since the solutions have to satisfy the homogenous boundaries at $z=0$ and $z=L$. Therefore, one just follows the procedures of finding homogeneous solutions for interior domain to obtain the solutions. To do this, one can express the displacement and stress fields in terms of

displacement-stress vector at the top surface ($z=0$) of the layered medium like the procedure to obtain Eqs. (2-4) and (2-10) except the Bessel function matrix \bar{J} is replaced with Hankel function matrix \bar{H} . Matrix \bar{H} is similar to matrix \bar{J} in Eq. (A1) except the element $J_n(kr)$ and $J'_n(kr)$ are replaced by the second kind of Hankel functions $H_n(kr)$ and $H'_n(kr)$. Then the displacement and stress at the vertical surface s_1+s_3 in Fig. 2-1 can be written by the combination of a finite number of modes with unknown participation factors similar to Eqs. (2-13) and (2-14).

$$\mathbf{u}_{h,s_1+s_3}^{(e)}(z) = \mathbf{N}^{(e)}(z)\boldsymbol{\alpha}^{(e)} \quad , \quad r = a_0 \quad (2-37)$$

and

$$\mathbf{t}_{h,s_1+s_3}^{(e)}(z) = \mathbf{G}^{(e)}(z)\boldsymbol{\alpha}^{(e)} \quad , \quad r = a_0 \quad (2-38)$$



where matrices $\mathbf{N}^{(e)}(z)$ and $\mathbf{G}^{(e)}(z)$ contain all the considered modal shapes of displacement and stress respectively, and $\boldsymbol{\alpha}^{(e)}$ is the vector of unknown modal participation factors.

2.2 Formulation of impedance matrix

In Fig. 2-2, the solutions at the boundaries of interior domain and exterior domain have been shown by using of Eqs. (2-37) and (2-38) for exterior domain and Eqs. (2-3), (2-13)-(2-16), (2-20 or 2-29), (2-33), (2-35) and (2-36) for interior domain. Also, in the following derivations, the variation with respect to θ ($\cos(n\theta)$ or $\sin(n\theta)$) will be omitted in the expression, and the integrations with respect to θ will be automatically calculated.

By applying the stress continuity condition to vertical surface s_1+s_3 , the variational principle

$$\int_{S_1+S_3} \delta u^{(e)}(z)(t^{(e)}(z) - t^{(i)})dS = 0 \text{ gives}$$

$$K_{ee} \alpha^{(e)} - K_{eh} \alpha^{(i)} = K_{ep} P_2 - V_{b1} P_1 \quad (2-39)$$

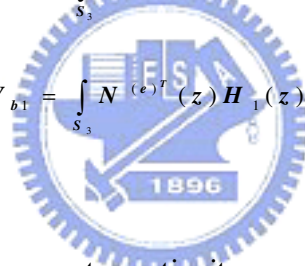
where

$$K_{ee} = \int_{S_1+S_3} N^{(e)T}(z) G_h^{(e)}(z) dS \quad (2-40)$$

$$K_{eh} = \int_{S_3} N^{(e)T}(z) G_{h.S_3}^{(i)}(z) dS \quad (2-41)$$

$$K_{ep} = \int_{S_3} N^{(e)T}(z) G_{p.S_3}^{(i)}(z) dS \quad (2-42)$$

$$V_{b1} = \int_{S_3} N^{(e)T}(z) H_1(z) dS \quad (2-43)$$



Similarly, imposing the displacement continuity condition, the variational principle of

$$\int_{S_3} \delta t^{(i)}(z)(u^{(i)}(z) - u^{(e)})dS = 0 \text{ gives}$$

$$-K_{he} \alpha^{(e)} + K_{hh} \alpha^{(i)} = -K_{hp} P_2 \quad (2-44)$$

where

$$K_{he} = \int_{S_3} G_{h.S_3}^{(i)T}(z) N^{(e)}(z) dS \quad (2-45)$$

$$K_{hh} = \int_{S_3} G_{h.S_3}^{(i)T}(z) N_{h.S_3}^{(i)}(z) dS \quad (2-46)$$

$$K_{hp} = \int_{S_3} G_{h.S_3}^{(i)T}(z) N_{p.S_3}^{(i)}(z) dS \quad (2-47)$$

Eqs. (2-39) and (2-44) can be combined as

$$\begin{bmatrix} K_{ee} & -K_{eh} \\ -K_{he} & K_{hh} \end{bmatrix} \begin{bmatrix} \alpha^{(e)} \\ \alpha^{(i)} \end{bmatrix} = \begin{bmatrix} K_{ep} \\ -K_{hp} \end{bmatrix} P_2 + \begin{bmatrix} -V_{b1} \\ 0 \end{bmatrix} P_1 \quad (2-48)$$

Therefore, the unknown modal participation factors of the homogeneous solutions in the exterior and interior domains can be expressed in terms of the stress intensity vectors P_1 and P_2 in Eqs. (2-18) and (2-20) respectively as follows:

$$\begin{bmatrix} \alpha^{(e)} \\ \alpha^{(i)} \end{bmatrix} = \begin{bmatrix} \xi_1 \\ \xi_2 \end{bmatrix} P_2 + \begin{bmatrix} \xi_3 \\ \xi_4 \end{bmatrix} P_1 \quad (2-49)$$

Consequently all the displacement and the stress components at any arbitrary location in the soil domain can be obtained for the arbitrarily prescribed piecewise linear tractions at the surface of cylindrical cavity. Now, referring to Fig. 2-2 and making use of Eqs. (2-49), (2-18) and (2-20), the displacement and traction at surfaces s_1 and s_2 can be written as

$$\mathbf{u}_0 = \begin{bmatrix} \mathbf{u}_{s_1}(z) \\ \mathbf{u}_{s_2}(r) \end{bmatrix} = \begin{bmatrix} N^{(e)}(z)\xi_3 & N^{(e)}(z)\xi_1 \\ N^{(i)}(r)\xi_4 & N^{(i)}(r)\xi_2 + N_{p,s_2}^{(i)}(r) \end{bmatrix} \begin{bmatrix} P_1 \\ P_2 \end{bmatrix} \quad (2-50)$$

and

$$\mathbf{t}_0 = \begin{bmatrix} \mathbf{t}_{s_1}(z) \\ \mathbf{t}_{s_2}(r) \end{bmatrix} = \begin{bmatrix} \mathbf{H}_1(z) & 0 \\ 0 & \mathbf{H}_2(r) \end{bmatrix} \begin{bmatrix} P_1 \\ P_2 \end{bmatrix} \quad (2-51)$$

To form the impedance matrix, one can use Eqs. (2-50) and (2-51). The variational

principle gives the virtual work of the system as follows :

$$\begin{aligned}
\delta W &= \int_{S_1+S_2} \delta \mathbf{t}_0^T \mathbf{u}_0 dS \\
&= \delta \mathbf{P}^T \int_{S_1+S_2} \begin{bmatrix} \mathbf{H}_1^T(z) & 0 \\ 0 & \mathbf{H}_2^T(r) \end{bmatrix} \begin{bmatrix} N^{(e)}(z) \xi_3 & N^{(e)}(z) \xi_1 \\ N_{h,S_2}^{(i)}(r) \xi_4 & (N_{h,S_2}^{(i)}(r) \xi_2 + N_{p,S_2}^{(i)}(r)) \end{bmatrix} dS \mathbf{P} \\
&= \delta \mathbf{P}^T \begin{bmatrix} \mathbf{Q}_{11} & \mathbf{Q}_{12} \\ \mathbf{Q}_{21} & \mathbf{Q}_{22} \end{bmatrix} \mathbf{P} = \delta \mathbf{P}^T \mathbf{Q} \mathbf{P}
\end{aligned} \tag{2-52}$$

where

$$\mathbf{Q}_{11} = \int_0^d \mathbf{H}_1^T(z) N^{(e)}(z) dz \xi_3 \tag{2-53}$$

$$\mathbf{Q}_{12} = \int_0^d \mathbf{H}_1^T(z) N^{(e)}(z) dz \xi_1 \tag{2-54}$$

$$\mathbf{Q}_{21} = \int_0^{a_0} \mathbf{H}_2^T(r) N_{h,S_2}^{(i)}(r) r dr \xi_4 \tag{2-55}$$

and

$$\mathbf{Q}_{22} = \int_0^{a_0} \mathbf{H}_2^T(r) [N_{h,S_2}^{(i)}(r) \xi_2 + N_{p,S_2}^{(i)}(r)] r dr \tag{2-56}$$

For the foundation itself, the displacement field of the foundation for the n^{th} Fourier component (either a symmetric or an anti-symmetric component as shown in Eqs.(2-1) or (2-2)) can be assumed as

$$\bar{\mathbf{u}}_0 = N \mathbf{v} \tag{2-57}$$

where matrix N is comprised of the displacement shape functions at the interface between foundation and surrounding soil, and vector \mathbf{v} is comprised of the generalized displacements at the nodal rings of the finite element model of foundation. Similarly, the virtual work of the system is obtained by applying the variational principle

$$\delta W = \int_{S_1+S_2} \delta \mathbf{t}_0^T \bar{\mathbf{u}}_0 dS = \delta \mathbf{P}^T \int_{S_1+S_2} \mathbf{H}^T N dS \mathbf{v} = \delta \mathbf{P}^T \mathbf{B} \mathbf{v} \tag{2-58}$$

Equating Eq. (2-52) to Eq. (2-58) and factoring out $\delta \mathbf{P}^T$, it is obtained.

$$\mathbf{QP} = \mathbf{Bv} \quad (2-59)$$

or

$$\mathbf{V} = \mathbf{Bv} \quad (2-60)$$

where the elements of vector \mathbf{V} are the generalized displacements at the nodal rings of the assumed piecewise linear traction model. Eq. (2-60) gives the relationship between the nodal generalized displacements of the assumed stress model of Eqs. (2-18) and (2-20) and the finite element model of Eq. (2-57). To obtain the corresponding force-stress relationship for both models, the reciprocal theorem can be used. This leads to the following equation.



$$\mathbf{F} = \mathbf{B}^T \mathbf{P} \quad (2-61)$$

where the elements of vector \mathbf{F} are the generalized forces at the nodal rings of the finite element model. Substituting $\mathbf{P} = \mathbf{Q}^{-1} \mathbf{Bv}$ from Eq. (2-59) into Eq. (2-61) yields

$$\mathbf{F} = \mathbf{B}^T \mathbf{Q}^{-1} \mathbf{Bv} = \mathbf{Iv} \quad (2-62)$$

where the matrix \mathbf{I} is the impedance matrix for the n^{th} Fourier component. It is noted that \mathbf{I} matrix is symmetric matrix.

2.3 Numerical investigations

A rigid massless circular foundation embedded in a stratum of single layer subjected to time harmonic torsional, vertical, rocking and horizontal excitations is used as an example to demonstrate the effectiveness and efficiency of the presented scheme. In this example, 0.05 hysteretic damping ratio is chosen for soil medium and the poisson ratio of soil is assumed to be 0.33. For the torsional time-harmonic and vertical time-harmonic vibrations of foundation, the anti-symmetric and symmetric Fourier components with $n=0$ in Eqs. (2-57), (2-1) and (2-2) are involved respectively in the analysis. For the rocking and horizontal time-harmonic vibrations of foundation, the Fourier component involved in the analysis is the symmetric component with $n=1$ in Eqs. (2-57), (2-1) and (2-2).

Since the Love modes and Rayleigh modes are involved in the homogeneous solutions, Eq. (2-8) and Eq. (2-9) are employed to find the wave numbers for homogeneous solutions of interior domain. And a similar way can be used to find the homogeneous solutions for exterior domain.

To obtain the Love and Rayleigh wave numbers of Eqs. (2-8) and (2-9) numerically, reference 8 proposed a scheme to locate approximately all the roots in a specified region on complex plane. Then, Mullers method is employed to find the more accurate roots [19].

For validation of the proposed numerical scheme, the convergence study is performed

first. In the study, $\frac{L}{a_0} = 2$ with $\frac{d}{a_0} = 0$ (see Fig. 2-1) and non-dimensional frequency

$\frac{\omega a_0}{\text{Re}(C_s)} = 0.01$ are chosen. The results for the case are shown in Table 2-1~2-5. In these

tables, i and j are the numbers of homogeneous modes for exterior and interior domains respectively (Eq. (2-8)) or (Eq. (2-9)) used in the analysis, l is the number of particular modes for interior domain (Eq. (2-22)), m_1 is the number of subintervals for piecewise

linear in z direction (Eq. (2-17)), m_2 is the number of subintervals for piecewise linear in r direction (Eq. (2-20)), $\text{Re}(C_s)$ is the real part of shear wave velocity of soil medium, K_{TT} is the torsional impedance, K_{VV} is the vertical impedance, K_{HH} is the horizontal impedance, $K_{RH} = K_{HR}$ are the coupling impedance, K_{RR} is the rocking impedance, G is the shear modulus of soil medium and ω is frequency. Also, one should notice that for torsional impedance, i and j are the numbers of Love modes for respective exterior and interior domains, and m_2 and l are the numbers of subintervals and roots of $J_1(ka) = 0$ (Eq.2-22) respectively for traction $\tau_{\theta z}$, for vertical impedance i and j are the numbers of Rayleigh modes for respective domains, m_2 is the number of subintervals for both tractions τ_{rz} and σ_{zz} and l is the number of roots of $J_0(ka) = 0$ and $J_1(ka) = 0$ (the total number of roots is $2l$), and for horizontal, coupling and rocking impedances, i and j are the numbers of Love or Rayleigh modes for respective domains (the total numbers are $2i$ and $2j$), m_2 is the numbers of subintervals for tractions τ_{rz} , σ_{zz} and $\tau_{\theta z}$ and l is the number of roots of $J_0(ka) = 0$, $J_1(ka) = 0$ and $J_2(ka) = 0$ (the total number of roots is $3l$). In the tables, $i = 10$ and $j = 15$ are enough for exterior and interior domains respectively, when non-dimensionalized frequency $\frac{\omega a_0}{\text{Re}(C_s)} = 0.01$. However, for higher frequency i and j should be larger.

From Table 2-1~2-5, one can see that as l and m_2 become larger, the results are converging and approaching the results of Liou and Lee [11]. Also one can observe from these tables that the number of particular solutions must be larger than the number of sub-interval m_2 . This means $l \geq m_2 + 1$. The reason to this restriction is that the number of particular modes employed in the analysis must be greater than the number of unknown

nodal intensities of piecewise linear traction. If $l < m_2 + 1$, then matrix Q in Eq. (2-52) will be singular.

From the preliminary study, 20 Love or Rayleigh homogeneous modes for both exterior and interior domains are enough for obtaining results of torsional and vertical impedances with good accuracy in the frequency range $\frac{\omega a_0}{2\pi \text{Re}(C_s)} = 0 \sim 1$. For the horizontal, coupling and rocking impedances, 40 homogeneous modes (20 Love modes and 20 Rayleigh modes) are enough for obtaining results with good accuracy in the frequency range mentioned previously.

For the case of rigid foundation on one layer stratum, Figs. 2-3~2-7 show the numerical results of impedance functions with $m_2 = 2, 3, 4, 5$. In these figures, $i = j = 20$ and $l = 6$ are selected after some convergence study has been performed. From these figures, one can observe that the results are approaching the results by Liou and Lee [11], as m_2 becomes larger.

In order to investigate the effects of embedment on impedance functions, the ratios of embedded depth to the radius of foundation $(\frac{d}{a_0})$ are selected to be $0, \frac{1}{4}, \frac{2}{4}, \frac{3}{4}$ and 1. In the investigation, $i = j = 20$, $m_2 = 5$ and $m_1 = 5$, in which m_1 is the number of the subintervals for vertical surface S_1 in Fig.2-2, are employed according to the preliminary numerical study. Also, the results for the case $\frac{d}{a_0} = 1$ are compared to that by Tassoulas and Kausel [14] and good consistency of both results is observed. Figs.2-8~2-12 show the results of torsional, vertical, horizontal, coupling and rocking impedances for rigid circular foundation embedded in one layer stratum. From these figures, one can see that the impedances except coupling impedance are generally getting larger especially in low

frequency range as the embedded depth increases. This means embedment effect is very important.

2.4 Concluding remarks

After generating torsional, vertical, horizontal, coupling and rocking impedances numerically for foundation embedded in different depth, the following observations can be obtained : (1) The presented scheme can be easily employed to calculate impedances for foundation embedded in a multiple layer stratum. (2) From the above derivation, the scheme can be extended to calculate the impedances for flexible foundation with arbitrary shape. (3) The computational cost for generating impedances by the presented scheme is much inexpensive while compared to that by other traditional methods; e.g. Finite Element Method and Boundary Element Method. (4) The presented scheme can also be extended to approximately calculate all impedance functions for foundation in layered half-space medium, if the bottom layer of stratum is thick enough.

Table 2-1 Non-dimensionalized Torsional Impedance $\frac{K_{TT}}{Ga_0^3}$ for $\frac{d}{a_0} = 0$, $\frac{L}{a_0} = 2$ and $\frac{\omega a_0}{\text{Re}(C_s)} = 0.01$

i	j	l	$m_2=2$	$m_2=3$	$m_2=4$	$m_2=5$
10	15	3	4.79+0.00059i	—	—	—
10	15	4	4.83+0.00058i	4.91+0.00061i	—	—
10	15	5	4.91+0.00056i	5.01+0.00057i	5.07+0.00055i	—
10	15	6	4.99+0.00056i	5.02+0.00053i	5.11+0.00051i	5.21+0.00048i
Liou and Lee [11]			5.254282+0.00044i			

Table 2-2 Non-dimensionalized Vertical Impedance $\frac{K_{VV}}{Ga_0}$ for $\frac{d}{a_0} = 0$, $\frac{L}{a_0} = 2$ and $\frac{\omega a_0}{\text{Re}(C_s)} = 0.01$

i	j	l	$m_2=2$	$m_2=3$	$m_2=4$	$m_2=5$
10	15	3	9.27+0.0115i	—	—	—
10	15	4	9.32+0.0114i	9.38+0.0121i	—	—
10	15	5	9.33+0.0114i	9.41+0.0111i	9.43+0.0107i	—
10	15	6	9.33+0.0114i	9.43+0.0108i	9.46+0.0105i	9.62+0.0089i
Liou and Lee [11]			9.852558+0.000158 i			

Table 2-3 Non-dimensionalized Horizontal Impedance $\frac{K_{HH}}{Ga_0^3}$ for $\frac{d}{a_0} = 0$, $\frac{L}{a_0} = 2$ and $\frac{\omega a_0}{\text{Re}(C_s)} = 0.01$

i	j	l	$m_2=2$	$m_2=3$	$m_2=4$	$m_2=5$
10	15	3	5.746+0.0143i	—	—	—
10	15	4	5.787+0.01458i	5.846+0.0158i	—	—
10	15	5	5.783+0.01454i	5.841+0.0157i	5.921+0.00173i	—
10	15	6	5.788+0.01459i	5.855+0.0159i	5.891+0.00168i	5.966+0.0184i
Liou and Lee [11]			6.003748 +0.000148 i			

Table 2-4 Non-dimensionalized Coupling Impedance $\frac{K_{RH}}{Ga_0^3}$ for $\frac{d}{a_0} = 0$, $\frac{L}{a_0} = 2$ and $\frac{\omega a_0}{\text{Re}(C_s)} = 0.01$

i	j	l	$m_2=2$	$m_2=3$	$m_2=4$	$m_2=5$
10	15	3	-0.2498+0.0081i	—	—	—
10	15	4	-0.251+0.00855i	-0.219+0.0111i	—	—
10	15	5	-0.249+0.00848i	-0.227+0.0113i	-0.194+0.014i	—
10	15	6	-0.2508+0.00859i	-0.225+0.0113i	-0.204+0.0134i	-0.183+0.0167i
Liou and Lee [11]			-0.3105359-0.00003881 i			

Table 2-5 Non-dimensionalized Rocking Impedance $\frac{K_{RR}}{Ga_0^3}$ for $\frac{d}{a_0} = 0$, $\frac{L}{a_0} = 2$ and $\frac{\omega a_0}{\text{Re}(C_s)} = 0.01$

i	j	l	$m_2=2$	$m_2=3$	$m_2=4$	$m_2=5$
10	15	3	3.828+0.00761i	—	—	—
10	15	4	3.907+0.00761i	3.97+0.01041i	—	—
10	15	5	3.873+0.00766i	3.986+0.01033i	4.07+0.0132i	—
10	15	6	3.893+0.00758i	3.992+0.01036i	4.04+0.0129i	4.191+0.0125i
Liou and Lee [11]			4.214673 +0.0003247 i			

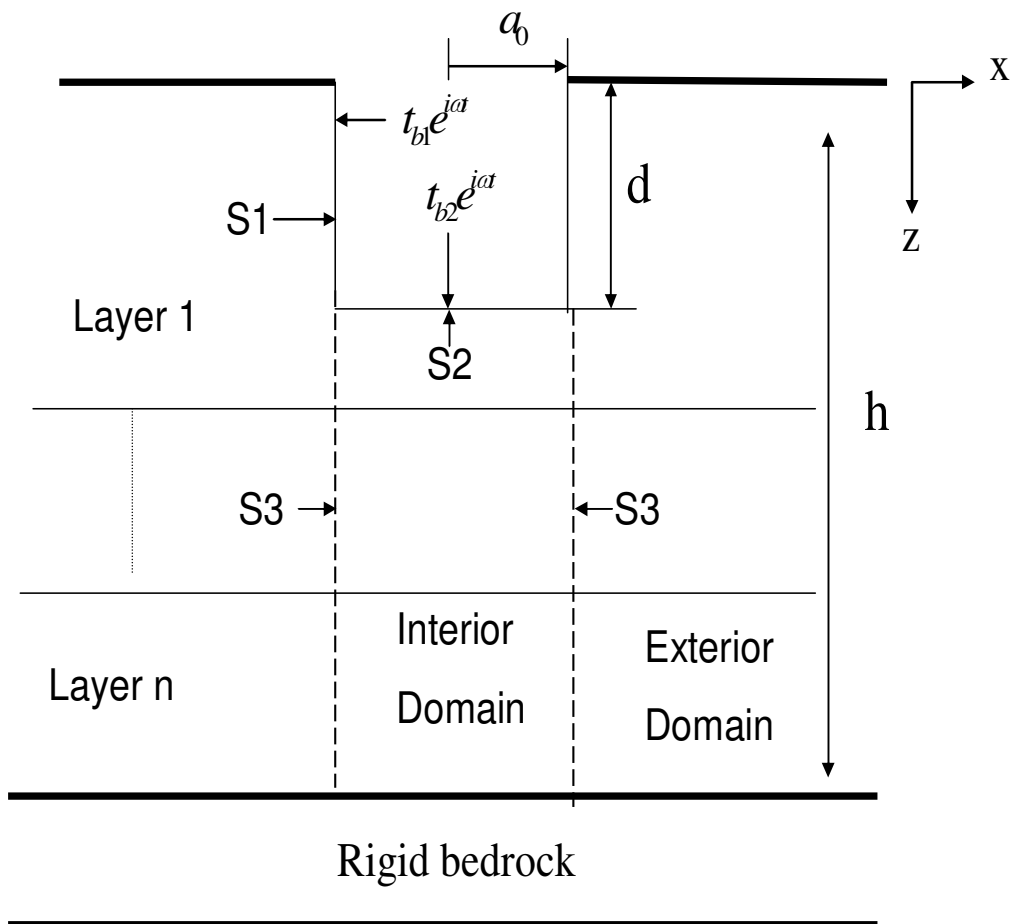


Fig. 2-1 Total soil system with prescribed tractions.

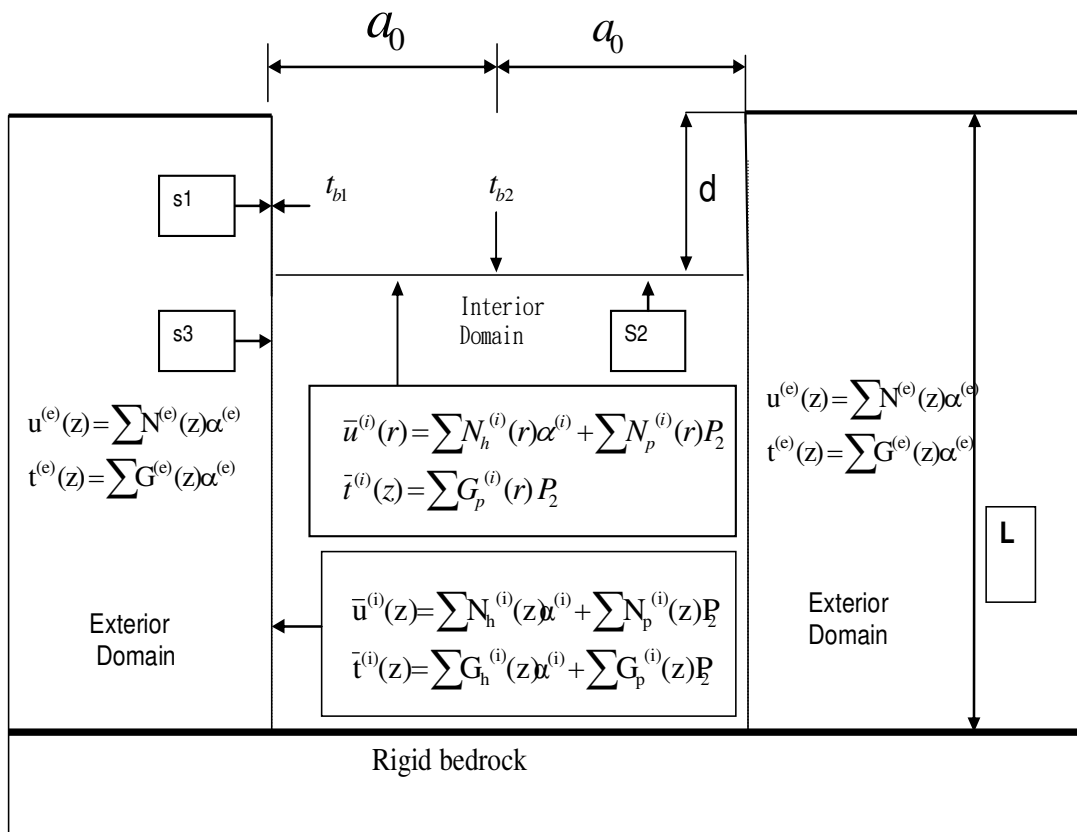


Fig. 2-2 Solution at interfaces

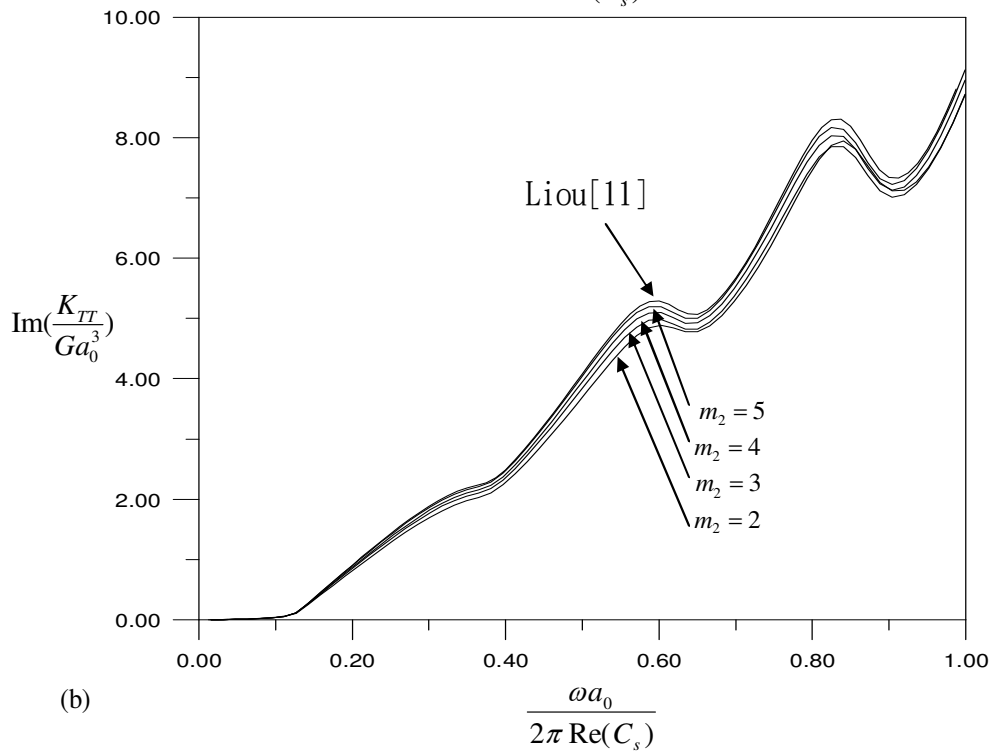
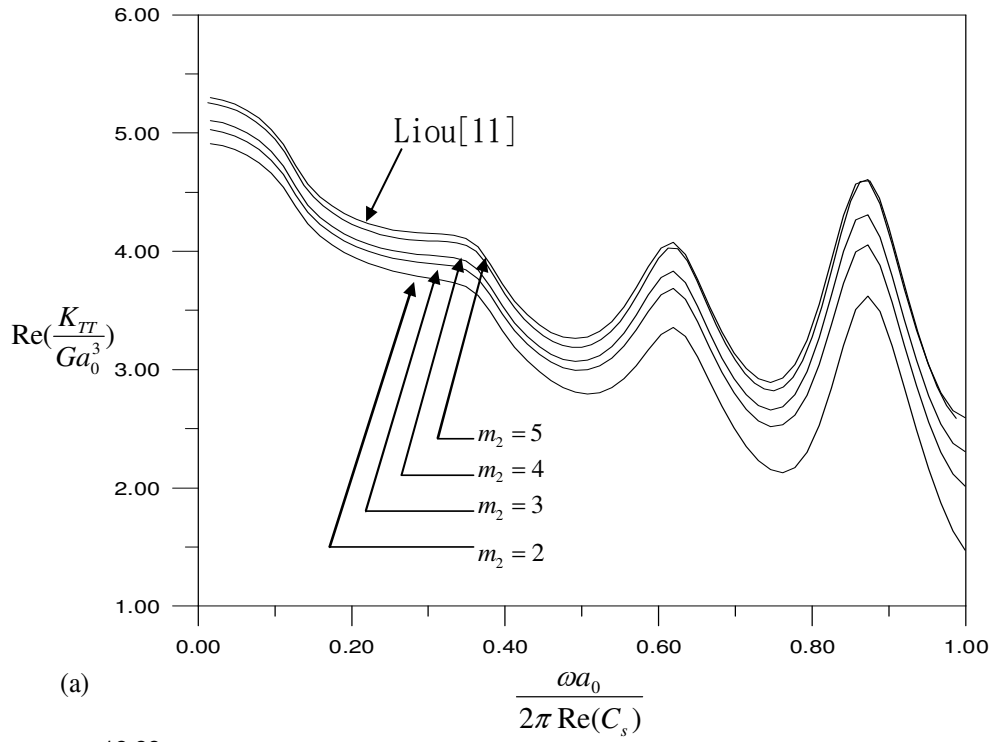


Fig. 2-3. Comparison of non-dimensionalized torsional impedance with Liou's results for $L/a_0 = 2$

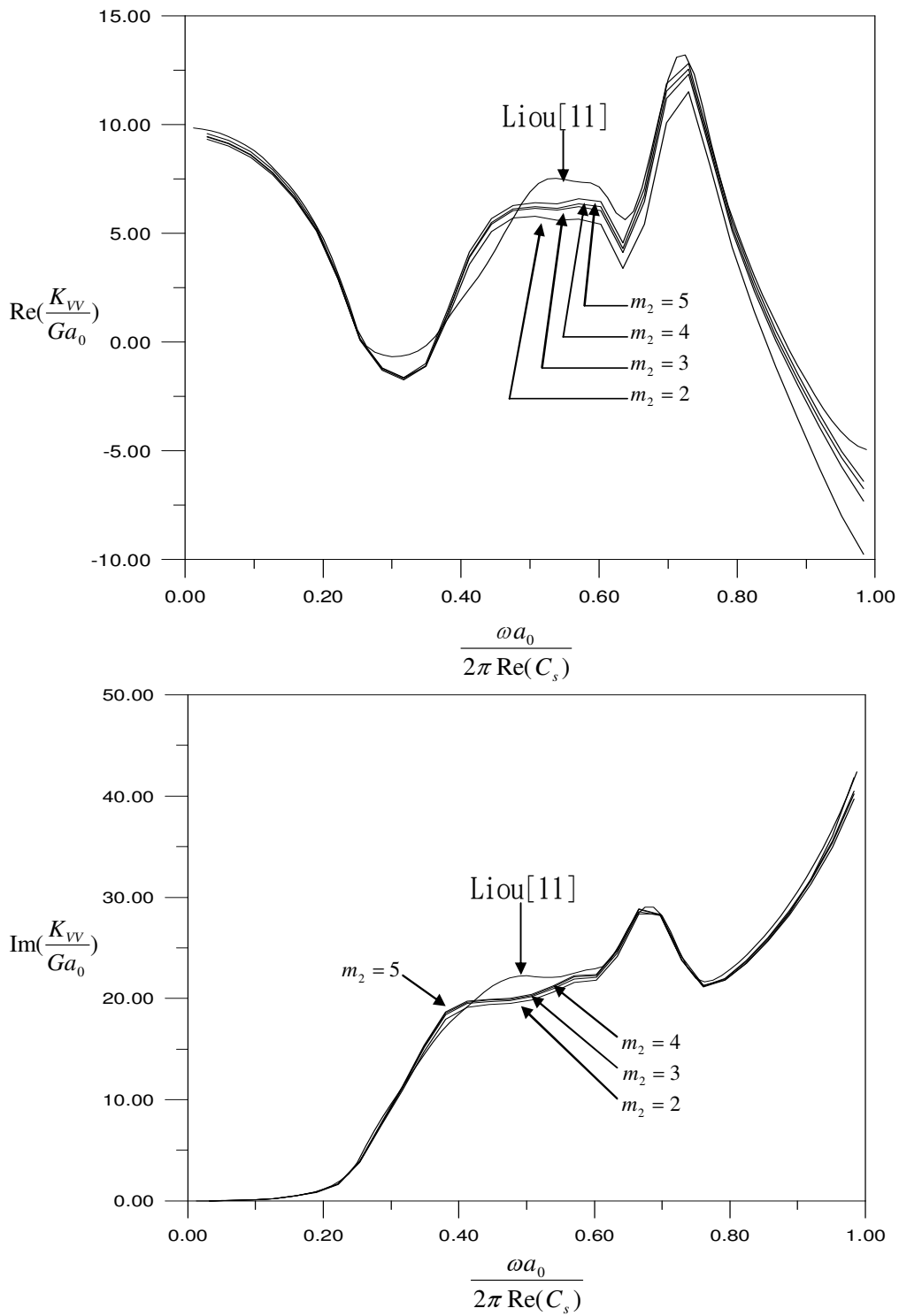


Fig. 2-4 Comparison of non-dimensionalized vertical impedance with Liou's results for $L/a_0 = 2$

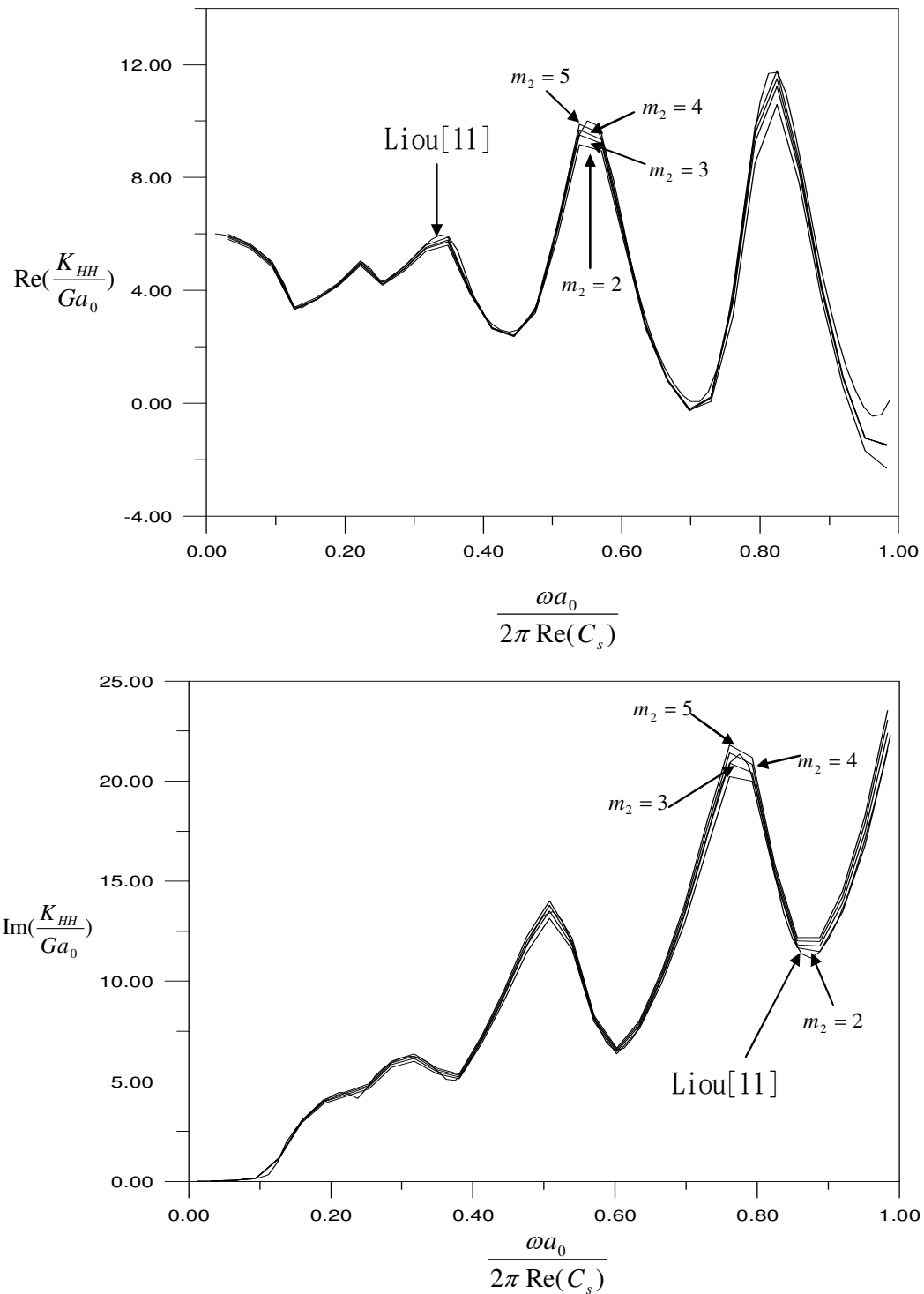


Fig. 2-5 Comparison of non-dimensionalized horizontal impedance with Liou's results for $L/a = 2$

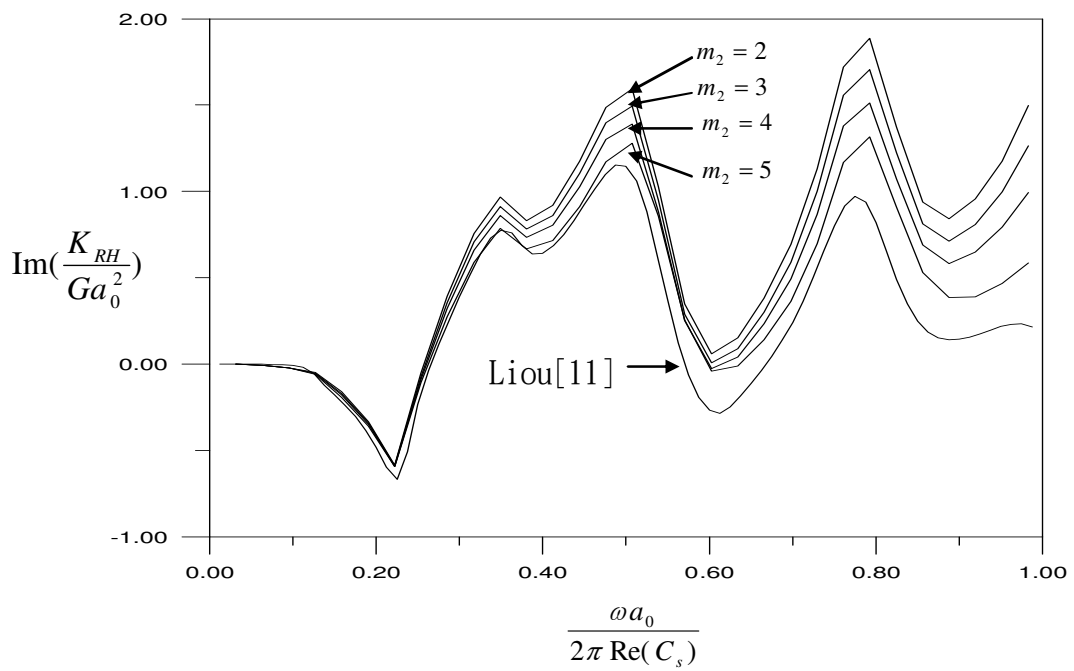
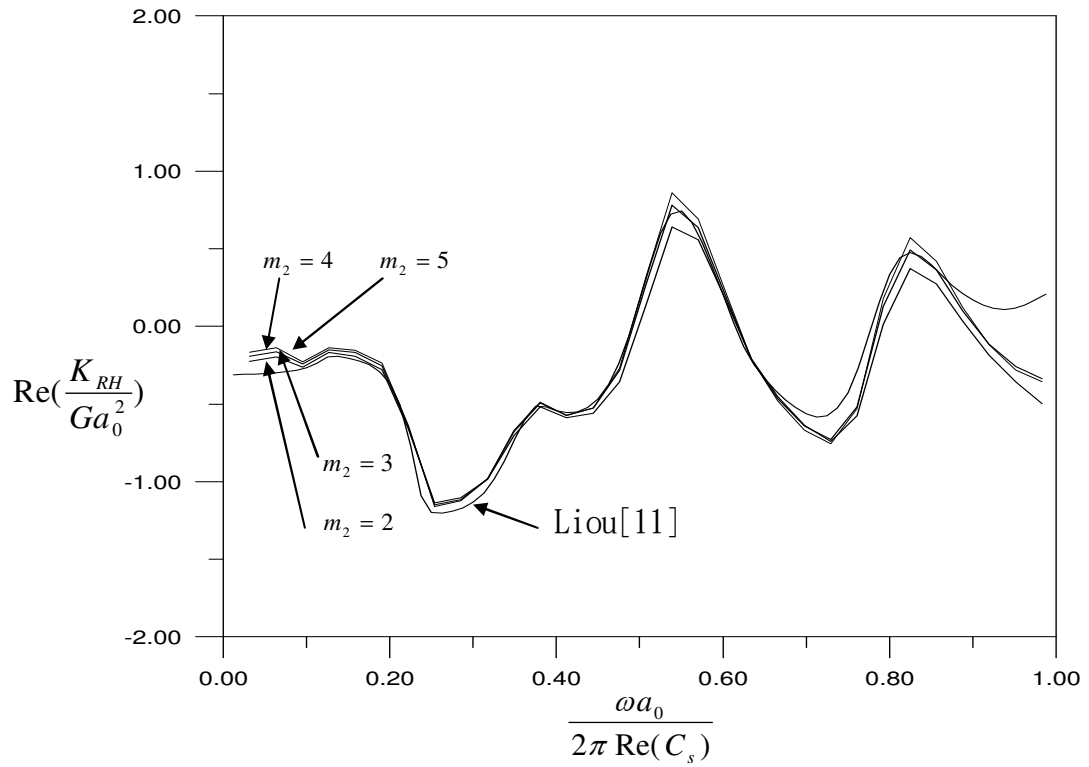


Fig. 2-6 Comparison of non-dimensionalized coupling impedance with Liou's results for $L/a_0 = 2$

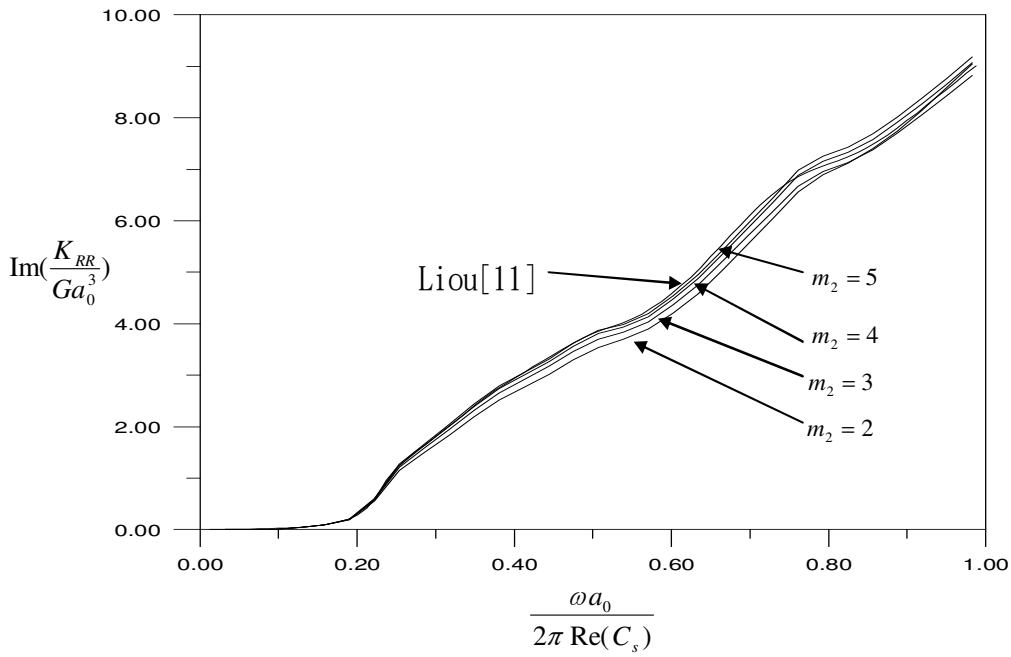
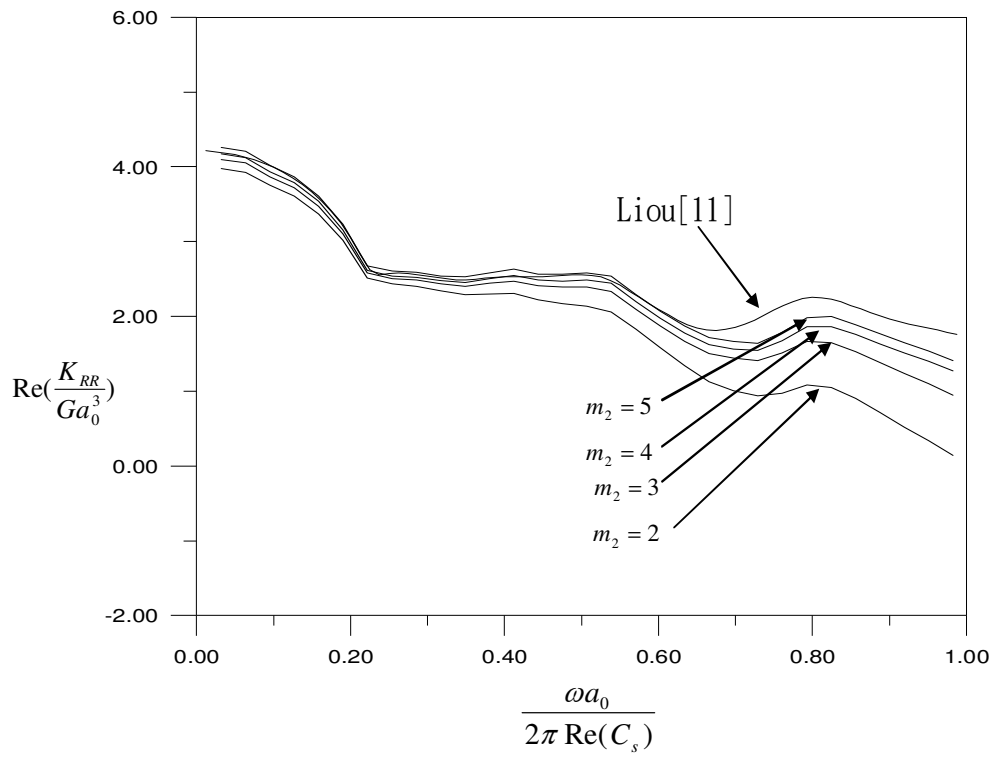


Fig. 2-7 Comparison of non-dimensionalized rocking impedance with Liou's results for $L/a = 2$

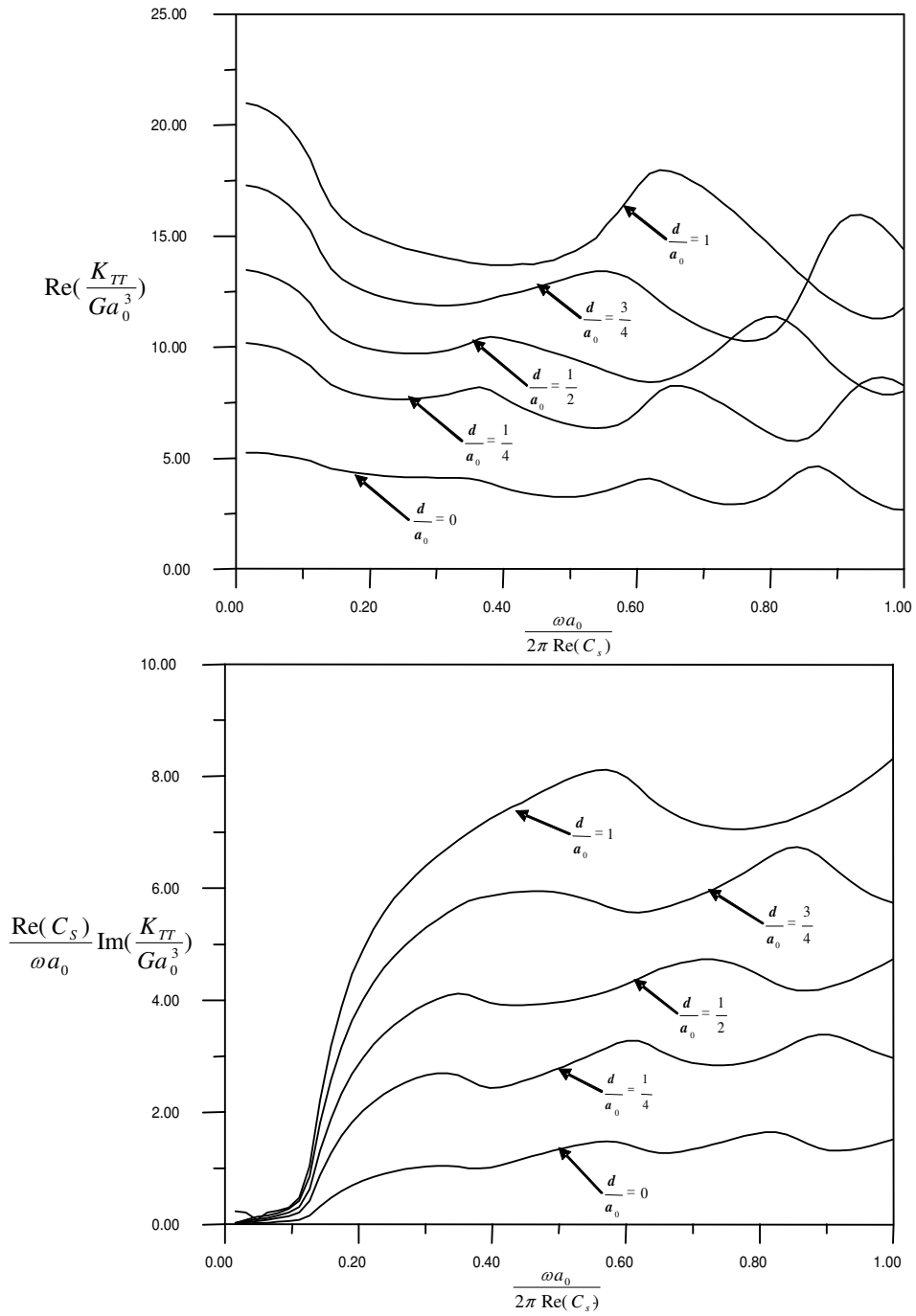


Fig. 2-8 Non-dimensionalized torsional impedance with different depths for $L/a_0 = 2$

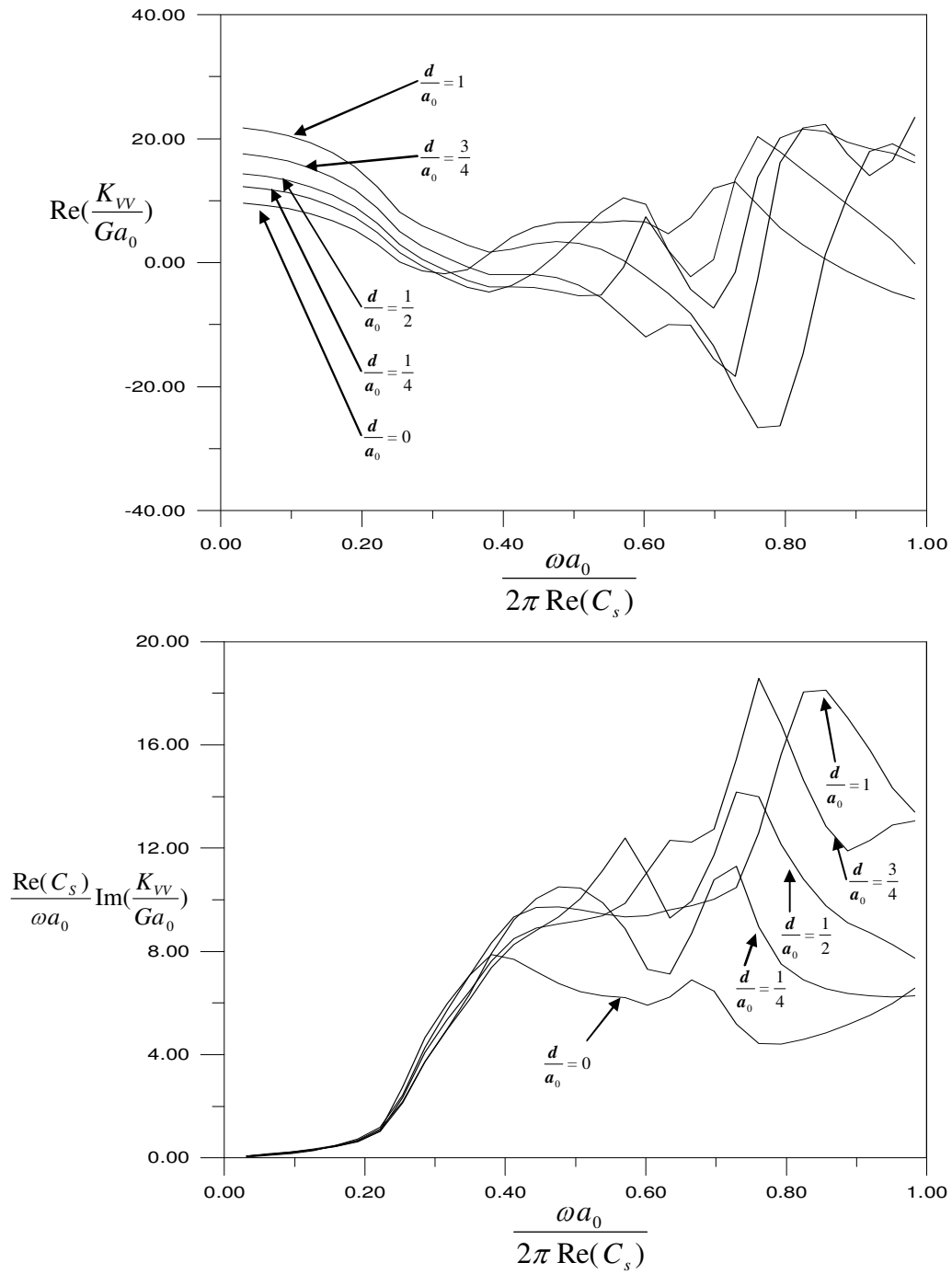


Fig. 2-9 Non-dimensionalized vertical impedance with different depths for $L/a_0 = 2$

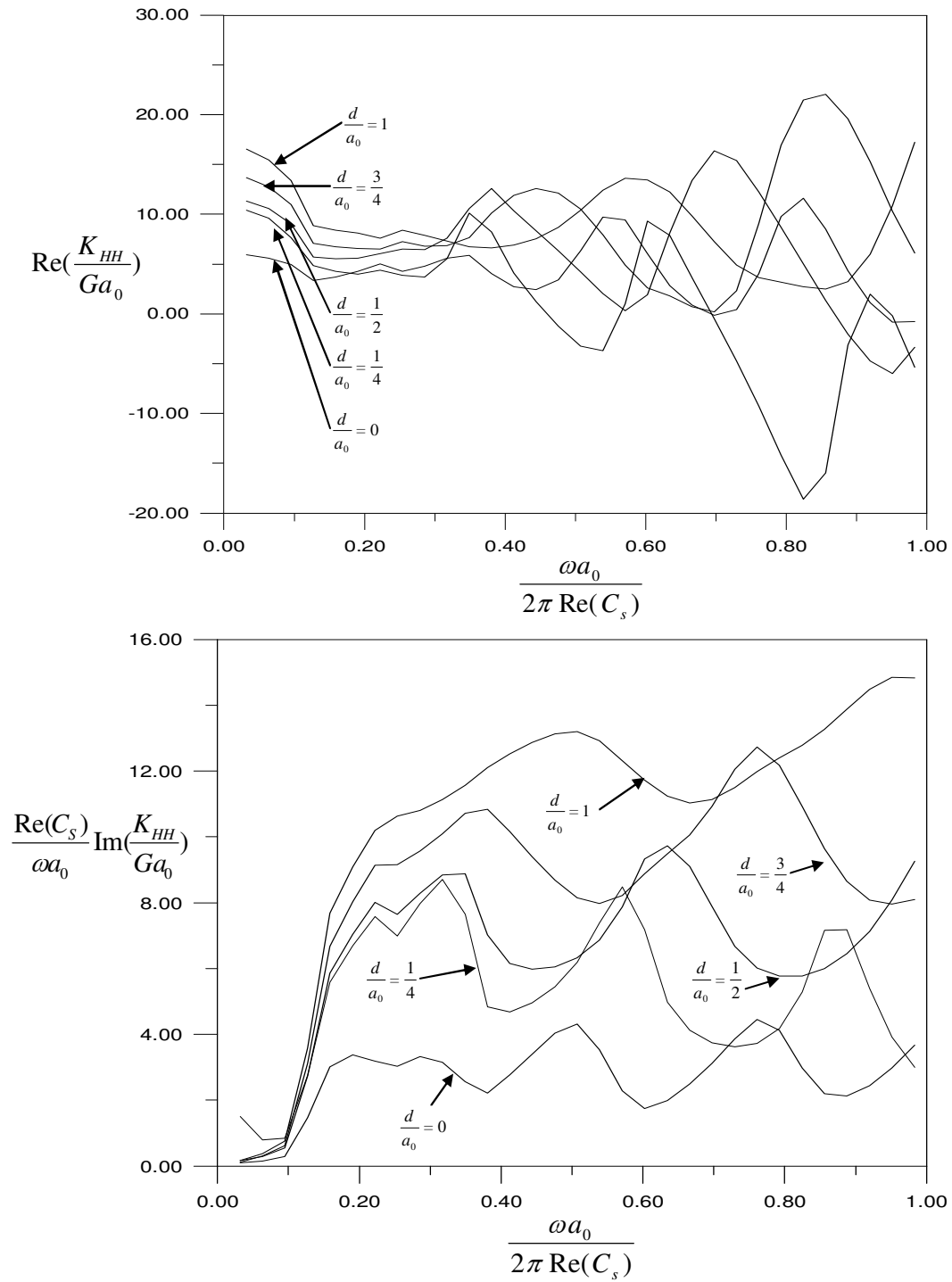


Fig. 2-10 Non-dimensionalized horizontal impedance with different depths for $L/a_0 = 2$

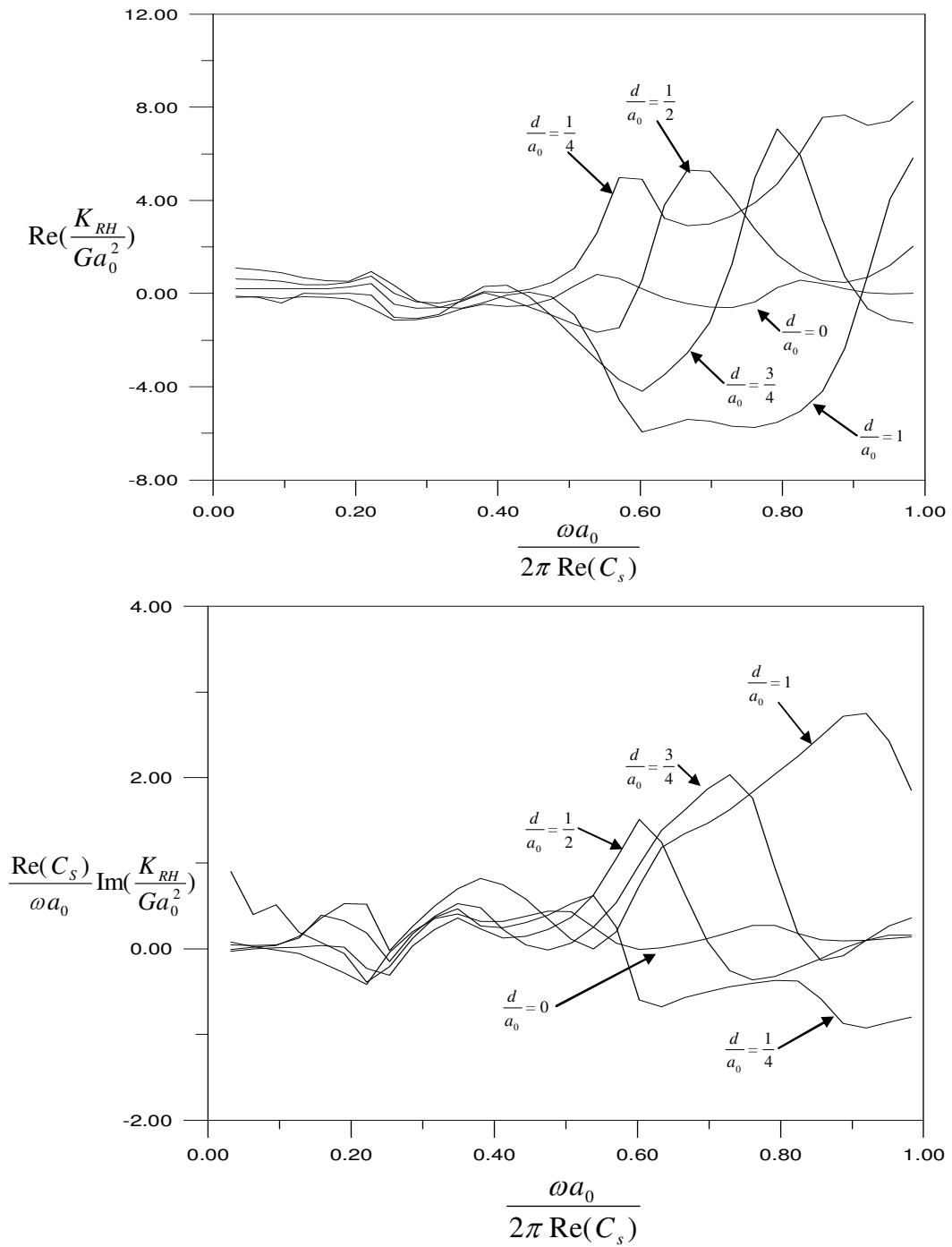


Fig. 2-11. Non-dimensionalized coupling impedance with different depths for $L/a_0 = 2$

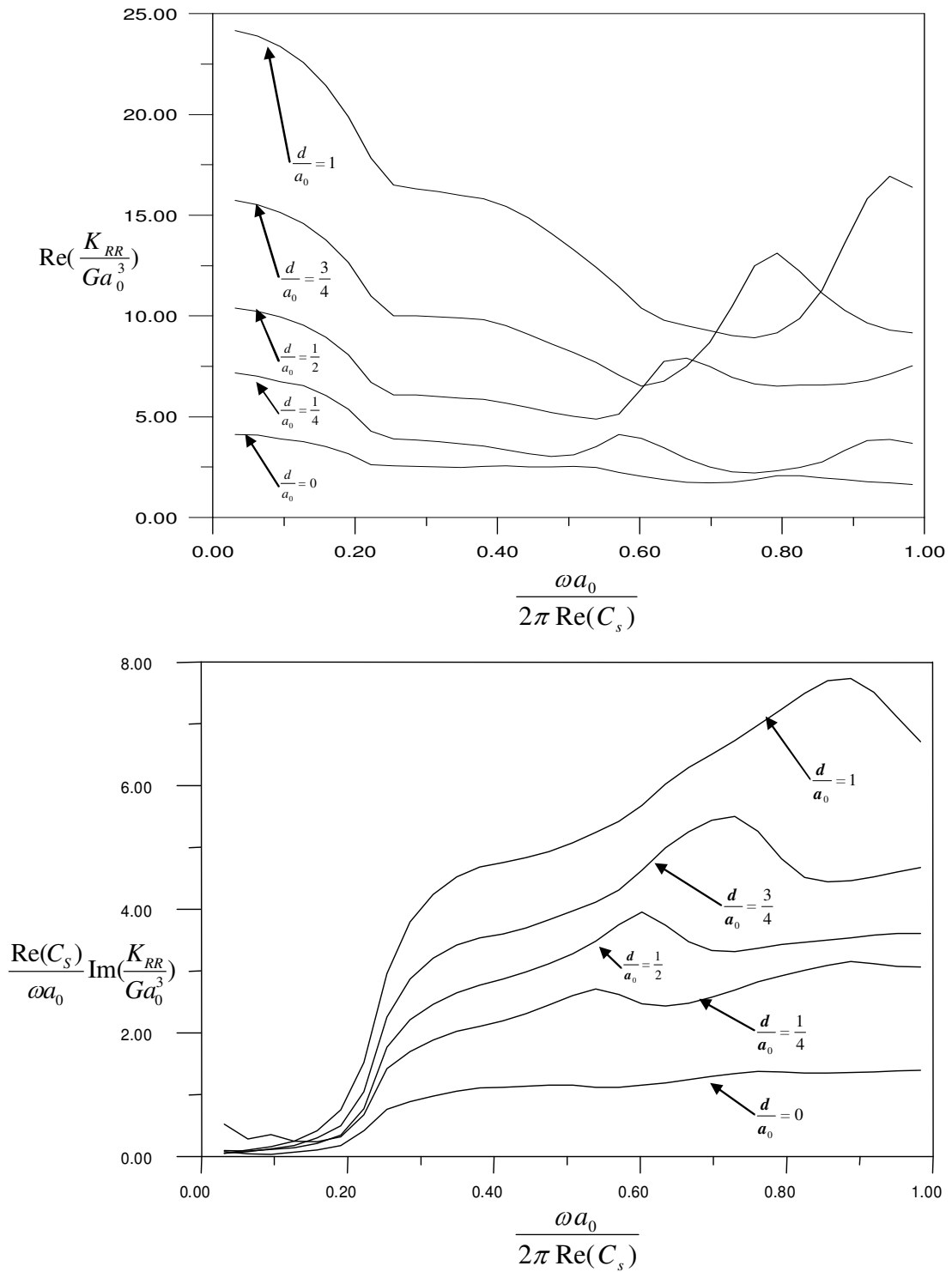


Fig. 2-12 Non-dimensionalized rocking impedance with different depths for $L/a_0 = 2$

Chapter 3

Solving of the transcendental equations for the analysis of transient wave propagation in layered media

Summary

In this chapter, we use an efficient method to solve the wave numbers of transient wave propagation in layered media. The whole soil domain is divided into interior and exterior domains. To solve those problems, the analytic solution for the interior domain is the combination of a homogeneous solution and a particular solution, the exterior domain is described by a homogeneous solution only. To obtain the homogeneous solution, one has challenge to solve the complex root of the transcendental equations will be discussed. For the soil-structure interaction problem, the wave number of transient wave propagation in layered media will be used for the impedance matrix of embedded axial symmetric foundation.

3.1 Analytical derivations for three-dimensional wave propagation problems

The total system is shown in Fig. 2-1. The whole soil domain is divided into interior and exterior domain. The general equation of wave propagation for the homogeneous solution was derived in chapter 2. The wave number k'_s are responding to the exterior domains of the complex roots equations. For the case of the wave number k is representing Love modes, we obtain

$$t_{55} = \text{Cosh}[v'L] = 0 \quad (3-1)$$

where k is the wave number of the mode, $v = \sqrt{k^2 - \left(\frac{\omega^2}{C_P^2}\right)}$, $v' = \sqrt{k^2 - \left(\frac{\omega^2}{C_S^2}\right)}$, C_S is

the shear wave velocity and C_p is the compressional wave velocity, ω is natural frequency. Methods to solving the wave problem from equation (3-1) can be expressed as

$$\text{Cosh}[v'L] = \text{Cos}[iv'L] = 0 \quad (3-2)$$

The wave number k can be determined as

$$k_N = \pm \sqrt{\frac{\omega^2}{C_s^2} - \frac{\pi^2(N+0.5)^2}{h^2}}, N = 0,1,2,3 \dots \quad (3-3)$$

Where $C_s = \sqrt{\frac{G}{\rho}}$ and $G = 1 + 2\xi i$.

For the case of the wave number k is representing Rayleigh modes, we obtain

$$t_{11}t_{22} - t_{12}t_{21} = 0 \quad (3-4)$$

For the Eq. (3-4), we will use an efficient method to solve the wave numbers of transient wave propagation in layered media.

Due to Eqs. (3-1) and (3-4) have an infinite number of root, all the roots must satisfying the radiation condition in exterior domain. As $r \rightarrow \infty$, $H_n^{(2)}(kr)$ is the Hankel function of the second kind of order n . It can be expressed as asymptotic form:

$$H_n^{(2)}(kr) \approx \left(\frac{2}{\pi kr}\right) \exp\left(-ikr + \frac{n\pi}{2} - \frac{\pi}{4}\right) \left[1 + \frac{4n^2 - 1}{1!(8ikr)} + \dots\right] \quad (3-5)$$

If $k = A + iB$ is an eigenvalue with eigenvector, then $-k$ is another pair. In order to satisfying the radiation condition in Eq. (3-5), we should choose the wave number k which is $B < 0$.

3.2 Root searching scheme for transcendental equations

Eqs. (3-1) and (3-4) have an infinite number of roots on the complex plane. The transcendental function can be expressed as

$$f(z) = \Phi(x, y) + i\Psi(x, y) \quad (3-6)$$

Where $z = x + iy$ is a complex variable, $\Phi(x, y)$ and $\Psi(x, y)$ are the real and the imaginary parts of $f(z)$. The scheme is to find the approximate z such that

$$f(z) = \Phi(x, y) + i\Psi(x, y) \approx 0 \quad (3-7)$$

To find all the approximate root's, one needs to divide the region into the mesh shown in Fig. 3-1. Fig. 3-2 show typical grid pattern. If any two function values at the four corners of the grid have different signs. To determine the root above two functions, we have two linear equations :

$$l_r(x, y) = a_1x + b_1y + c_1 = 0 \quad (3-8)$$

$$l_i(x, y) = a_2x + b_2y + c_2 = 0 \quad (3-9)$$

Where $a_1 = y_5 - y_6$, $b_1 = x_6 - x_5$, $c_1 = x_5y_6 - x_6y_5$, $a_2 = y_7 - y_8$, $b_2 = x_8 - x_7$ and $c_2 = x_7y_8 - x_8y_7$, to determine the root in the grid, the approximate root is

$$z_n = x_n + iy_n \quad (3-10)$$

Where $y_n = \frac{c_1a_2 - c_2a_1}{b_2a_1 - b_1a_2}$, $x_n = -\frac{(b_1y_n + c_1)}{a_1}$, if $a_1 \geq a_2$, $x_n = -\frac{(b_2y_n + c_2)}{a_2}$, if

$a_2 \geq a_1$.

3.3 Numerical investigations

A rigid massless circular plate resting on a single layer stratum is shown in Fig. 4. Form Love mode of Eq. (3-1), Figs. 3-4 ~3-6 are show $\omega = 0.4$, $\omega = 2$ and $\omega = 6$ of an analytical wave numbers of undamping system of real part k versus imaginary part k .

From the Fig. 3-4, when $N = 0, 1, 2, \dots$ are show the position of analytical complex wave numbers, we can find that the analytical complex wave numbers of k_N only exist in imaginary axial and \bar{k}_N is another pair of the roots. The Fig. 3-5 and Fig 3-6 are show when the natural frequency is increasing, the analytical complex wave numbers from imaginary axial close to real axial. Figs. 3-7 ~3-9 are show $\omega = 0.4$, $\omega = 2$ and $\omega = 6$ of an analytical wave numbers of 0.05 hysteretic damping ratio is chosen. At the same time, it is observation that analytical complex wave numbers exist in both real part and imaginary part.

Figs. 3-10~3-12 are shown the numerical wave numbers of undamping system for real part k versus imaginary part k on $\omega = 0.4$, $\omega = 2$ and $\omega = 6$, and Figs. 3-13~3-15 are shown the numerical wave numbers of 0.05 hysteretic damping ratio on $\omega = 0.4$, $\omega = 2$ and $\omega = 6$. Respectively, it is interesting to find that the analytical solution of Figs. 3-4~3-9 match well the numerical solution in Figs. 3-10~3-15. From Rayleigh modes, we can use the numerical method to solve the transcendental equations of Rayleigh wave numbers in Eq. (3-4). Figs. 3-16~3-18 are shown numerical wave numbers of 0.05 hysteretic damping ratio on $\omega = 0.4$, $\omega = 2$ and $\omega = 6$.

3.4 Concluding remarks

We have used an efficient technique to solve the complex roots in the transcendental equations. In this procedure, the wave numbers of transient wave propagation can be calculated numerically and analytically, the mathematical model of the transient wave propagation is being used for constructing the impedance matrices of foundation embedded in layered medium.

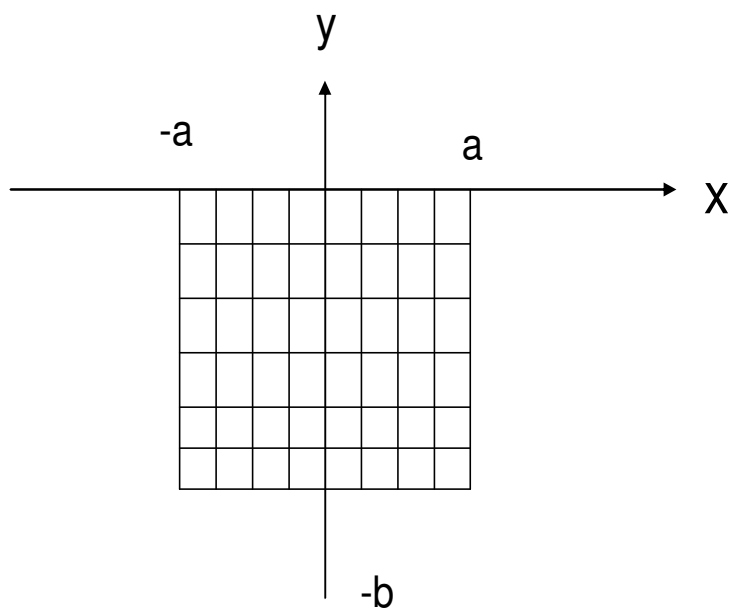


Fig.3-1 Mesh of the region $-a \leq x \leq a$ and $-b \leq y \leq 0$ on complex plane

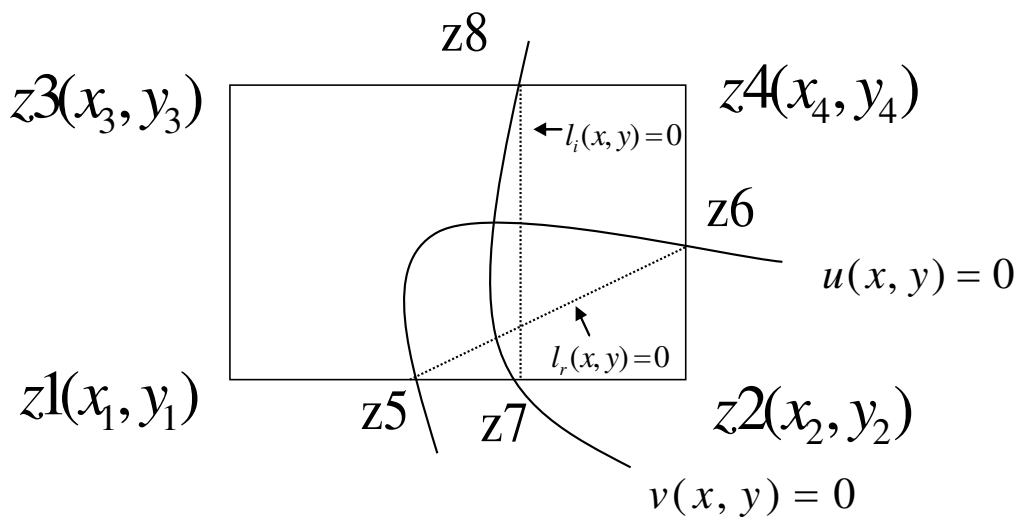


Fig. 3-2 typical grid patterns

Numerical example

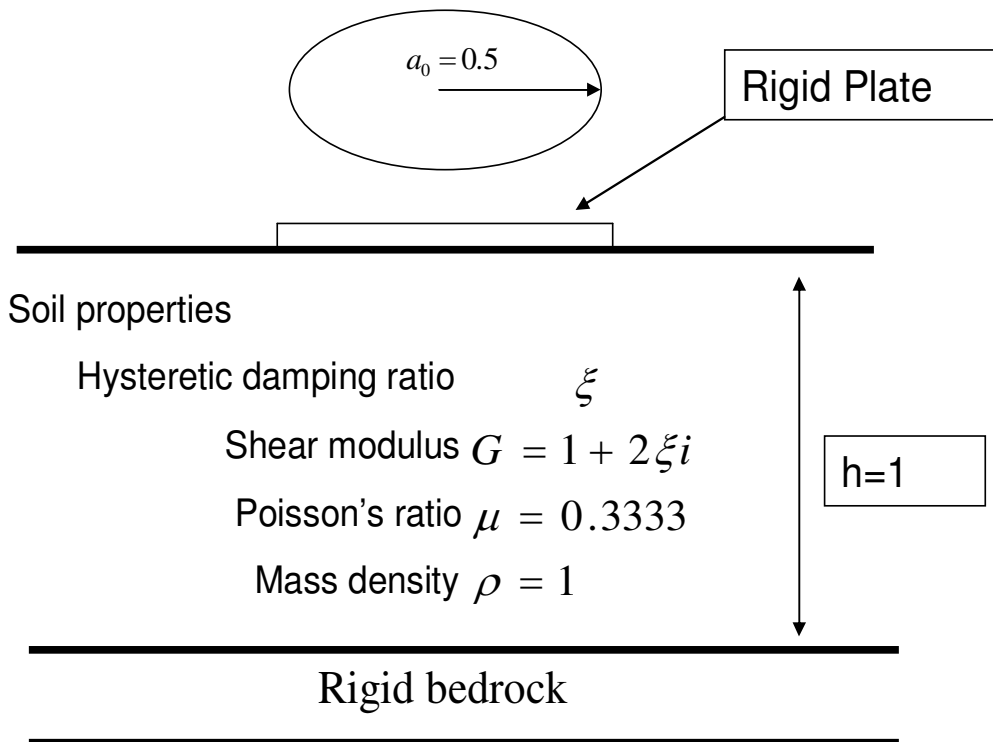


Fig. 3-3 Soil profile of example

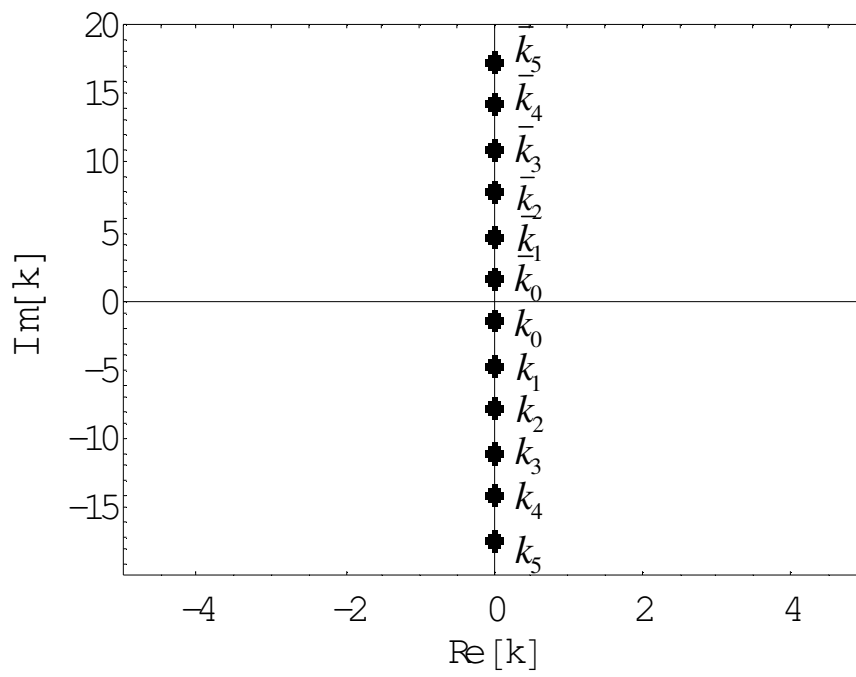


Fig. 3-4 Analytical wave number values of undamping system .

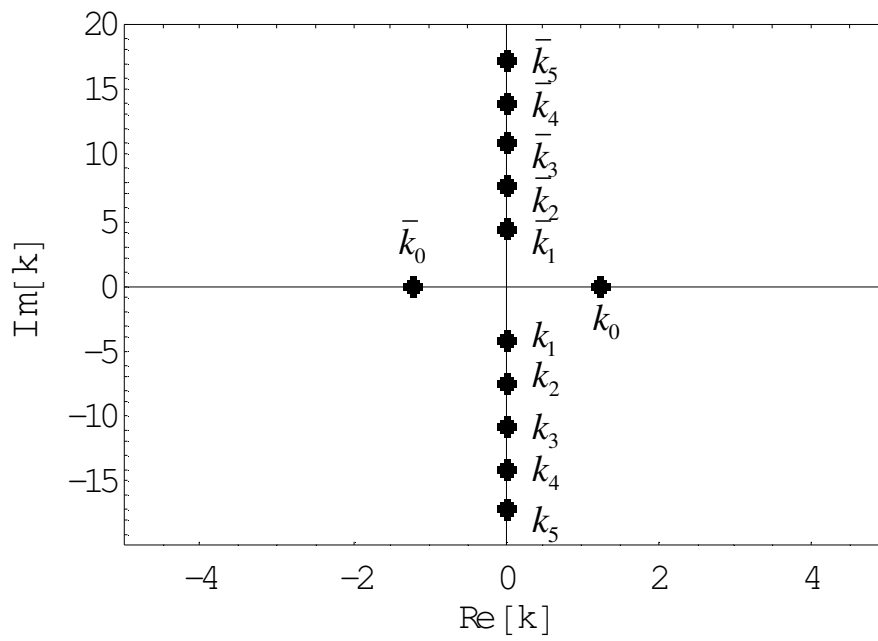


Fig. 3-5 Analytical wave number values of undamping system .

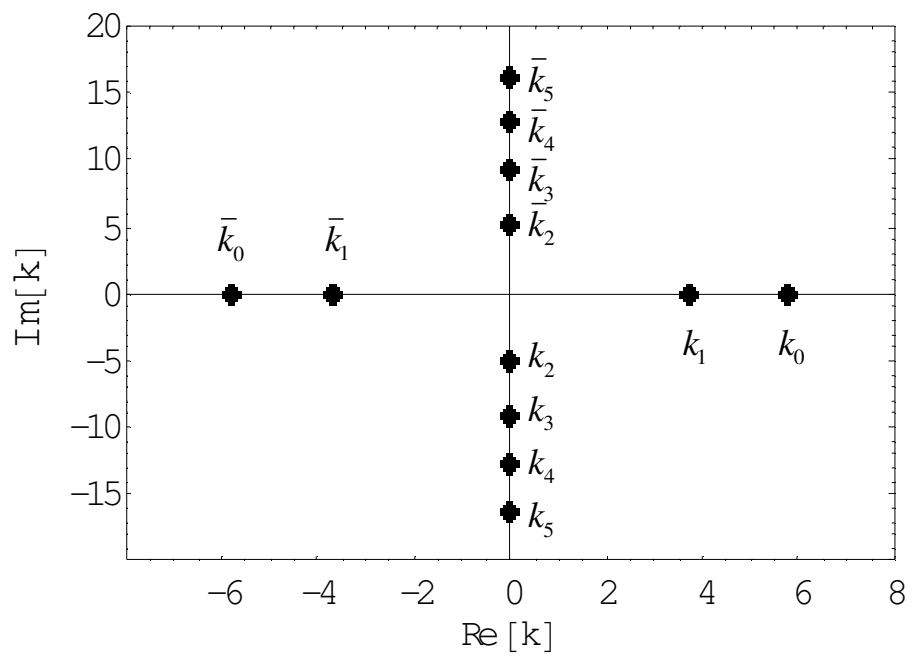


Fig. 3-6 Analytical wave number values of undamping system .

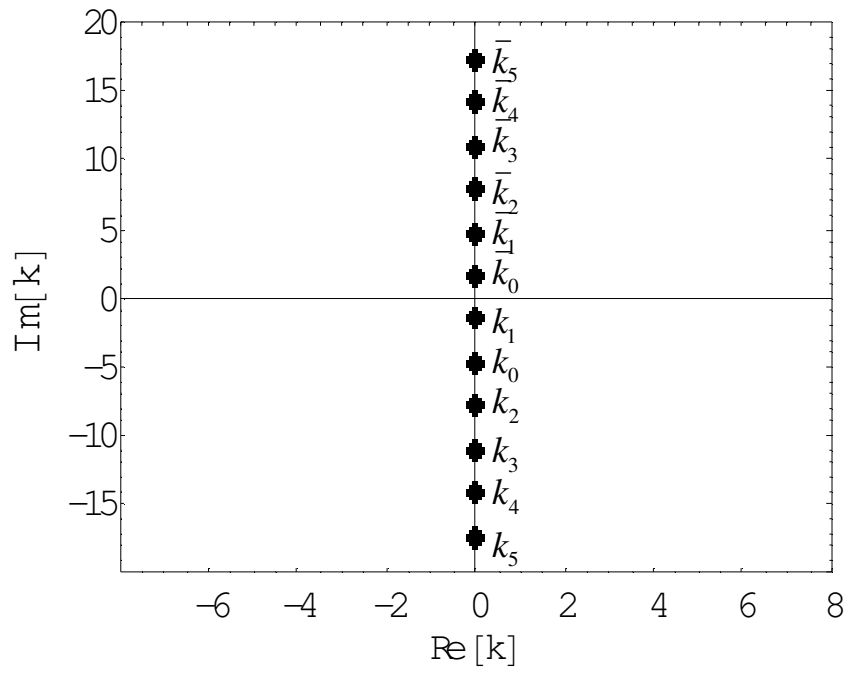


Fig. 3-7 Analytical wave number values of damping system .

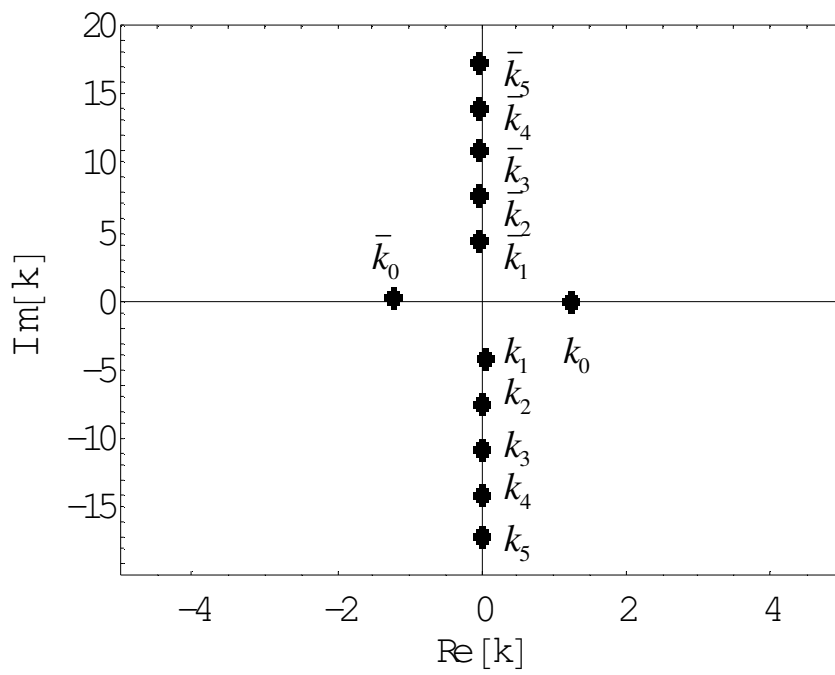


Fig. 3-8 Analytical wave number values of damping system .

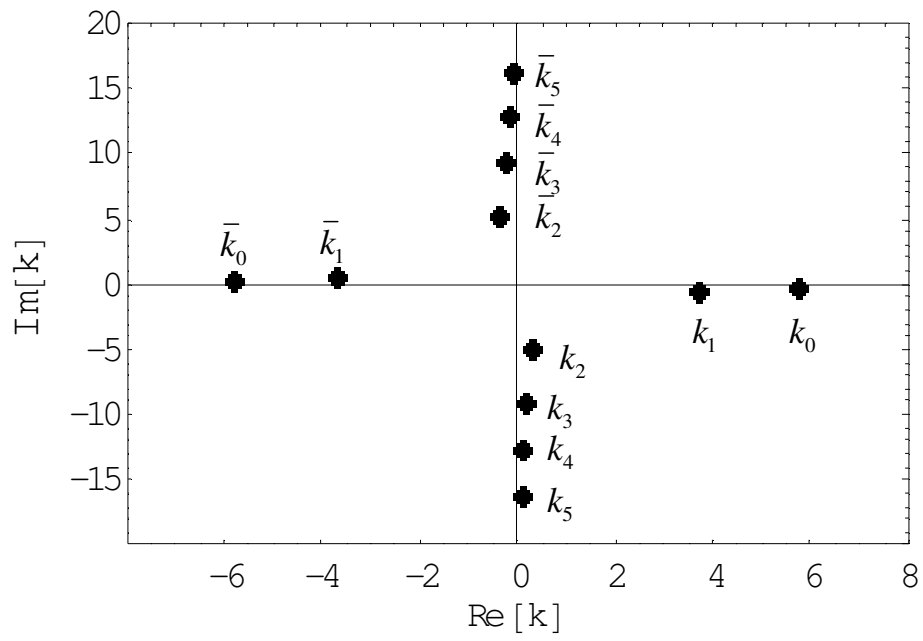


Fig. 3-9 Analytical wave number values of damping system .

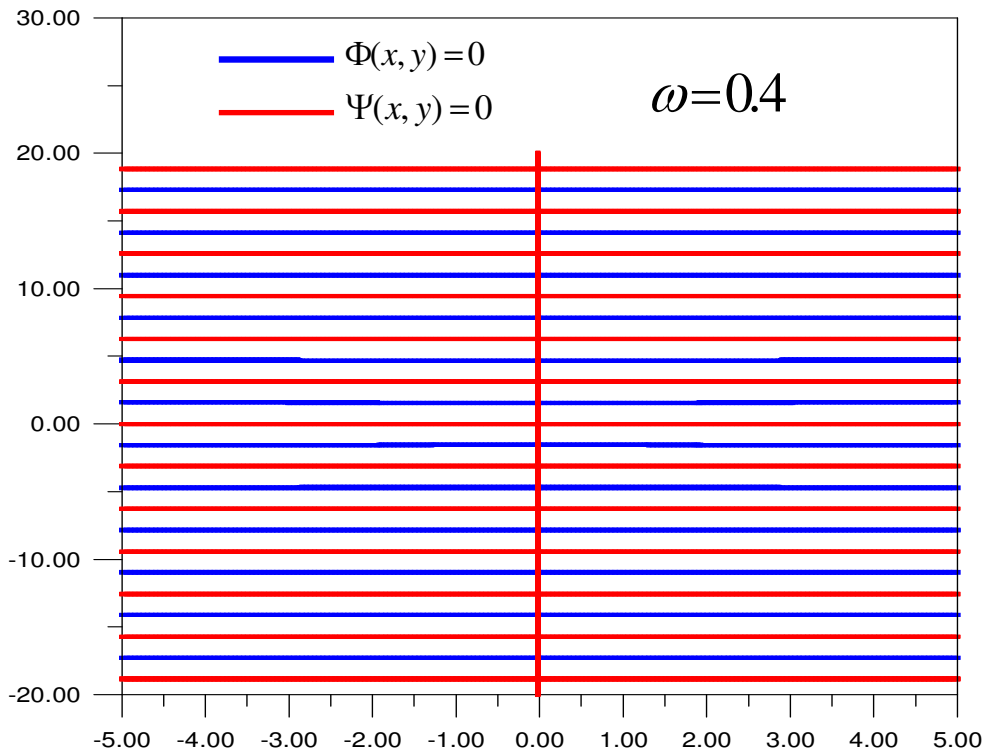


Fig. 3-10 (a) Numerical solution of $\Phi(x, y) = 0$ and $\Psi(x, y) = 0$

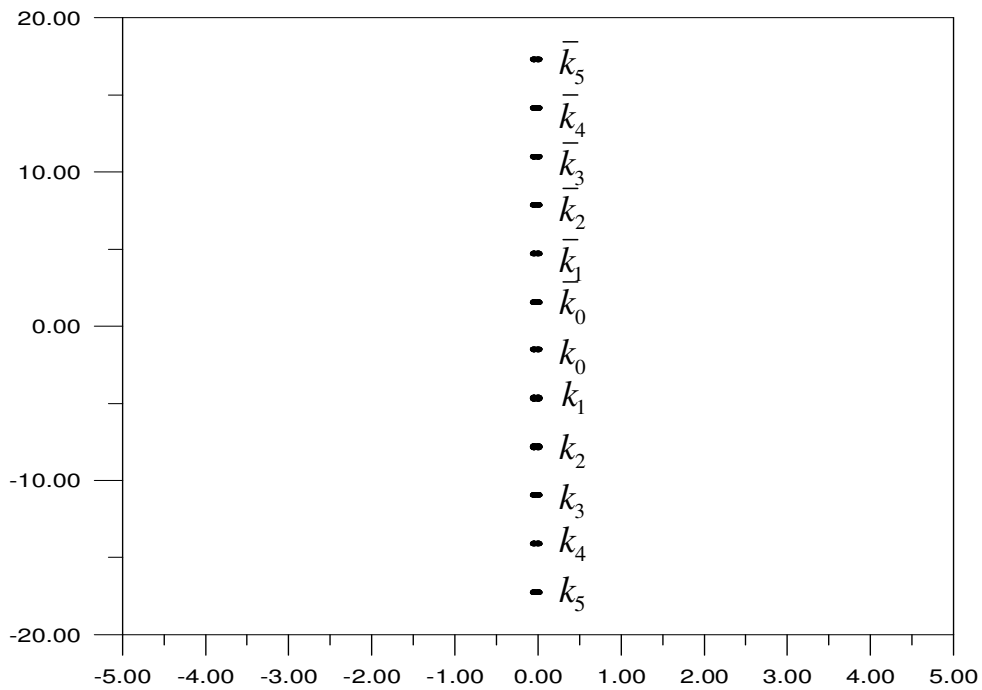


Fig. 3-10 (b) Numerical wave number values of undamping system .

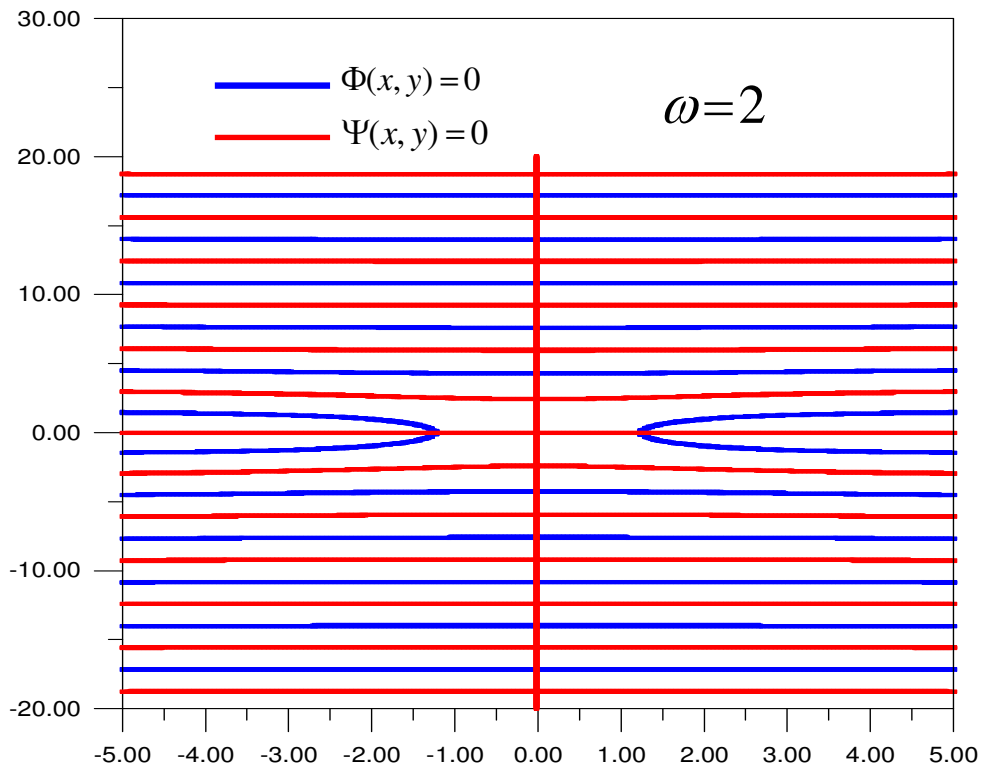


Fig. 3-11 (a) Numerical solution of $\Phi(x, y) = 0$ and $\Psi(x, y) = 0$

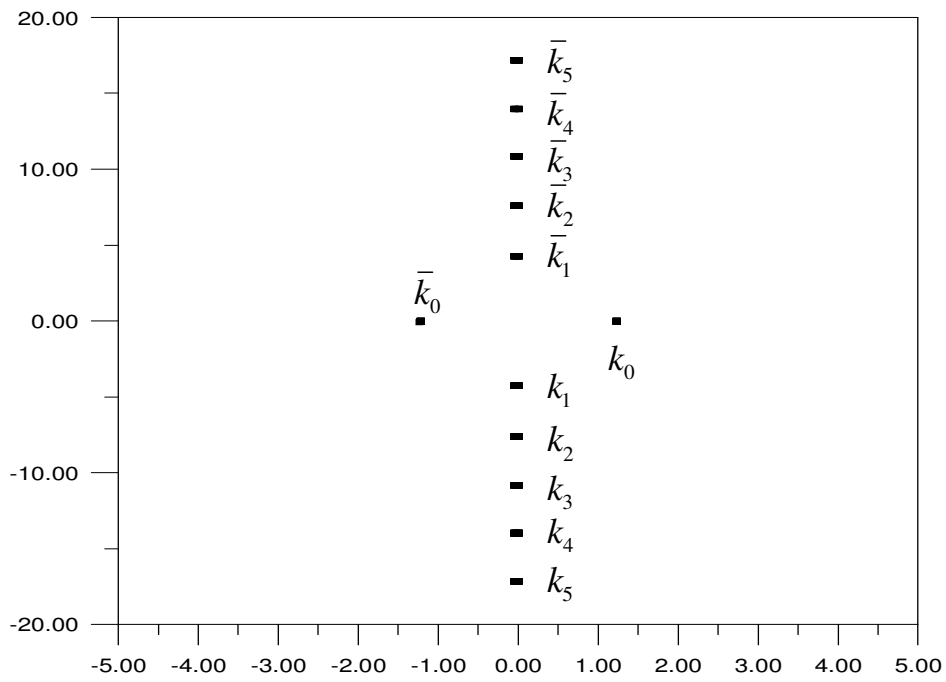


Fig. 3-11 (b) Numerical wave number values of undamping system .

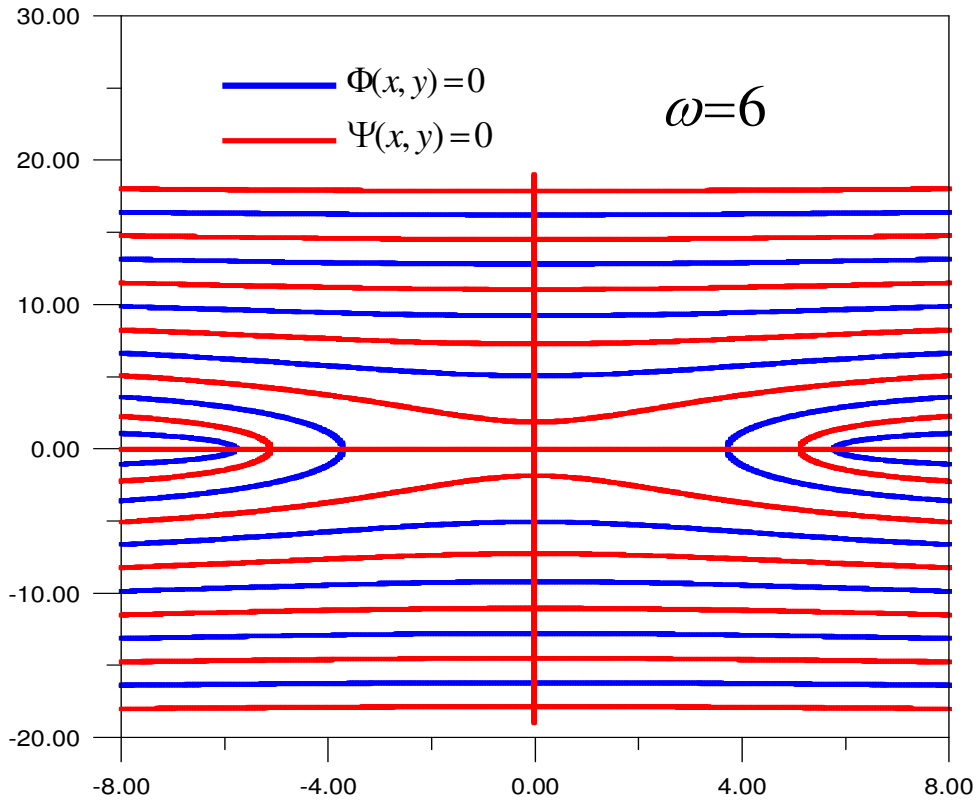


Fig. 3-12 (a) Numerical solution of $\Phi(x, y) = 0$ and $\Psi(x, y) = 0$

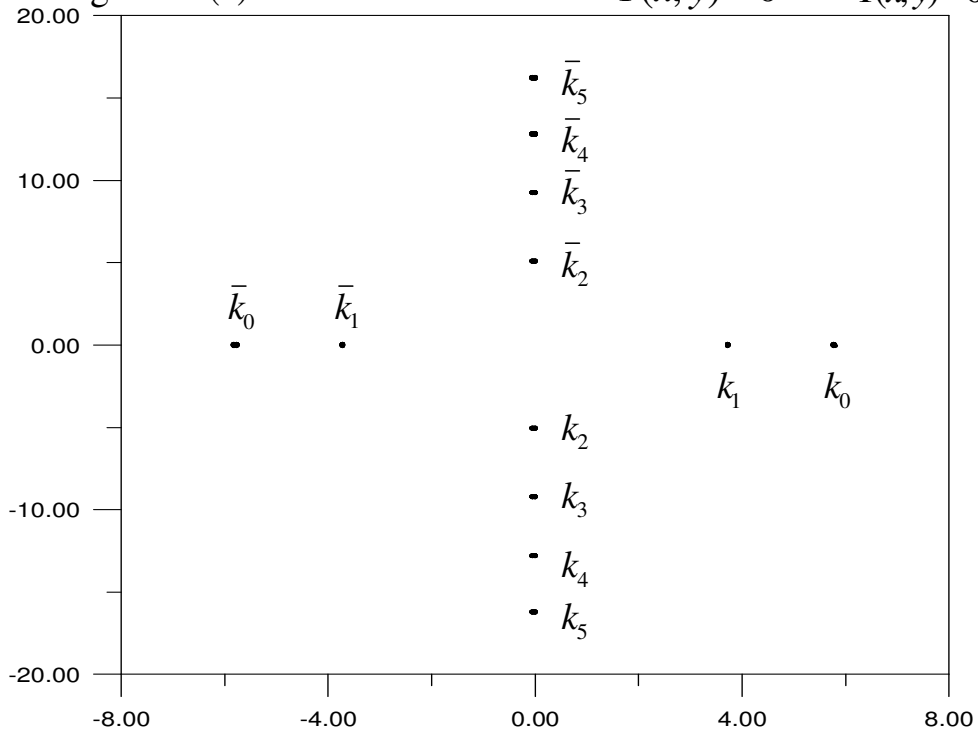


Fig. 3-12 (b) Numerical wave number values of undamping system .

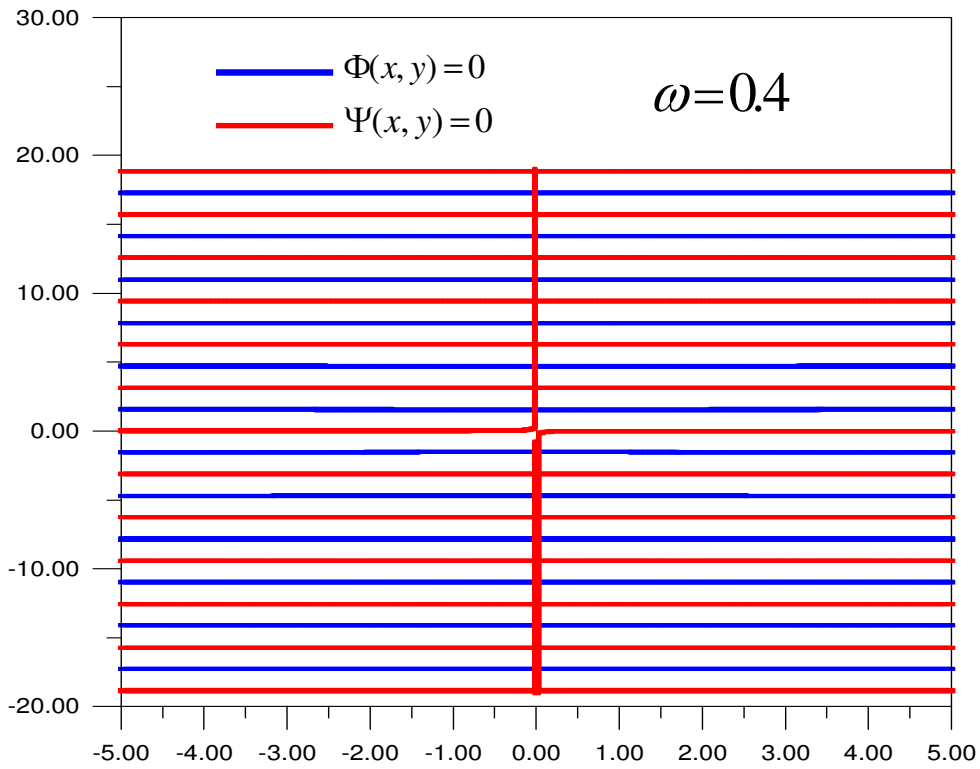


Fig. 3-13 (a) Numerical solution of $\Phi(x, y) = 0$ and $\Psi(x, y) = 0$

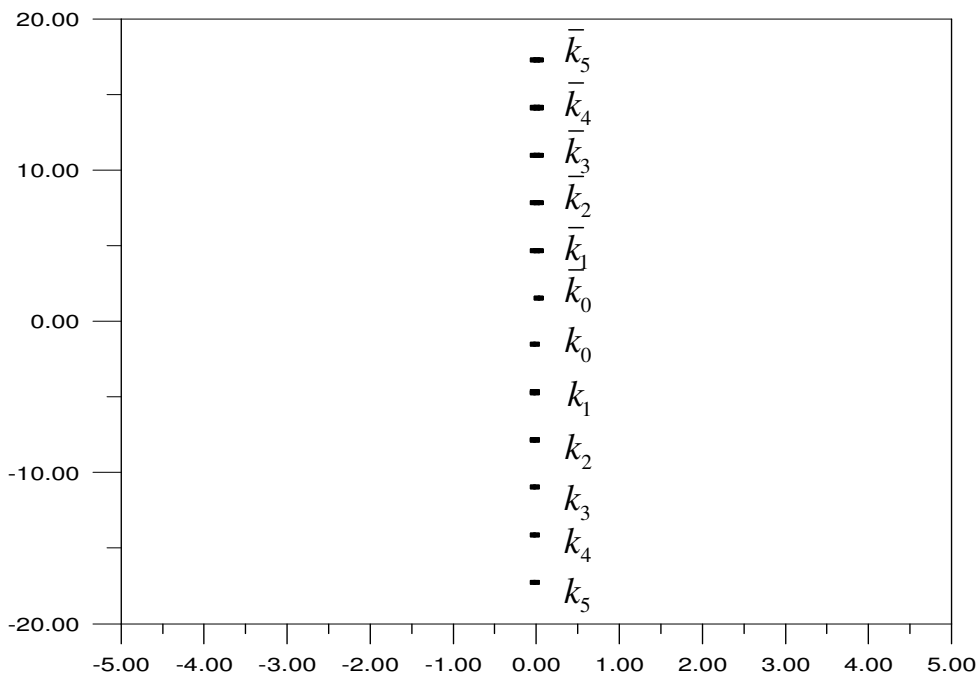


Fig. 3-13 (b) Numerical wave number values of damping system .

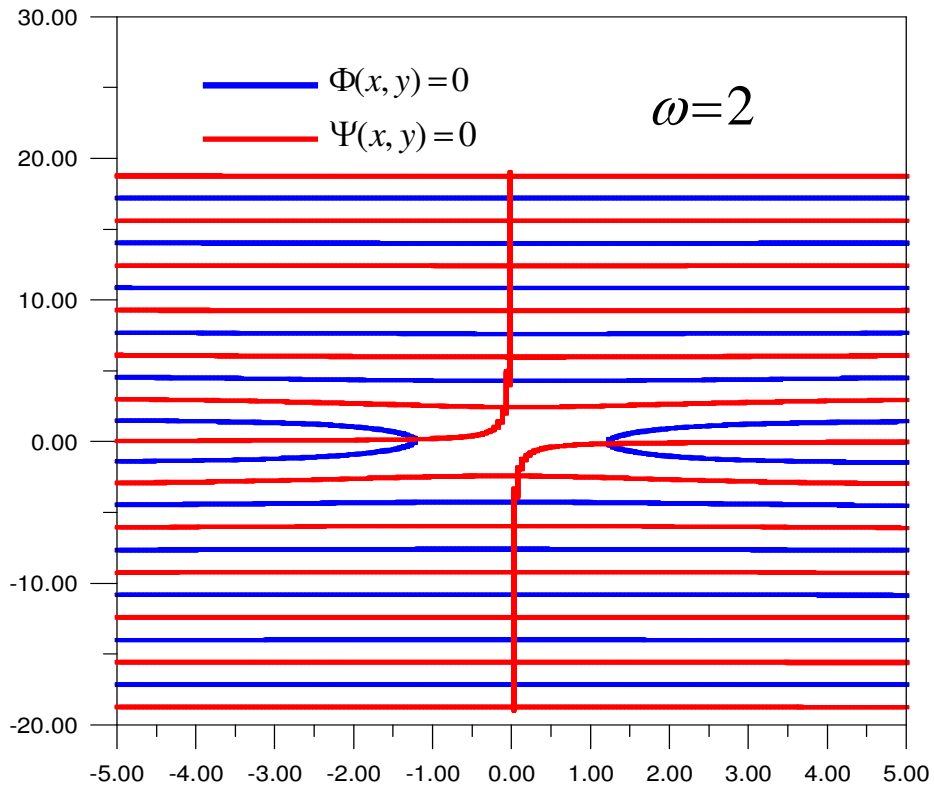


Fig. 3-14 (a) Numerical solution of $\Phi(x, y) = 0$ and $\Psi(x, y) = 0$

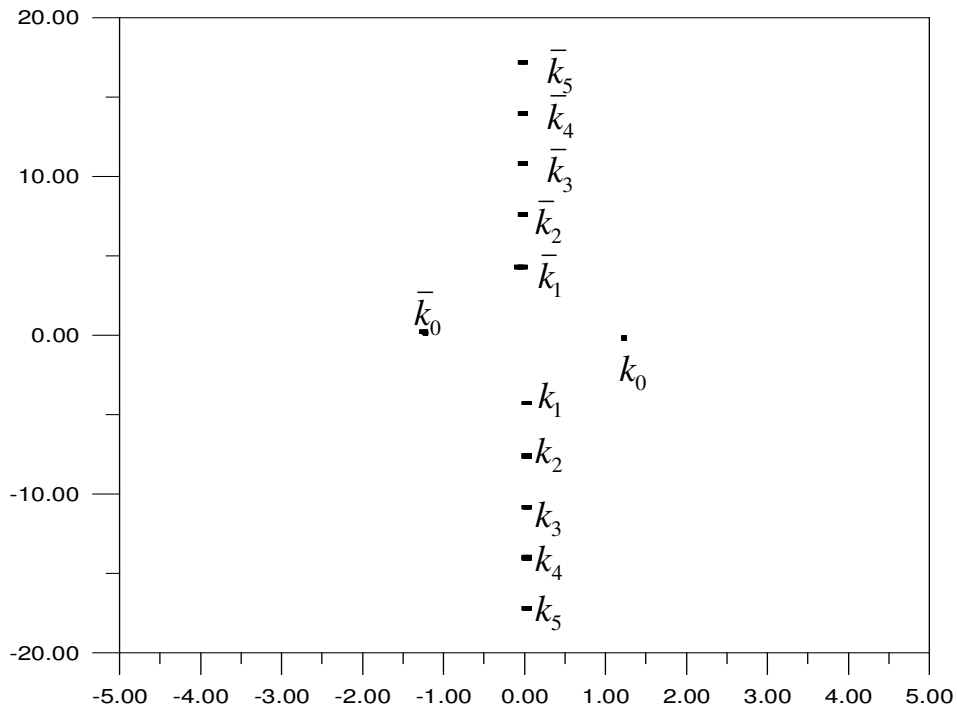


Fig. 3-14 (b) Numerical wave number values of damping system .

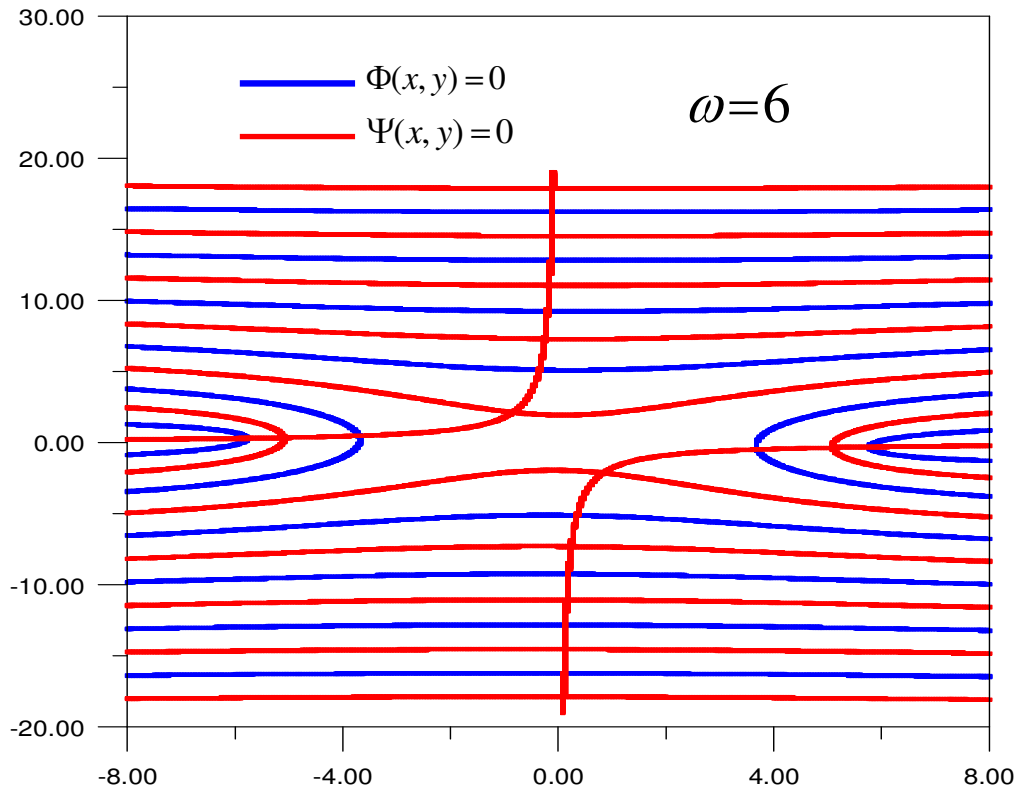


Fig. 3-15 (a) Numerical solution of $\Phi(x, y) = 0$ and $\Psi(x, y) = 0$

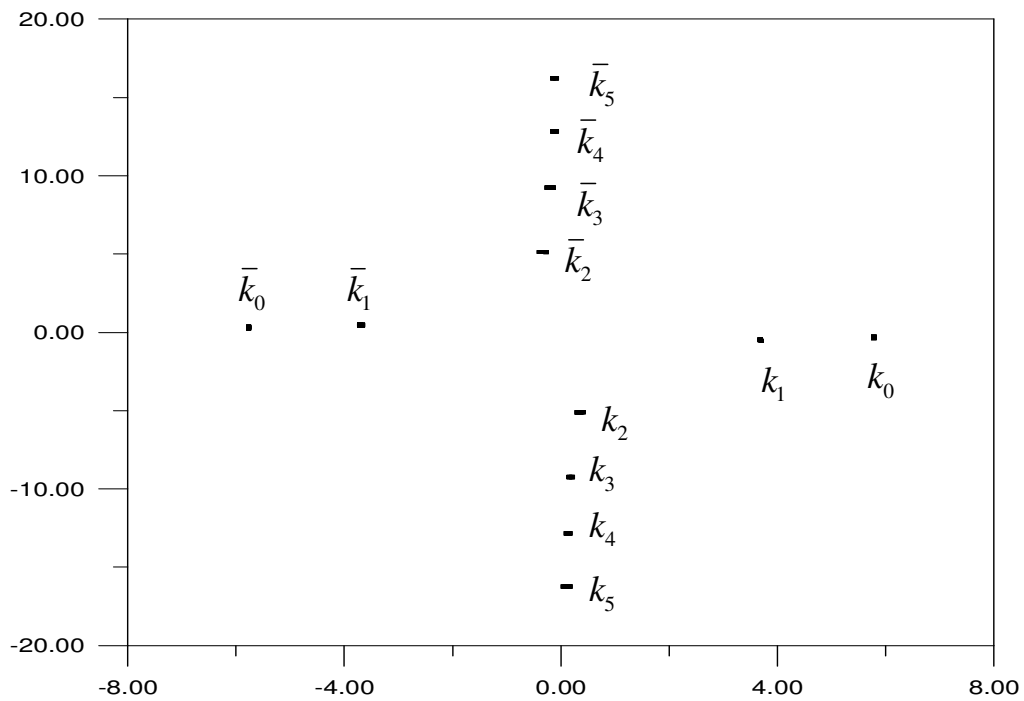


Fig. 3-15 (b) Numerical wave number values of damping system .

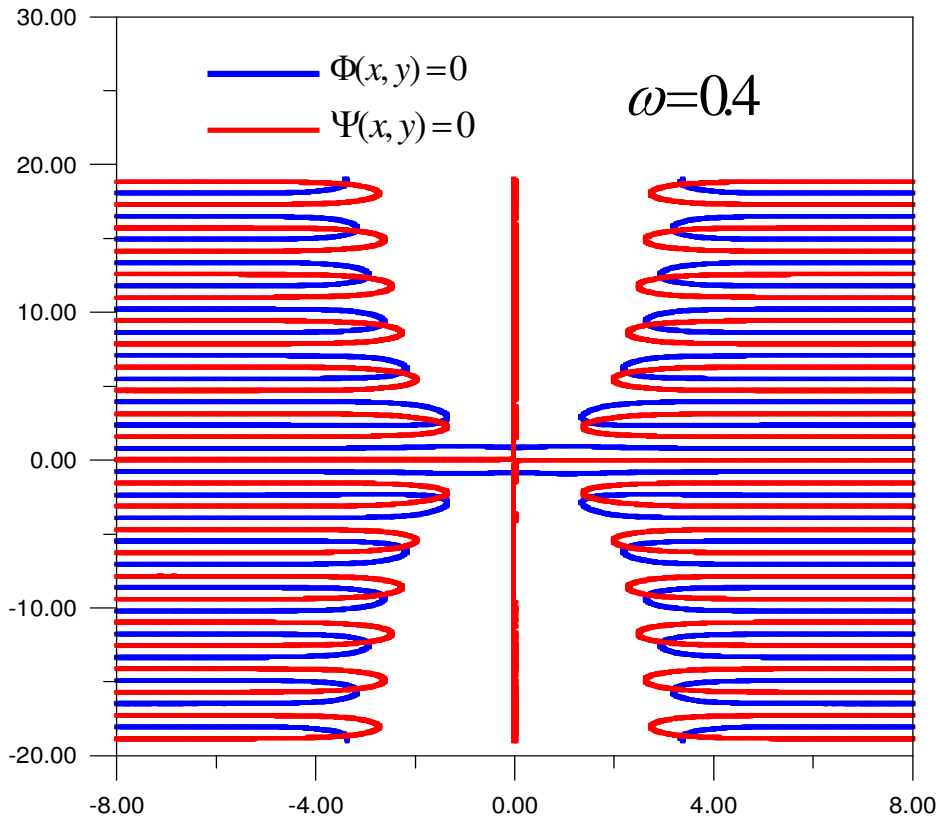


Fig. 3-16 (a) Numerical solution of $\Phi(x, y) = 0$ and $\Psi(x, y) = 0$

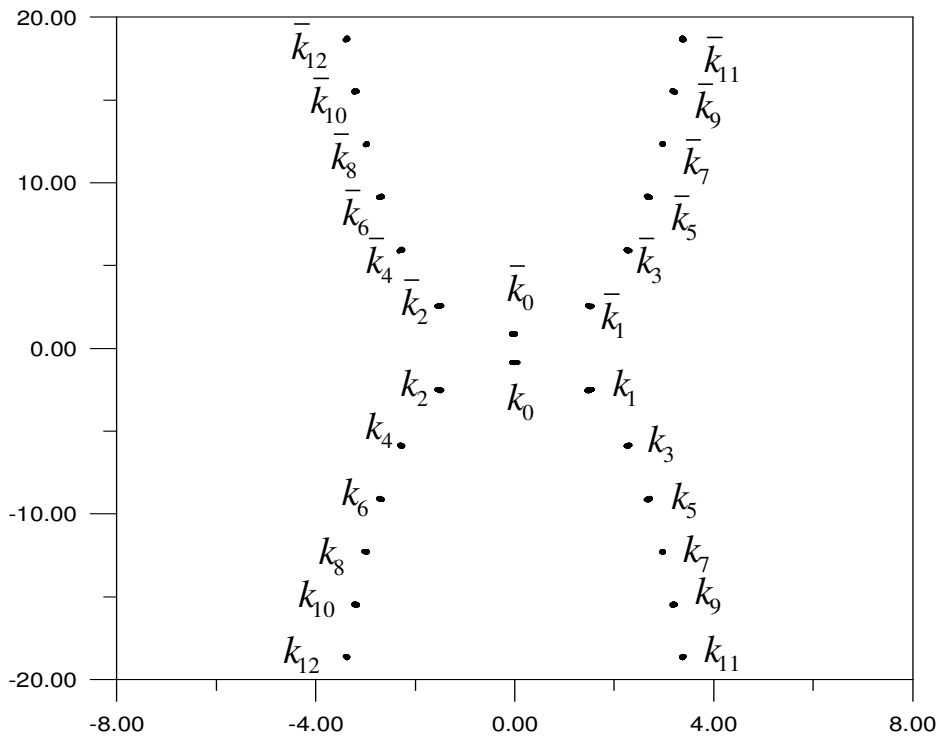


Fig. 3-16 (b) Numerical wave number values of damping system .

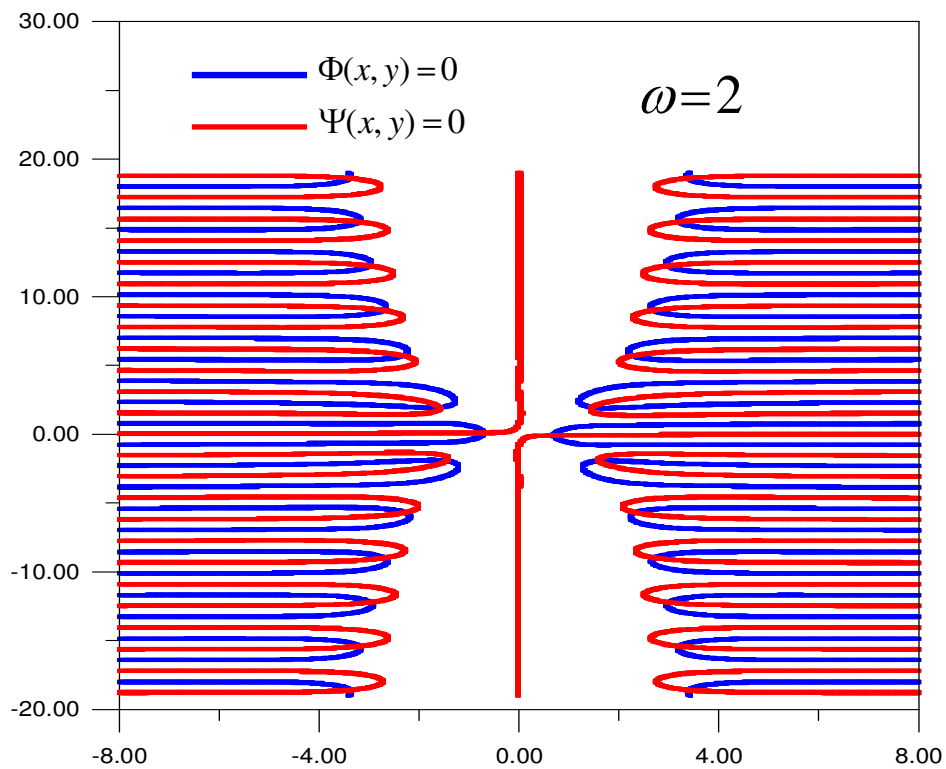


Fig. 3-17 (a) Numerical solution of $\Phi(x, y) = 0$ and $\Psi(x, y) = 0$

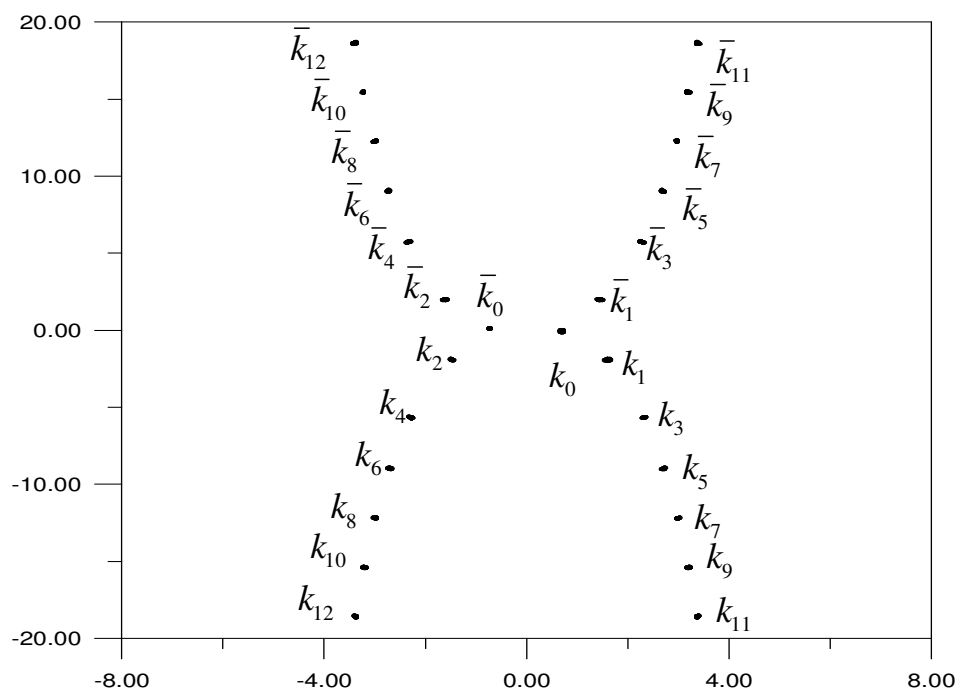


Fig. 3-17 (b) Numerical wave number values of damping system .

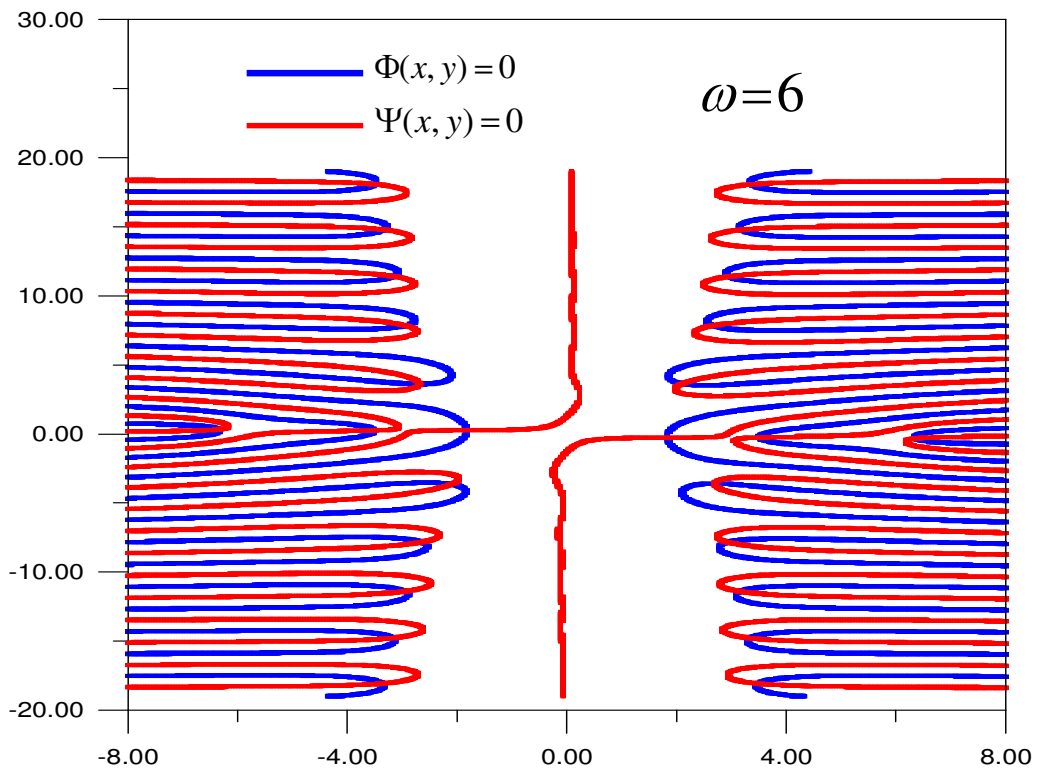


Fig. 3-18 (a) Numerical solution of $\Phi(x, y) = 0$ and $\Psi(x, y) = 0$

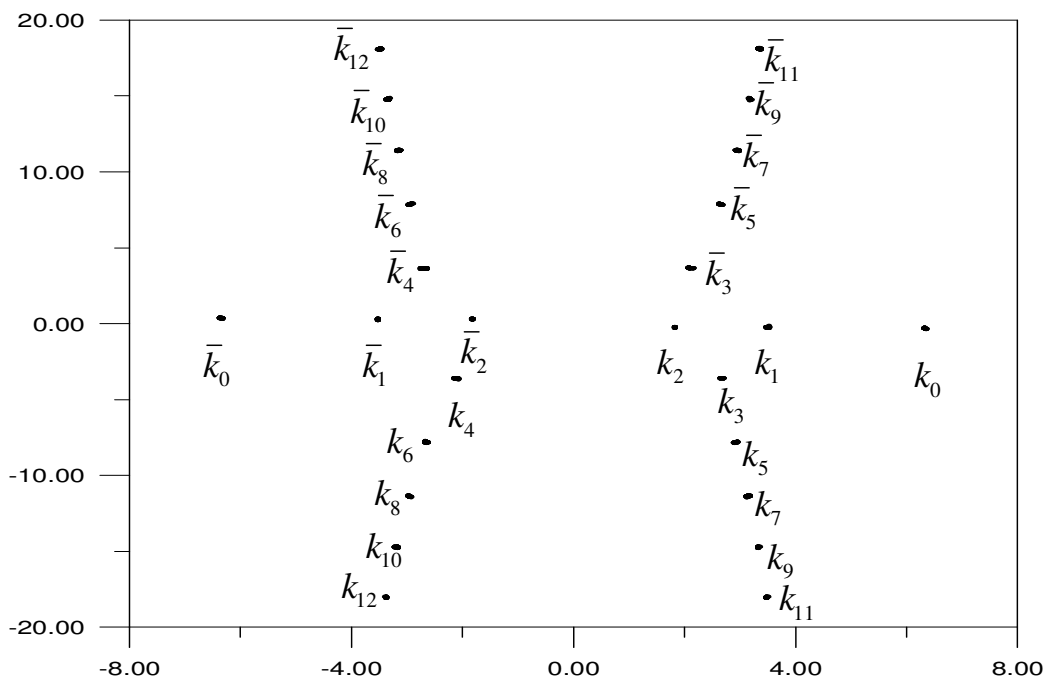


Fig. 3-18 (b) Numerical wave number values of damping system .

Chapter 4

Impedance matrices for axial symmetric foundation embedded in half-space medium by layered approximation

Summary

In this Chapter, the impedance matrices of axial-symmetric foundations embedded in an elastic half-space medium approximated using analytical solutions in layer. To approximate the situation of half-space medium, the thickness of one layer medium is gradually increased to see if the impedance function is approaching those for the case of half-space medium. However, as the thickness increases the numerical problem will arise due to extremely large numbers of $e^{v'L}$ and e^{vL} in which v' and v are appearing wave numbers in vertical direction for shear and compressional waves. To solve this numerical problem, a new scheme for the modes with large $e^{v'L}$ and e^{vL} will be developed. The numerical results show that the new numerical scheme is effective and the solutions in layered medium can be expanded to obtain the results for layered half-space medium. Some numerical results of torsional, vertical, horizontal, coupling and rocking impedances with different embedded depths will be presented and comments on the numerical scheme will be given.

4.1 Derivations of the approximate model shapes functions for exterior and interior domains

Impedance matrices for circular foundation embedded in layered medium was successful developed in chapter 2. All the solutions at the boundaries of interior domain and exterior

domain have been summarized in Fig. 2-2. In the figure, vector P_2 represents the nodal intensities of interaction tractions of piecewise linear model, matrices N and G represent all model shapes of displacements and tractions respectively interfaces, and vector $\alpha^{(i)}$ and $\alpha^{(e)}$ represent the unknown participation factors of all the modes of homogenous solutions for interior and exterior domains respectively. By intuition, it is possible to approximate impedance matrices for circular foundation embedded in half-space medium by using the same method. In order to find the impedance matrices by Liou's method for circular foundation embedded in half-space medium, the thickness L of layer should be gradually increased until the impedance value approaching that for half-space case [10]. However, as L increases, the magnitudes difference between $e^{\nu L}$ and $e^{-\nu L}$ will become enormously huge for the modes with large real part of νL , and the truncation error will contain the numerical results. Therefore, some measure has to be taken in order to avoid this containing for these modes. This containing is due to the order of $e^{\nu L}$ (or $e^{-\nu L}$) is much greater than $e^{\nu L}$ (or $e^{-\nu L}$). This will cause significant figures lose in the process of calculation and $e^{\nu z}$ (or $e^{-\nu z}$) represents the vertical variation of upward propagation wave. This does not exist in half-space medium case. So, this upward propagation waves must be suppressed in order to simulate the case of half-space medium. The procedure to find the impedance matrix for foundation embedded in half-space medium is similar to that for the case of layered medium which has been presented in details in chapter 2, except for the modes with large real part of νL , the expressions of displacements and tractions at the interfaces between interior and exterior domains, interior domain and foundation, and exterior domain and foundation, must be revised by neglecting upward propagation wave. Therefore, the followings will briefly give the revisions.

Sezawa [18] have solved the wave equations for a homogeneous half-space in cylindrical coordinates. In the solutions, only downward propagation waves are taken into account. After some mathematical manipulation, the displacement field of each mode for interior and exterior domains can be expressed as

$$\mathbf{u} = \begin{Bmatrix} \mathbf{u}_r \\ \mathbf{u}_z \\ \mathbf{u}_\theta \end{Bmatrix} = \mathbf{H} \mathbf{K}_1 \mathbf{e}(z) \mathbf{A} \quad (4-1)$$

where

$$\mathbf{H} = \begin{bmatrix} H'_n(kr) & 0 & \frac{n}{r} H_n(kr) \\ 0 & kH_n(kr) & 0 \\ \frac{n}{r} H_n(kr) & 0 & H'_n(kr) \end{bmatrix} \quad (4-2)$$

$$\mathbf{K}_1 = \begin{bmatrix} k & -v' & 0 \\ -v & k & 0 \\ 0 & 0 & 1 \end{bmatrix} \quad (4-3)$$

vector $\mathbf{A} = (A_1 \ B_1 \ C_1)^T$ is the unknown coefficient will be determined by boundary conditions, matrix $\mathbf{e}(z) = \text{diag}(e^{-vz} \ e^{-v'z} \ e^{-v'z})$, $H_n(kr)$ is the second kind of Hankel function of order n , and $H'_n(kr) = \frac{dH_n(kr)}{dr}$, subscript n is n^{th} Fourier component with respect to θ , in Fig 2-1 and the Hankel function will be replaced by Bessel function $J_n(kr)$ for interior domain [8].

For the modes of particular solution of interior domain, the traction field on horizontal plane can be shown as [11]:

$$\mathbf{t} = \begin{Bmatrix} \boldsymbol{\tau}_{rz}(\mathbf{r}, z) \\ \boldsymbol{\sigma}_{zz}(\mathbf{r}, z) \\ \boldsymbol{\tau}_{\theta z}(\mathbf{r}, z) \end{Bmatrix} = \mathbf{JK}_2 \mathbf{e}(z-d) \mathbf{A} \quad (4-4)$$

where

$$\mathbf{K}_2 = \begin{bmatrix} -2kGv & G(2k^2 - k_\beta^2) & 0 \\ G(2k^2 - k_\beta^2) & -2kGv' & 0 \\ 0 & 0 & 1 \end{bmatrix} \quad (4-5)$$

in which $k_\beta = \sqrt{\frac{\omega^2}{C_s^2}}$, G is the shear modulus, and matrix \mathbf{J} is similar to \mathbf{H} of Eq(4-2)

except Hankel function $H_n(kr)$ are replaced by Bessel function $J_n(kr)$.

The modes for exterior domain contain only homogeneous solutions which satisfy the homogeneous boundaries at free surface $z=0$ and rigid base $z=L$. The unknown coefficients in vector \mathbf{A} in Eq. (4-1) can be expressed as follows:

$$\mathbf{A} = \mathbf{K}_1^{-1} \mathbf{H}^{-1} \mathbf{u}_0^{(e)} \quad (4-6)$$

where $\mathbf{u}_0^{(e)}$ is displacement vector at free surface ($z=0$). Substituting Eq. (4-6) into (4-1), one obtains


$$\mathbf{u}^{(e)} = \mathbf{H} \mathbf{a}_1(z) \mathbf{H}^{-1} \mathbf{u}_0^{(e)} \quad (4-7)$$

Where

$$\mathbf{a}_1(z) = \mathbf{K}_1 \mathbf{e}(z) \mathbf{K}_1^{-1} = \begin{bmatrix} \frac{k^2 e^{-\nu z} - \nu \nu' e^{-\nu' z}}{k^2 - \nu \nu'} & \frac{(e^{-\nu z} - e^{-\nu' z}) k \nu'}{k^2 - \nu \nu'} & 0 \\ \frac{(e^{-\nu' z} - e^{-\nu z}) k \nu}{k^2 - \nu \nu'} & \frac{k^2 e^{-\nu' z} - \nu \nu' e^{-\nu z}}{k^2 - \nu \nu'} & 0 \\ 0 & 0 & e^{-\nu' z} \end{bmatrix} \quad (4-8)$$

According reference 14, $\mathbf{H}^{-1} \mathbf{u}_0^{(e)}$ can be expressed as $(1 \ \xi_i \ 0)^T \alpha_i$ for Rayleigh modes and $(0 \ 0 \ 1)^T \alpha_i$ for Love modes. For the above expressions, α_i is unknown mode participation factor and ξ_i is the scale factor of the mode which is defined in reference 8.

Also, after some mathematical manipulation of using Eq(4-7), the tractions at depth z on the vertical interface ($s_1 + s_3$ in Fig. 2-1) for the exterior domain with only considering downward propagation wave can be expressed as the following:

$$\mathbf{t} = \begin{Bmatrix} \boldsymbol{\sigma}_{rr}(\mathbf{r}, z) \\ \boldsymbol{\tau}_{rz}(\mathbf{r}, z) \\ \boldsymbol{\tau}_{r\theta}(\mathbf{r}, z) \end{Bmatrix} = (\mathbf{H}_1 \mathbf{F}_1 + \mathbf{H}_2 \mathbf{F}_2) \mathbf{e}(z) \mathbf{K}_1^{-1} \mathbf{H}^{-1} \mathbf{u} \quad (4-9)$$


Where

$$\mathbf{H}_1 = \begin{bmatrix} 0 & kH_n(kr) & 0 \\ H'_n(kr) & 0 & \frac{n}{r} H_n(kr) \\ 0 & 0 & 0 \end{bmatrix} \quad (4-10)$$

$$\mathbf{H}_2 = \begin{bmatrix} -\left(\frac{H'_n(kr)}{r}\right) + \frac{n^2}{r^2} H_n(kr) & \frac{n}{r} H'_n(kr) - \frac{n}{r^2} H_n(kr) \\ 0 & 0 \\ \frac{n}{r} H'_n(kr) - \frac{n}{r^2} H_n(kr) & -\left(\frac{H'_n(kr)}{r}\right) + \left(\frac{n^2}{r^2} - \frac{k^2}{2}\right) H_n(kr) \end{bmatrix} \quad (4-11)$$

$$\mathbf{F}_1 = \begin{bmatrix} -2kGv & G(2k^2 - k_\beta^2) & 0 \\ G(2v^2 + k_\beta^2) & 2kGv' & 0 \\ 0 & 0 & -Gv' \end{bmatrix} \quad (4-12)$$

$$\mathbf{F}_2 = \begin{bmatrix} 2kG & -2Gv & 0 \\ 0 & 0 & 2G \end{bmatrix} \quad (4-13)$$

For the interior domain shown in Fig. 2-2, the solution is the combination of particular solution and homogeneous solution. For the modes of homogeneous solution, the expression for displacement and traction are similar to those shown in Eqs (4-1)~ (4-13) except the exponential functions $e^{-v'z}$ and e^{-vz} replaced with $e^{-v'(z-d)}$ and $e^{-v(z-d)}$ and Hankel matrices $\mathbf{H}, \mathbf{H}_1, \mathbf{H}_2$ is replaced with Bessel matrices $\mathbf{J}, \mathbf{J}_1, \mathbf{J}_2$ in which Hankel functions are replaced with Bessel functions. For the modes of particular solution, one should refer to reference 10 in which the transformation matrix \mathbf{Q}_n , which transform piecewise linear traction at $z = d$, should be revised as follow :

$$\mathbf{Q}_n = \mathbf{K}_1 \mathbf{K}_2^{-1} = \begin{bmatrix} \frac{-v'k_\beta^2}{G(4k^2vv' - (2k^2 - k_\beta^2)^2)} & \frac{k(2vv' - 2k^2 + k_\beta^2)}{G(4k^2vv' - (2k^2 - k_\beta^2)^2)} & 0 \\ \frac{k(2vv' - 2k^2 + k_\beta^2)}{G(4k^2vv' - (2k^2 - k_\beta^2)^2)} & \frac{-vk_\beta^2}{G(4k^2vv' - (2k^2 - k_\beta^2)^2)} & 0 \\ 0 & 0 & \frac{-1}{Gv'} \end{bmatrix} \quad (4-14)$$

The traction at the interface between interior and exterior domains for the mode can be obtained by using Eq. (4-8) with replacement of Hankel functions with respective Bessel

functions and $e^{-\nu'z}$ and $e^{-\nu z}$ with $e^{-\nu'(z-d)}$ and $e^{-\nu(z-d)}$ respectively.

The above expressions are only employed for the modes with large real part of $\nu'L$, saying $\text{Re}(\nu'L) \geq 25$. For the modes with smaller real part of $\nu'L$ (saying $\text{Re}(\nu'L) < 25$), the expression presented by Liou and Chung are explored [19]. Then, the compatibility condition variation principle and reciprocal theorem are employed to generate the impedance functions as reference chapter 2.

4.2 Numerical investigations

In this numerical study, 32 significant figures of numbers in calculation are used. This means that quadruple precision of numbers are defined in computer program. Therefore, after extensive study, if the real part of $\nu'L$ for the modes is greater than 25, the expression derived in previous section will be employed, one should also note that real part of $\nu'L$ is always greater than that of $\nu'L$ for these modes with real part of $\text{Re}(\nu'L) \geq 25$. For those modes with real part of $\nu'L$ smaller than 25, the expression in Reference 19 are employed.

In calculating the numerical results of impedance function, poisson ratio of soil medium is selected to be 0.33 and damping ratios is assigned to be 0.02, 0.05 and 0.1. All the impedance functions shown are non-dimensionalized by shear modulus G and foundation radius a , and the frequencies are non-dimensionalized by a and real part of complex shear wave velocity $\text{Re}(C_s)$, K_{TT} is the torsional impedance, K_{VV} is the vertical impedance, K_{HH} is the horizontal impedance, $K_{RH} = K_{HR}$ are the coupling impedance, K_{RR} is the rocking impedance and ω is frequency. In order to simulate the case of half-space, one has to increase the thickness of the layer and compare the results of impedance functions to that for the case of half-space medium. Figs 4-1~4-5 show

In these figures, damping ratio $\xi = 0.05$, the thickness of layer is gradually increased from

$\frac{a_0}{L} = 0.5$ to $\frac{a_0}{L} = 0.1$, and the numerical results are compared to that of Liou's previous work [10]. In general, one can observe that the results of impedance functions for the case of layer stratum is approaching that for the case of half-space medium, as $\frac{a_0}{L}$ is getting smaller. Also, the fluctuation of the result is getting less dramatic as the layer is getting thicker. The reason for the phenomenon is that the traveling path of waves become longer as L increases. This longer path will make the energy loss of reflection waves from rigid bedrock (upward propagation waves) larger. Furthermore, if one compares Fig. 4-1 with Fig. 4-5, one can see that the fluctuations in Fig. 4-1. is less severe and the torsional impedance for case of layered medium approaches that for half-space medium (Fig. 4-1) in terms of $\frac{a_0}{L}$ faster than the vertical impedance in Fig. 4-2.

This is because only shear waves are involved in calculating torsional impedance and shear wave length is shorter than compressional wave length which dominates in vertical vibration of foundation. This means the reflection shear waves need shorter distance to damp out energy. This kind of observation can also be found, if one compares Fig. 4-1 with Figs 4-2-4-5. Therefore, to simulate the case of half-space medium, thickness layer can be used for generating torsional impedance. From these figures (Figs 4-1-4-5), one can conclude that $\frac{a_0}{L} = 0.1$ is good enough for layered medium to simulate half-space medium, if

damping ratio is 0.05 for the media and non-dimensionalized frequency $\frac{\omega a_0}{2\pi \text{Re}(C_s)} = 0 \sim 1$.

For the cases of damping ratios $\xi = 0.1$ and $\xi = 0.02$ are show in Figs 4-6~4-10 and Figs 4-11~4-15, although investigation has been done just like the study for $\xi = 0.05$ presented above. The behaviors are similar to those presented above except the thicknesses of layer

medium need to simulate half-space are different for different damping ratio. In general, small damping ratio in the medium means thicker layer need to simulate half-space medium. For examples, for the case $\xi = 0.02$ $\frac{a_0}{L}$ must be 0.08 and $\frac{a_0}{L}$ just be 0.15 for the case $\xi = 0.1$. Figs 4-16~4-20 show the simulated numerical results of non-dimensionalized torsional, vertical, horizontal, coupling and rocking impedances respectively for circular formulation embedded in half-space medium with embedded depths $\frac{d}{a_0} = 0, \frac{1}{4}, \frac{1}{2}, \frac{3}{4}$, and 1. In the figures, the green curves are presented with the results for $\xi = 0.02$ are calculated by using $\frac{a_0}{L} = 0.08$, the blue curves are presented with the results for $\xi = 0.05$ are calculated by using $\frac{a_0}{L} = 0.1$ and the red curves are presented with the results for $\xi = 0.1$ are calculated by using $\frac{a_0}{L} = 0.15$. From these figures, one can observe that the impedance generally tend to be greater as the embedded depth increases. Also, higher damping will make the impedances a little higher.

4.3 Concluding remarks

The procedure to calculate impedance functions for foundation embedded in layered medium can be explored to calculate that for the case of half-space medium by using enough thickness of layered medium. Although increasing the thickness of layered medium will give rise to the numerical problem in the process of computation. One just needs to suppress the upward propagation waves for the modes with large real part of $v'L$. In the study, with quadruple precision number (about 32 significant figures) defined in computer program, the upward propagating waves for the modes with $\text{Re}(v'L) \geq 25$ should be

suppressed to avoid the values e^{vL} and e^{vL} contaminate the value e^{-vL} and e^{-vL} .

Also, to simulate the case of half-space medium, the thickness of layer can be less, if the

damping ratio is greater. For examples, $\frac{a_0}{L} = 0.15$ for $\xi = 0.1$, $\frac{a_0}{L} = 0.1$ for $\xi = 0.05$,

$\frac{a_0}{L} = 0.08$ for $\xi = 0.02$.



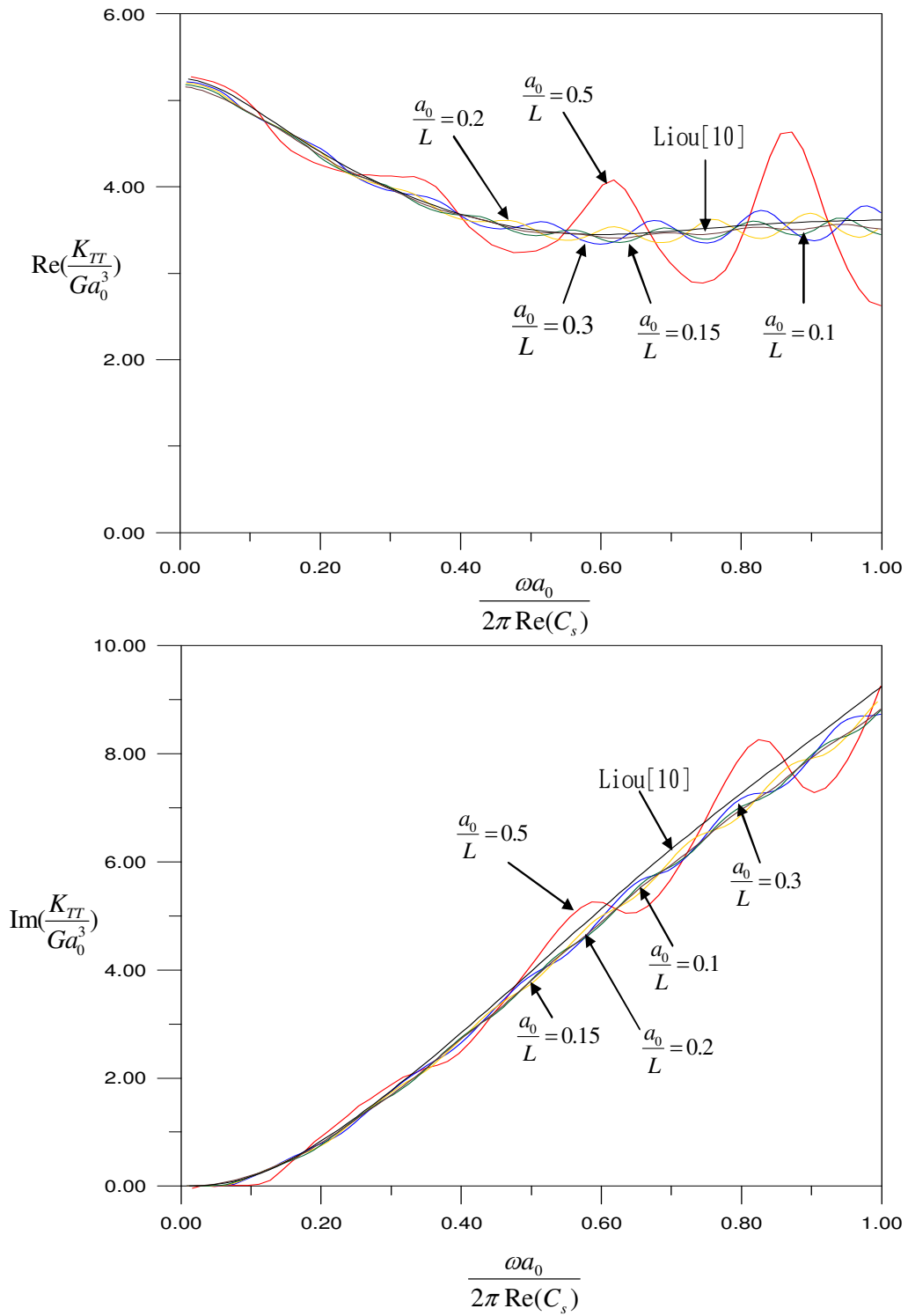


Fig. 4-1. Comparison of non-dimensionalized torsional impedance with Liou's results for $\frac{d}{a_0} = 0$

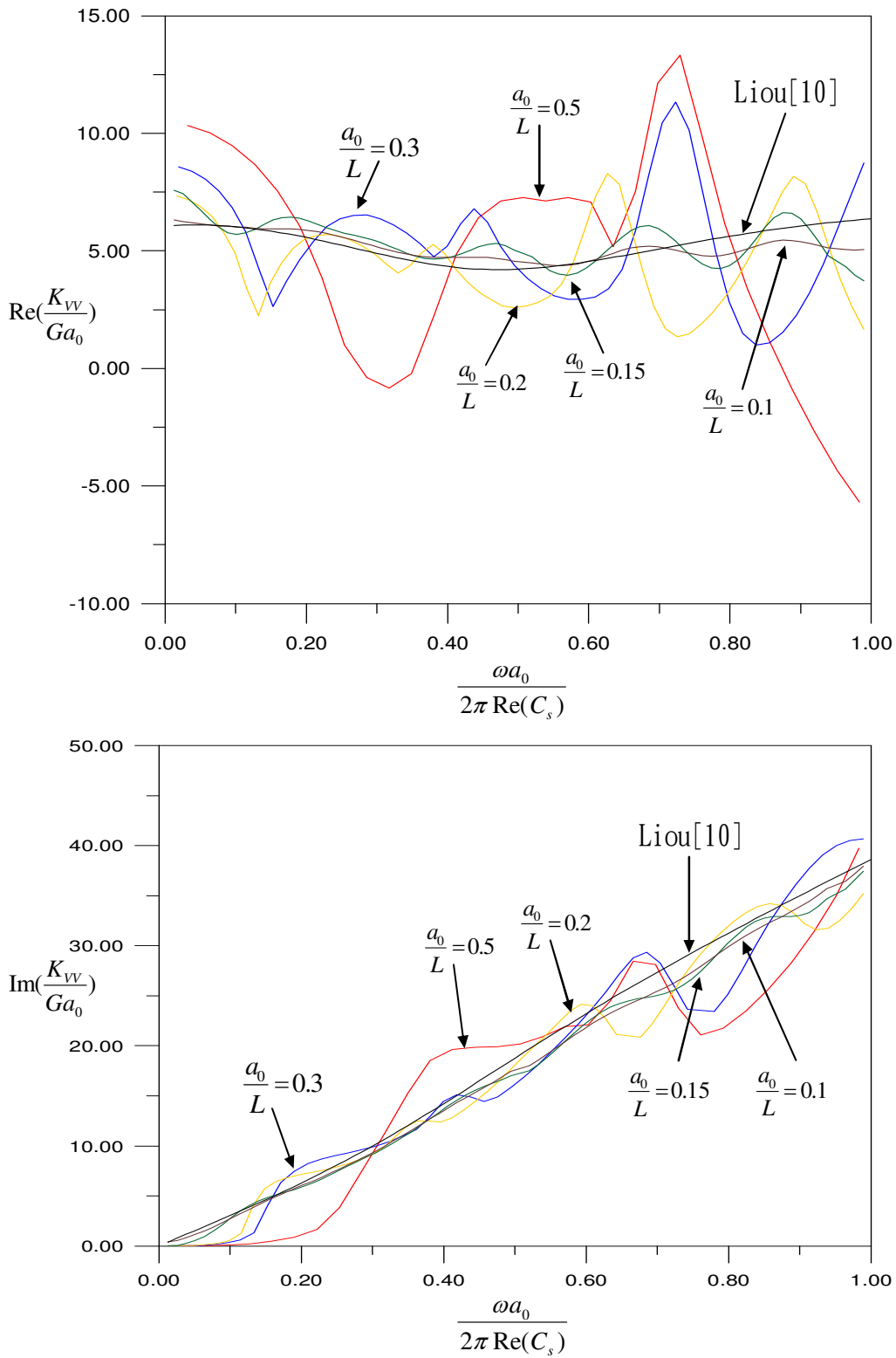


Fig. 4-2. Comparison of non-dimensionalized vertical impedance with Liou's results for $\frac{d}{a_0} = 0$

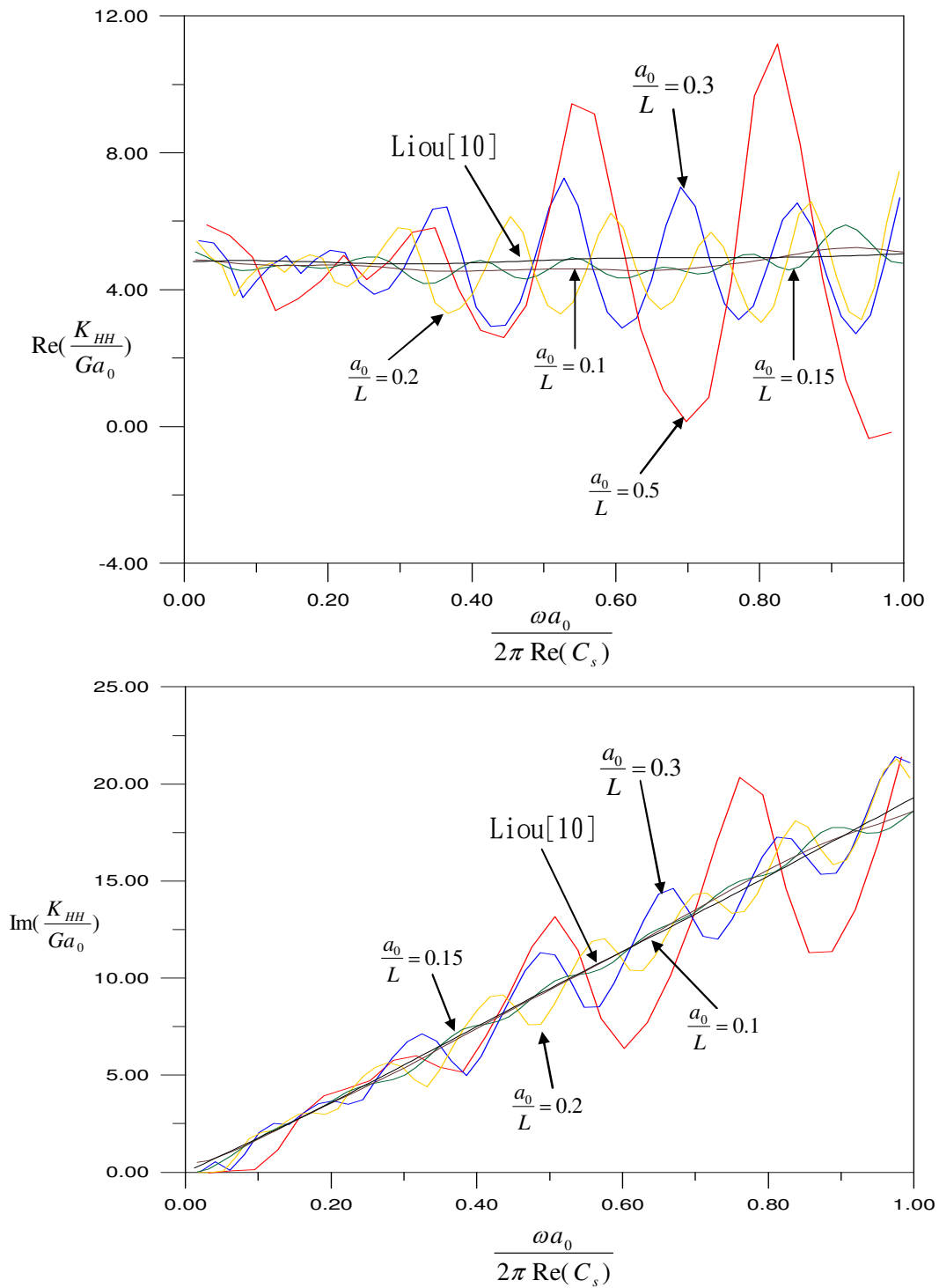


Fig. 4-3. Comparison of non-dimensionalized horizontal impedance with Liou's results for $\frac{d}{a_0} = 0$

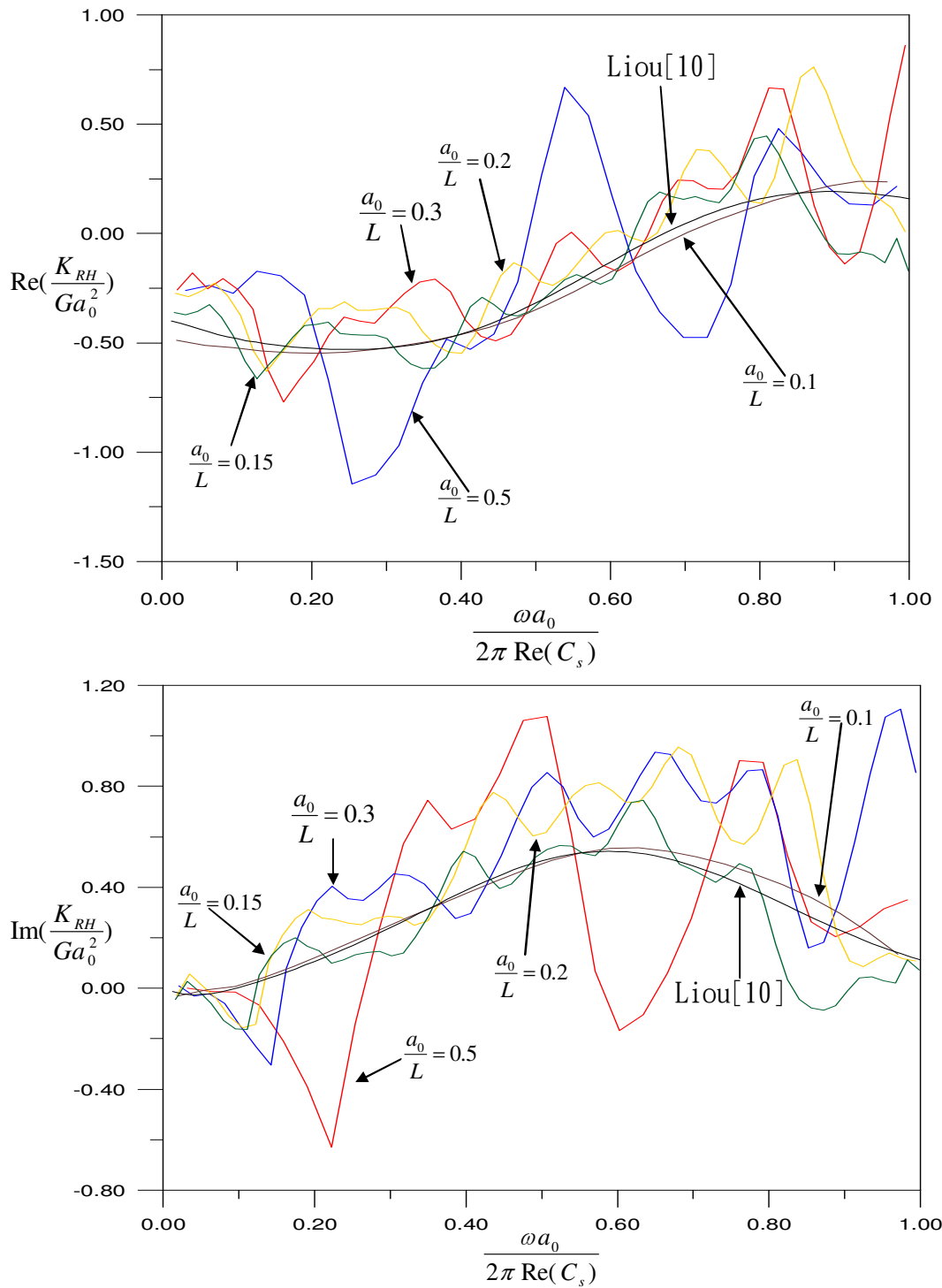


Fig. 4-4. Comparison of non-dimensionalized coupling impedance with Liou's results for $\frac{d}{a_0} = 0$

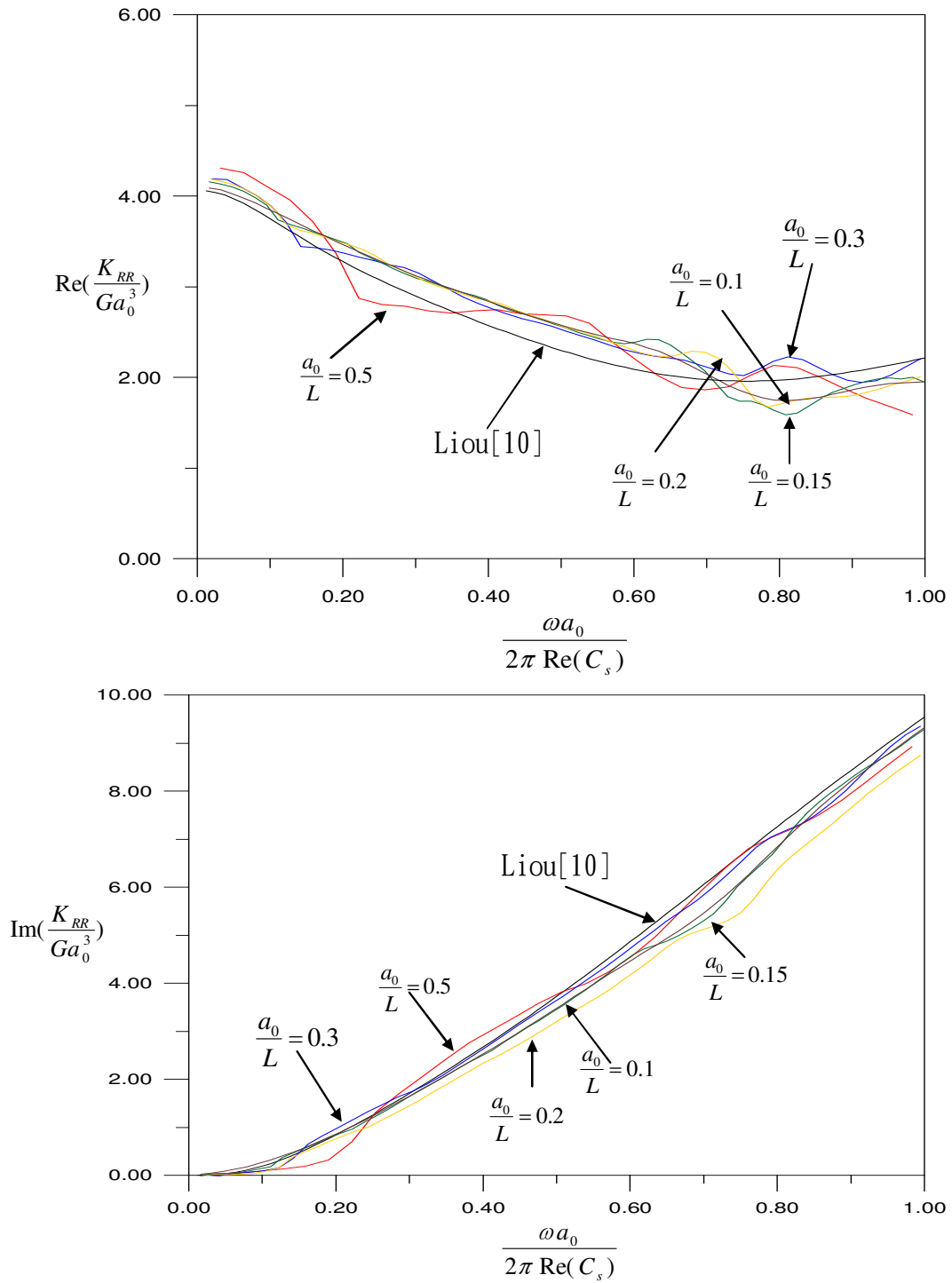


Fig. 4-5. Comparison of non-dimensionalized rocking impedance with Liou's results for $\frac{d}{a_0} = 0$

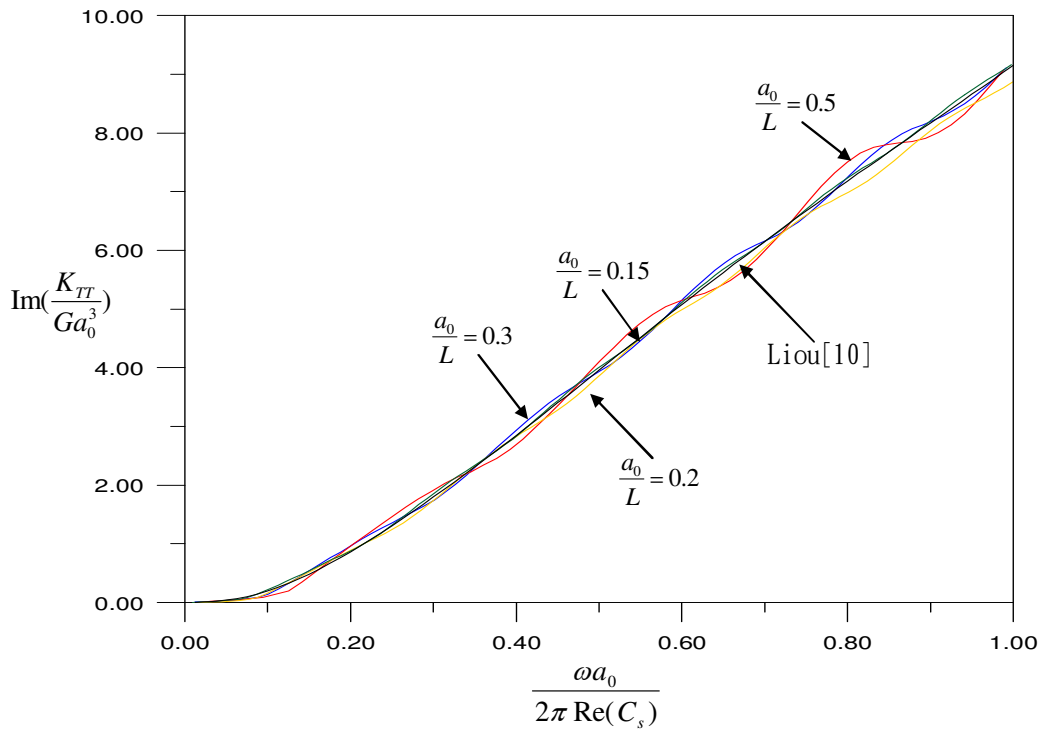
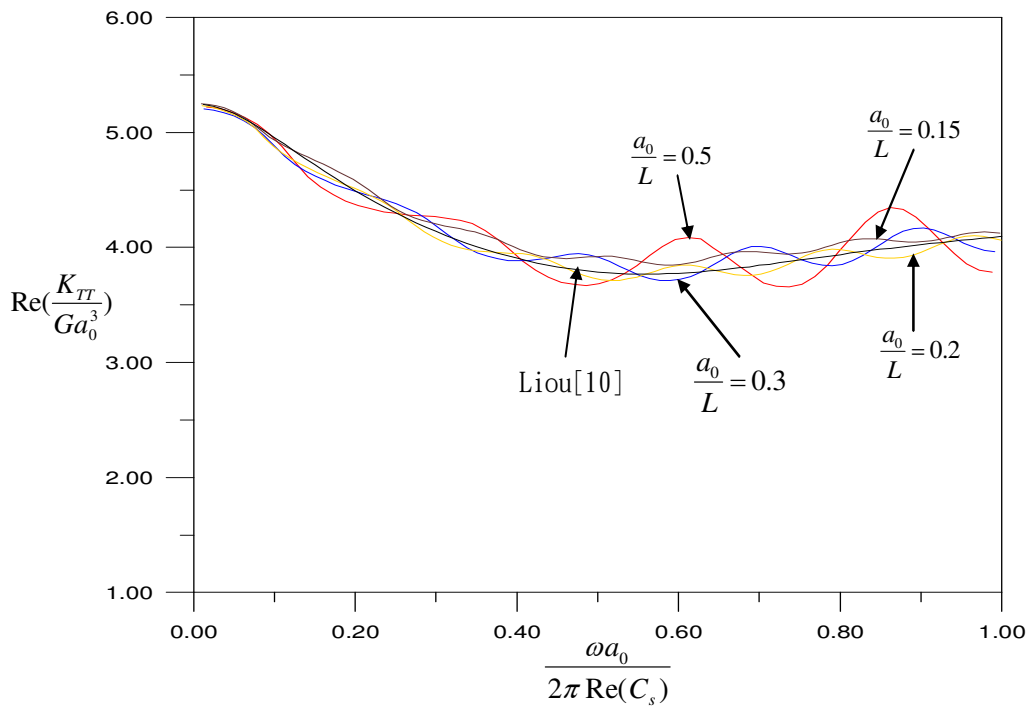


Fig. 4-6. Comparison of non-dimensionalized torsional impedance with Liou's results for $\frac{d}{a_0} = 0$

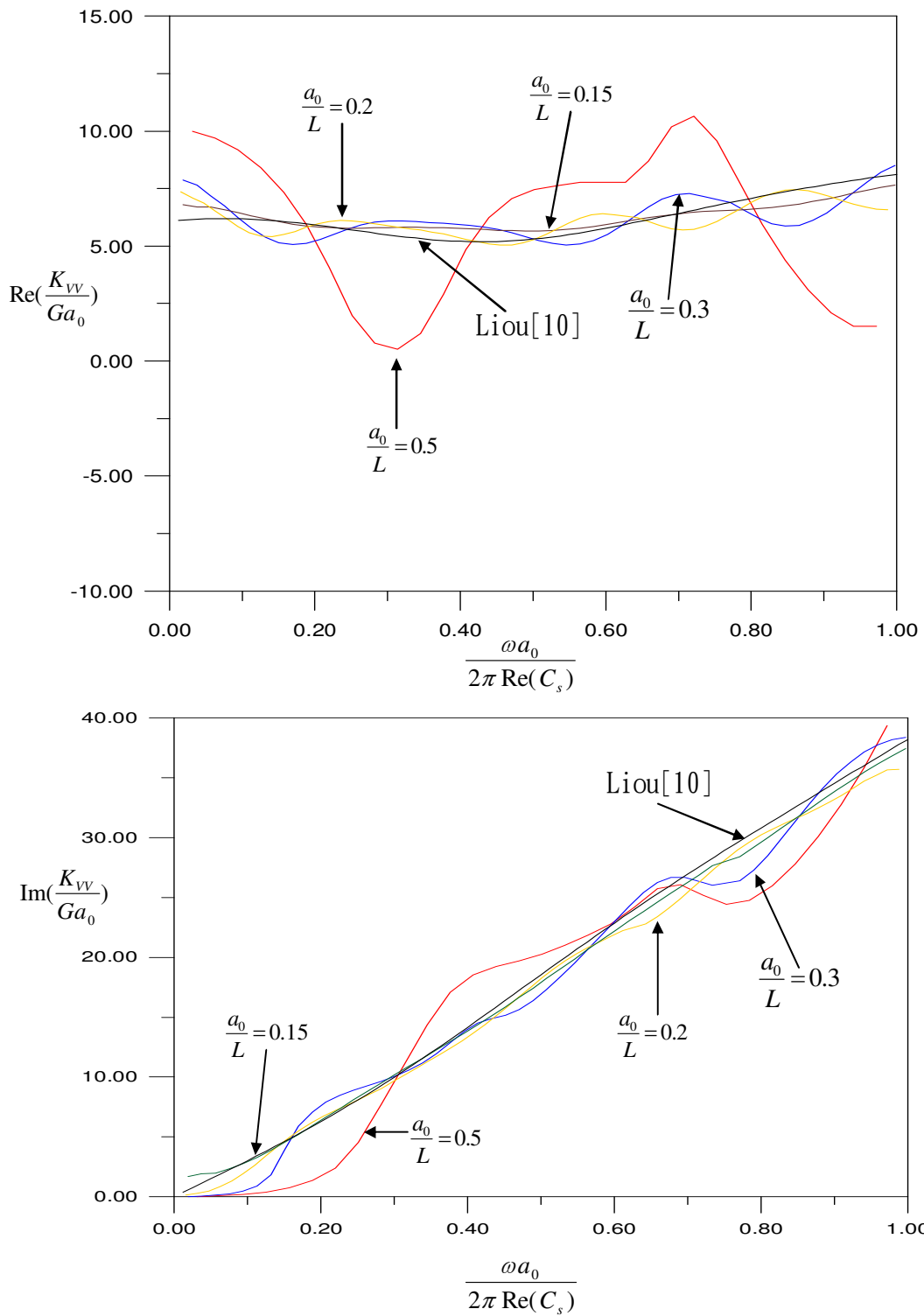


Fig. 4-7. Comparison of non-dimensionalized vertical impedance with Liou's results for $\frac{d}{a_0} = 0$

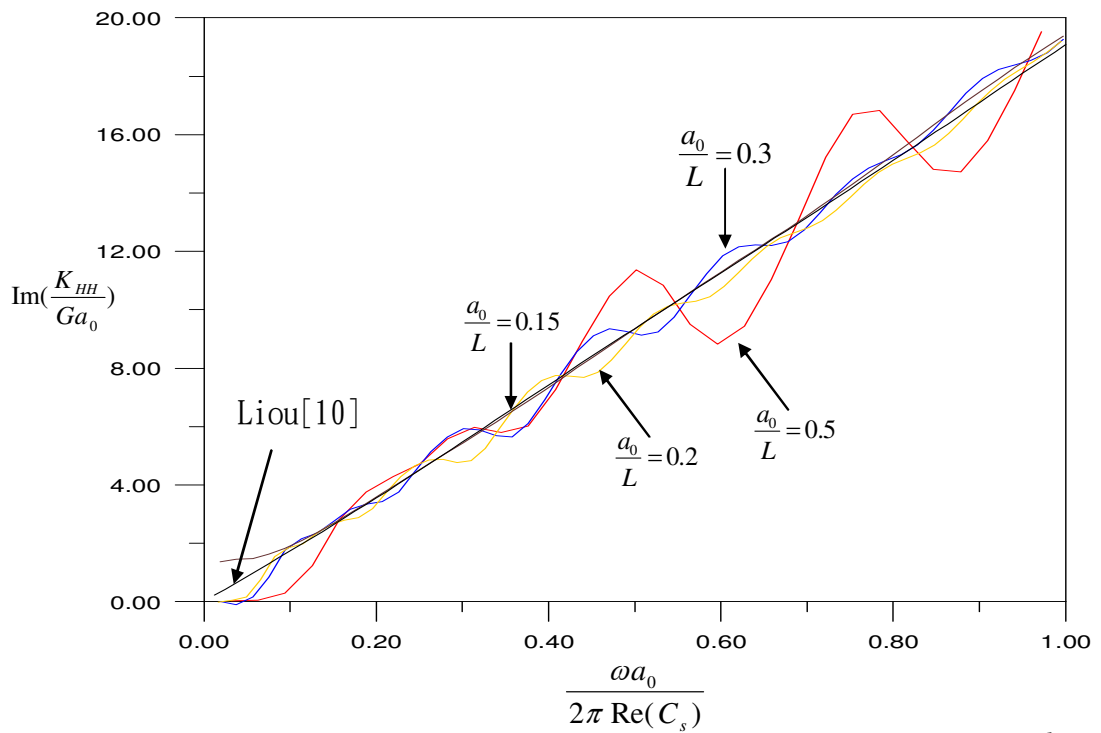
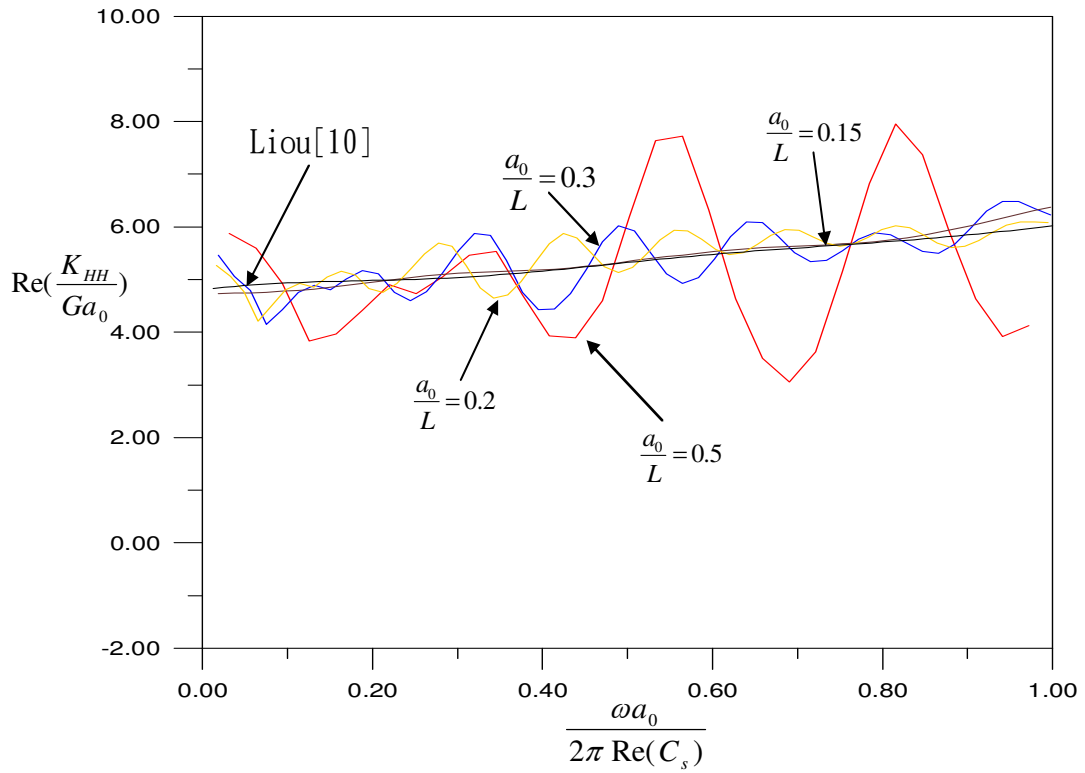


Fig. 4-8. Comparison of non-dimensionalized horizontal impedance with Liou's results for $\frac{d}{a_0} = 0$

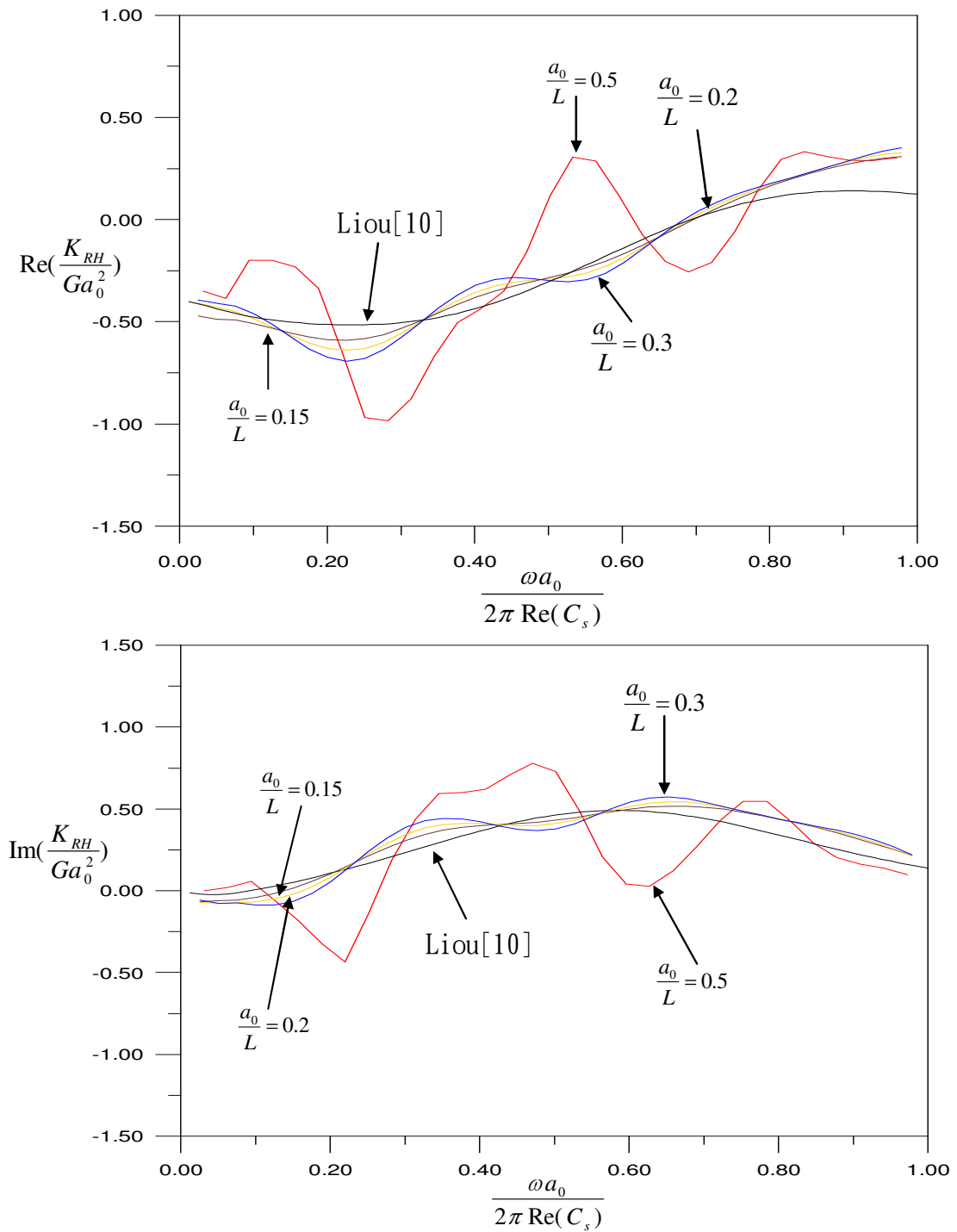


Fig. 4-9. Comparison of non-dimensionalized coupling impedance with Liou's results for $\frac{d}{a_0} = 0$

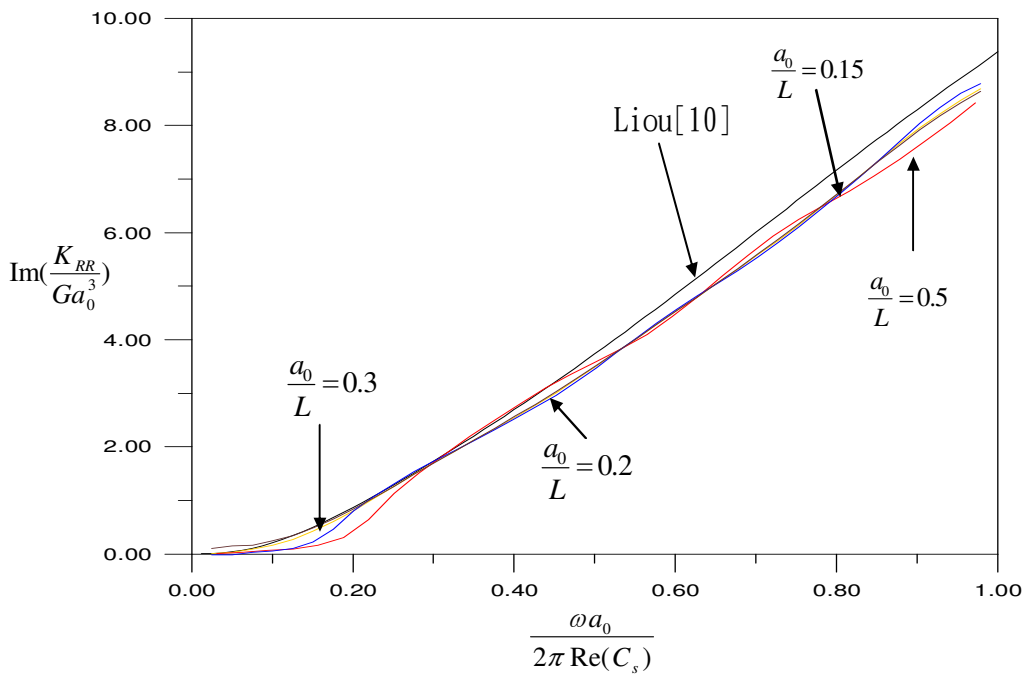
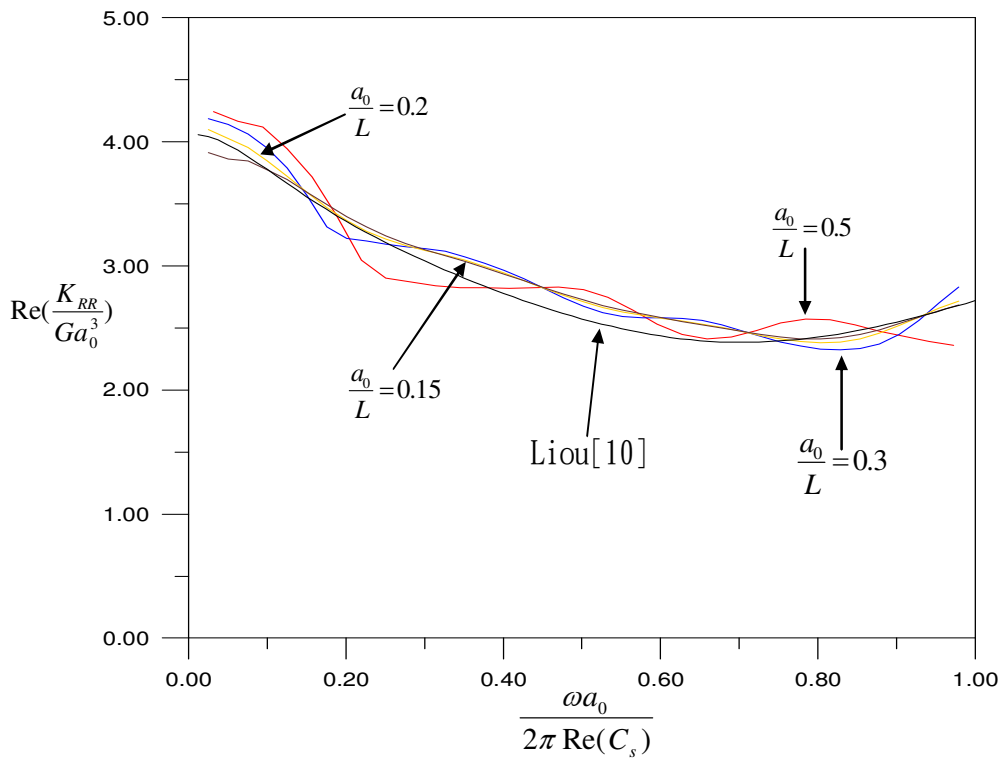


Fig. 4-10. Comparison of non-dimensionalized rocking impedance with Liou's results for $\frac{d}{a_0} = 0$

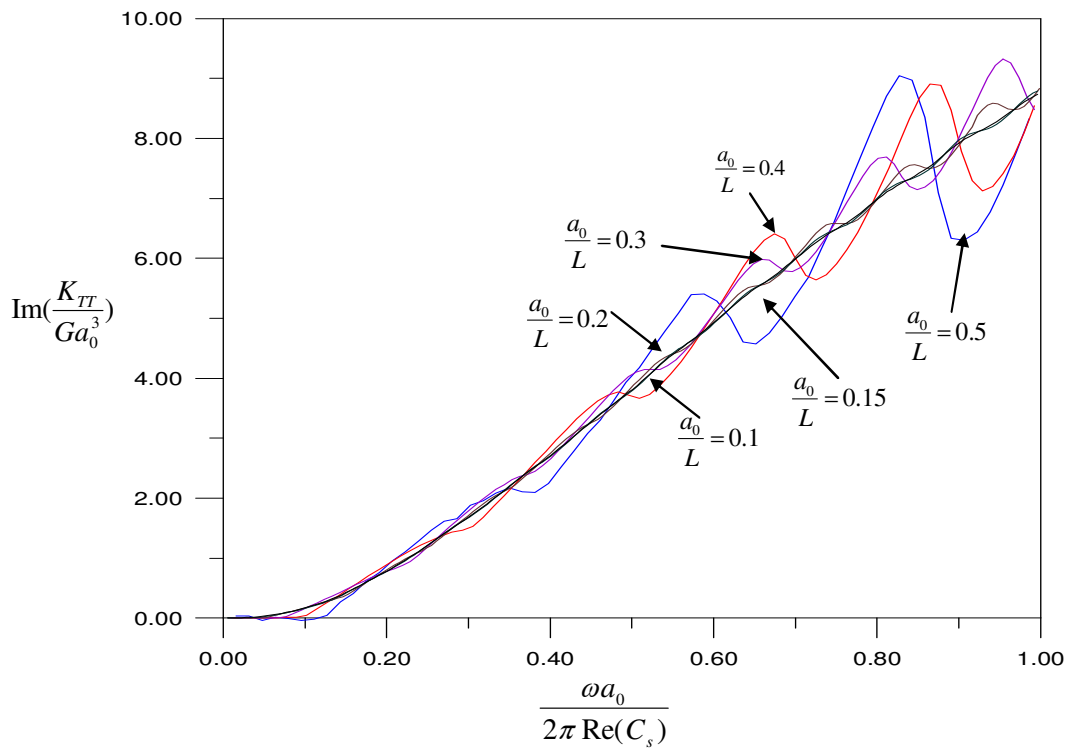
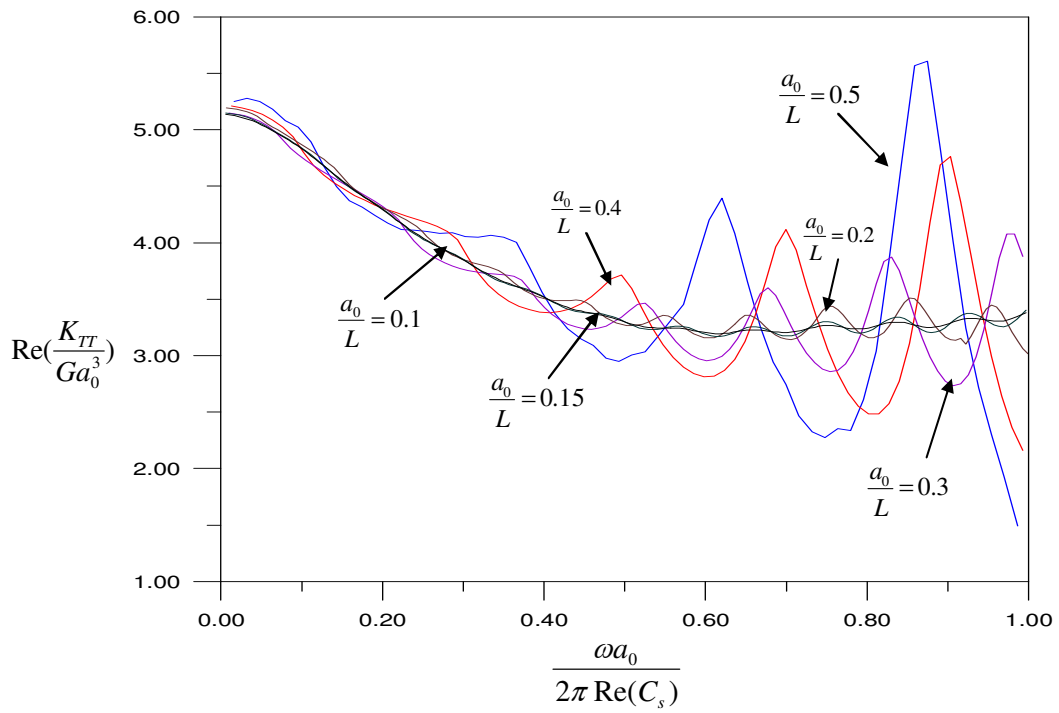


Fig. 4-11. torsional impedance for $\frac{d}{a_0} = 0$ with damp ratio 0.02

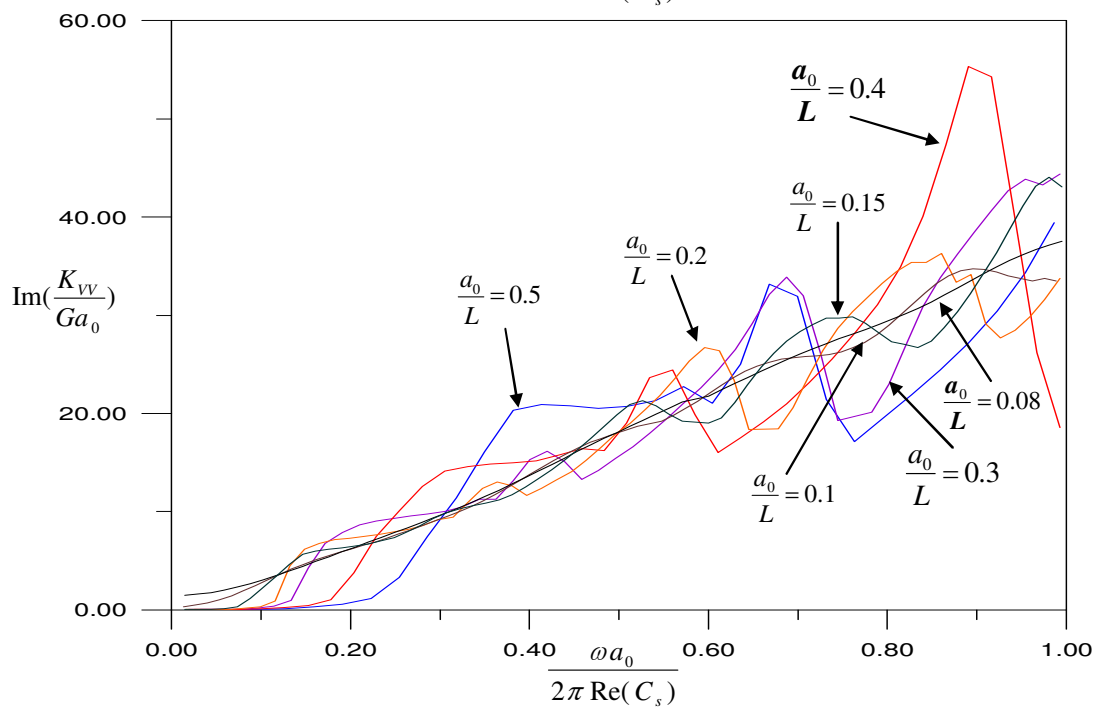
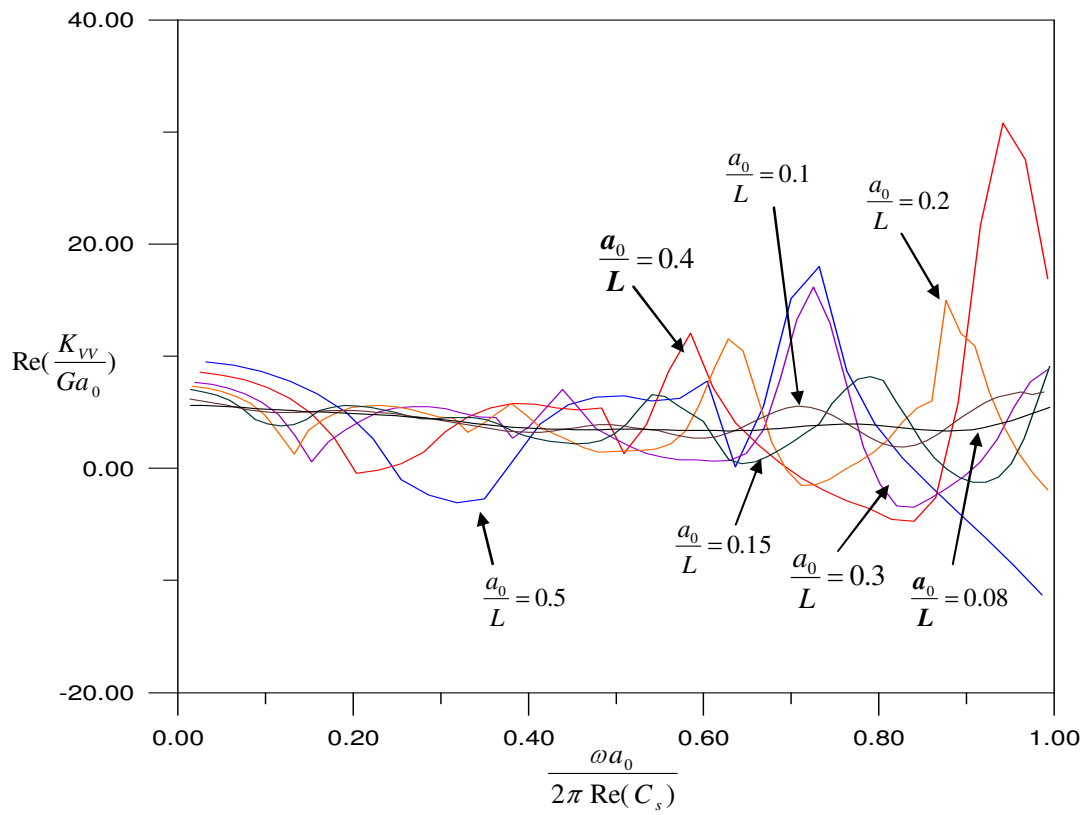


Fig. 4-12. vertical impedance for $\frac{d}{a_0} = 0$ with damp ratio 0.02

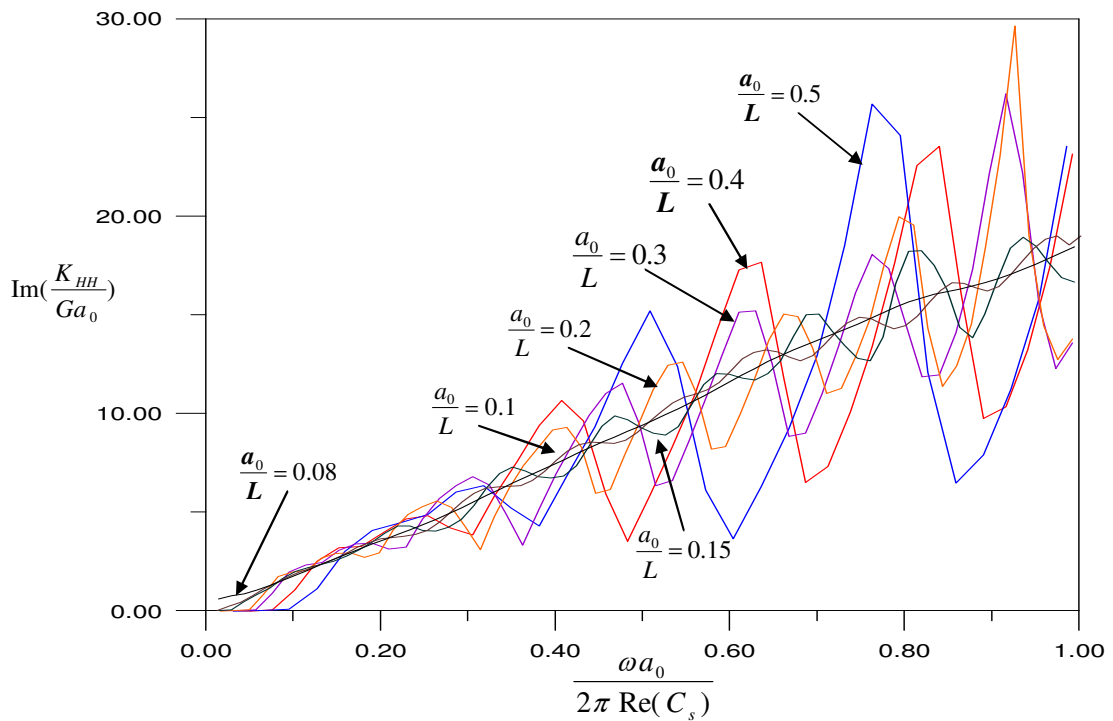
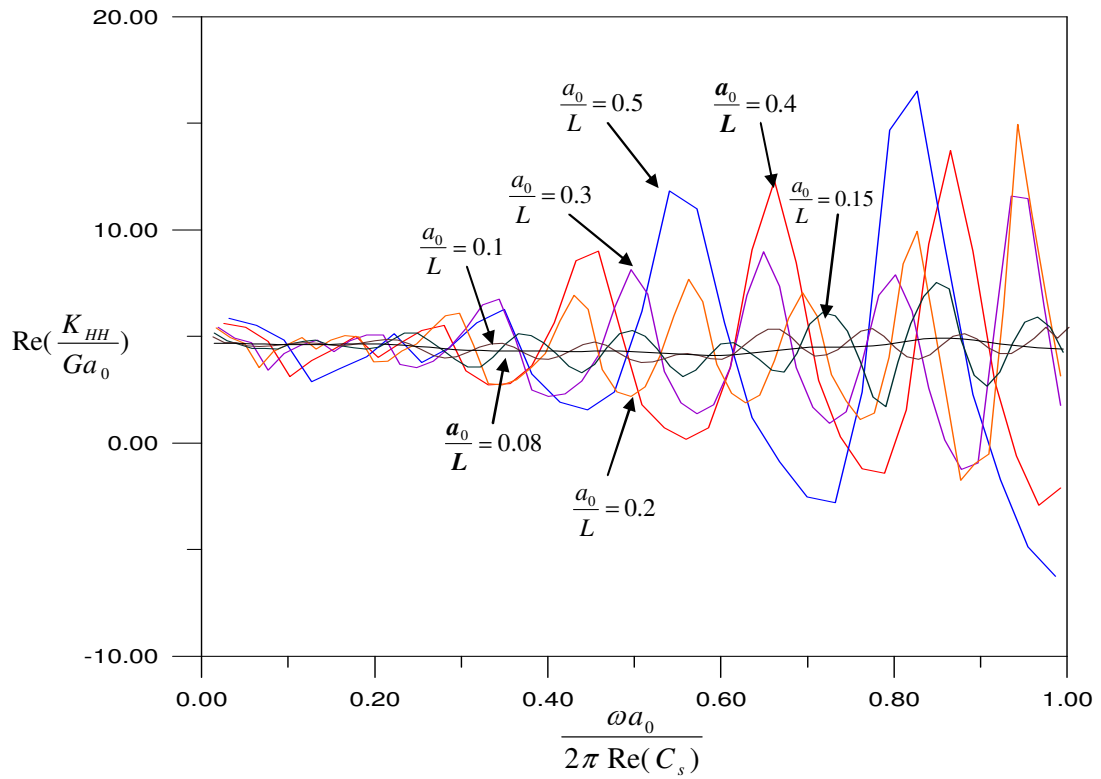


Fig. 4-13. horizontal impedance for $\frac{d}{a_0} = 0$ with damp ratio 0.02

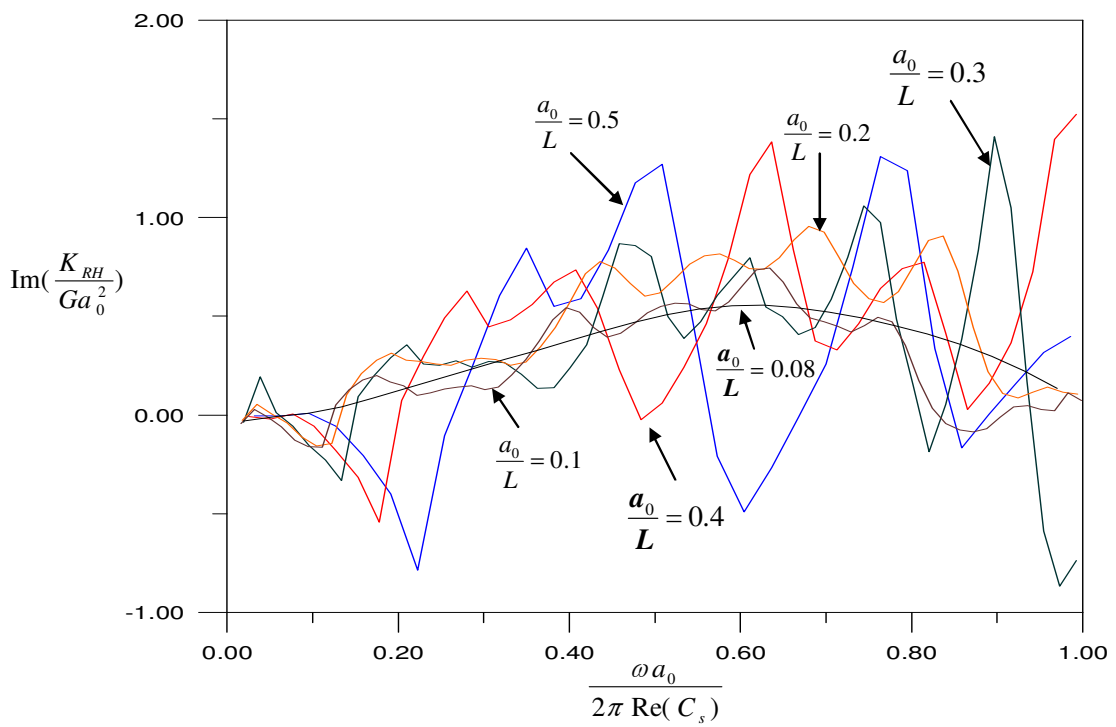
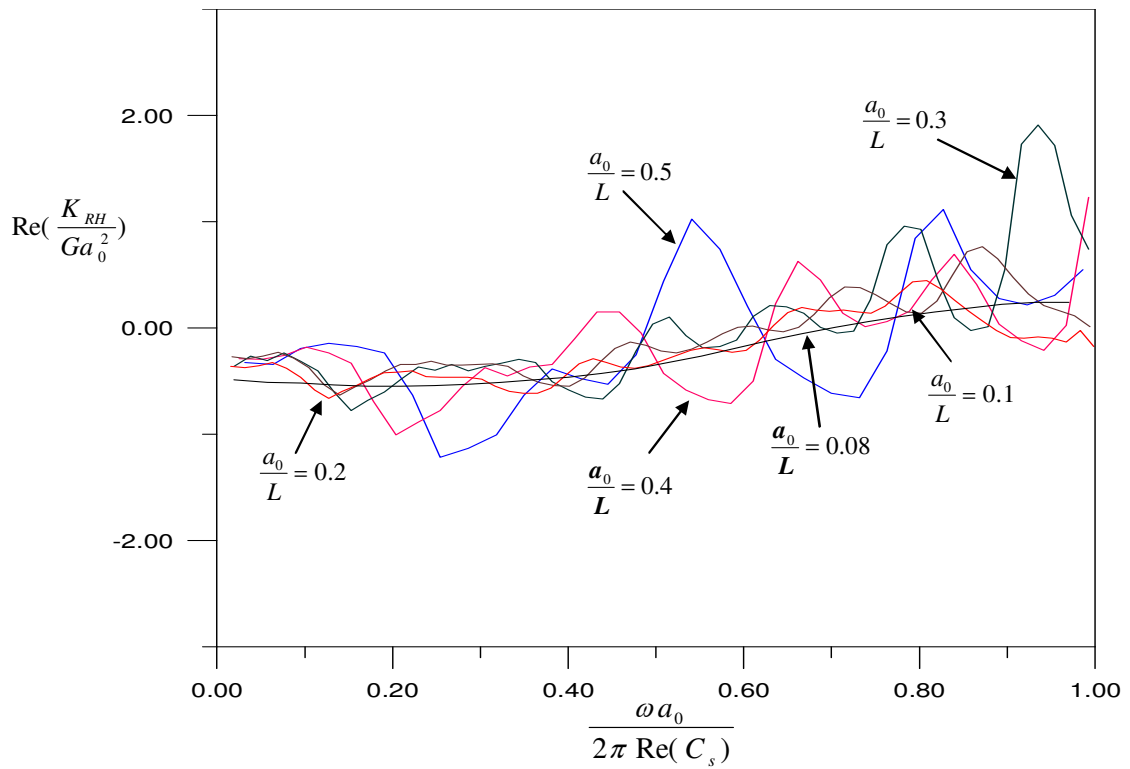


Fig. 4-14. Coupling impedance for $\frac{d}{a_0} = 0$ with damp ratio 0.02

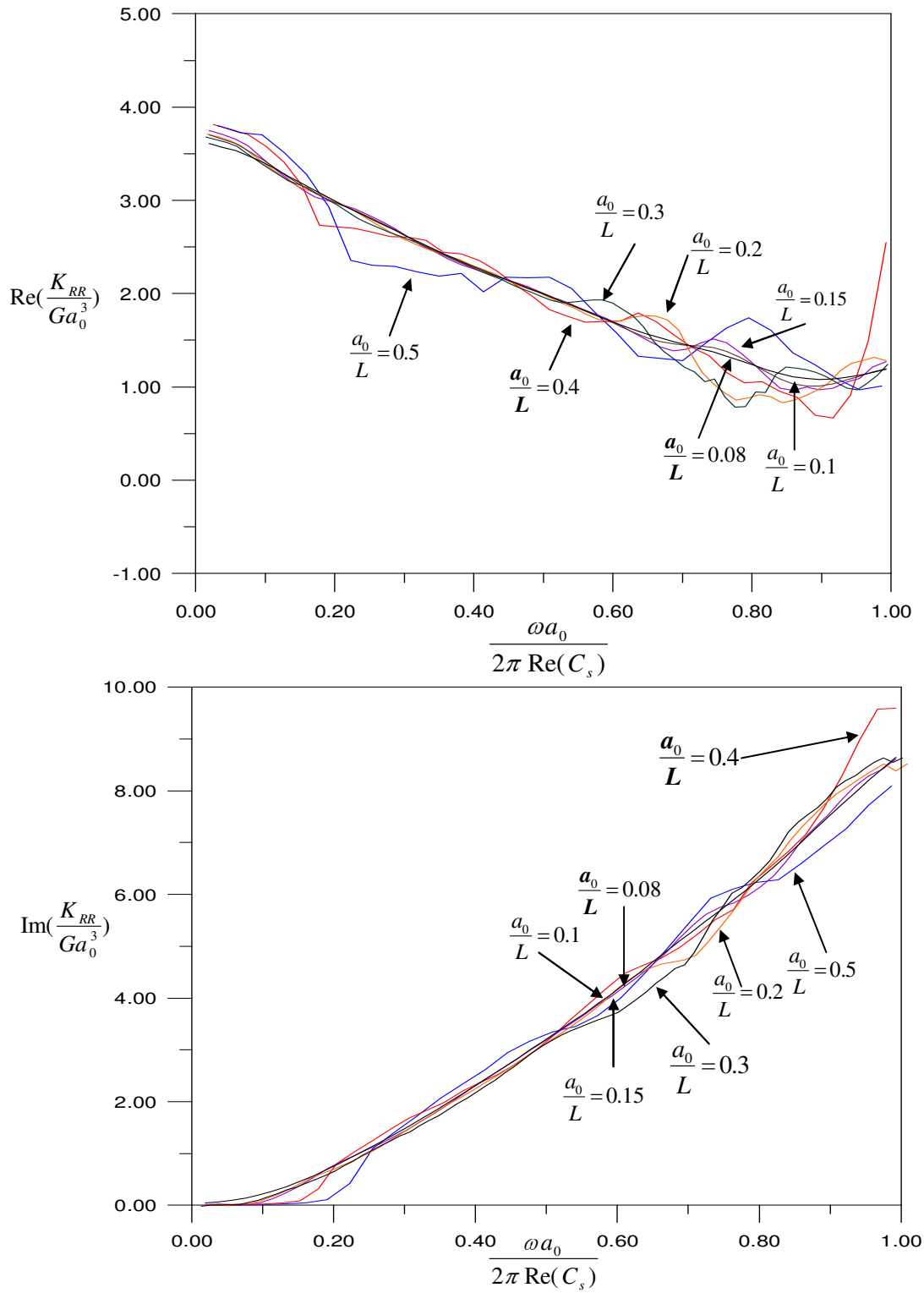


Fig. 4-15. rocking impedance for $\frac{d}{a_0} = 0$ with damp ratio 0.02

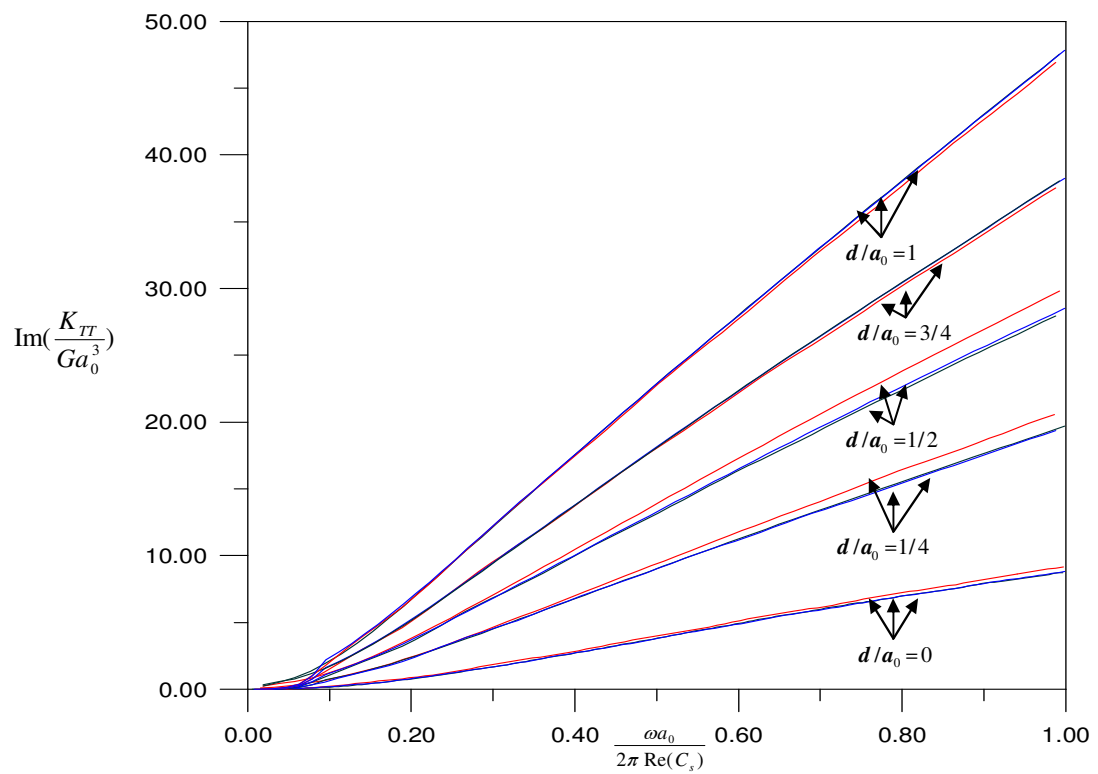
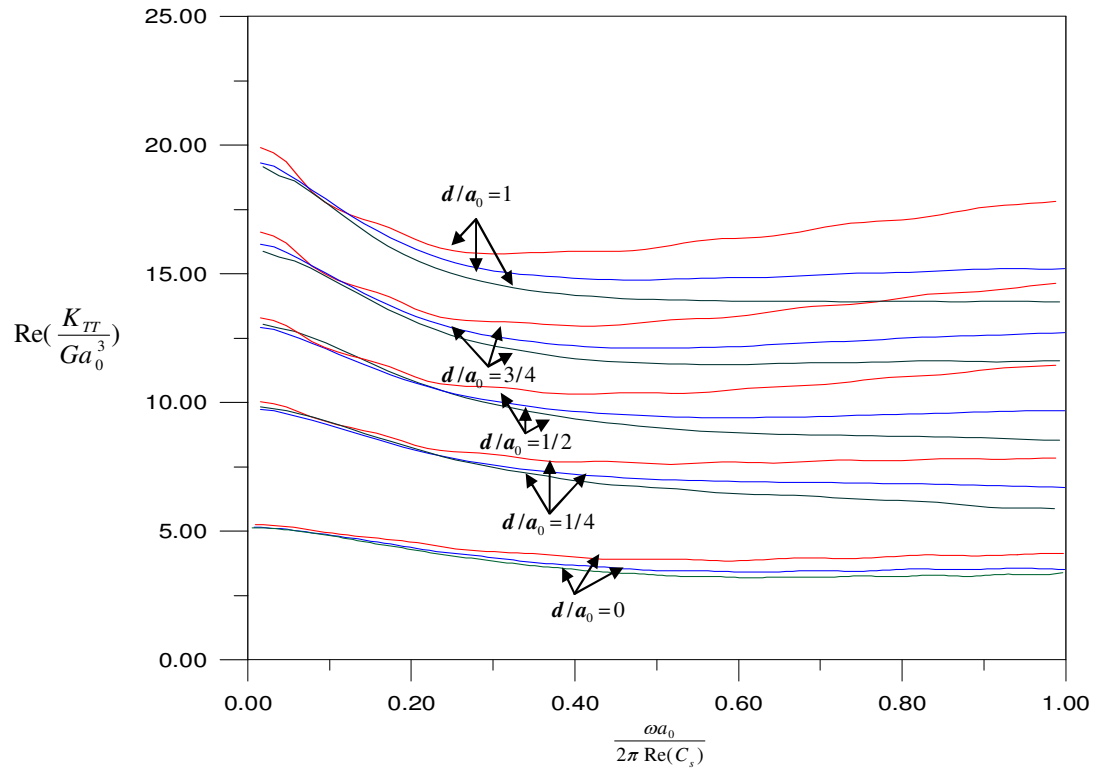


Fig. 4-16. Non-dimensionalized torsional impedance with different depths

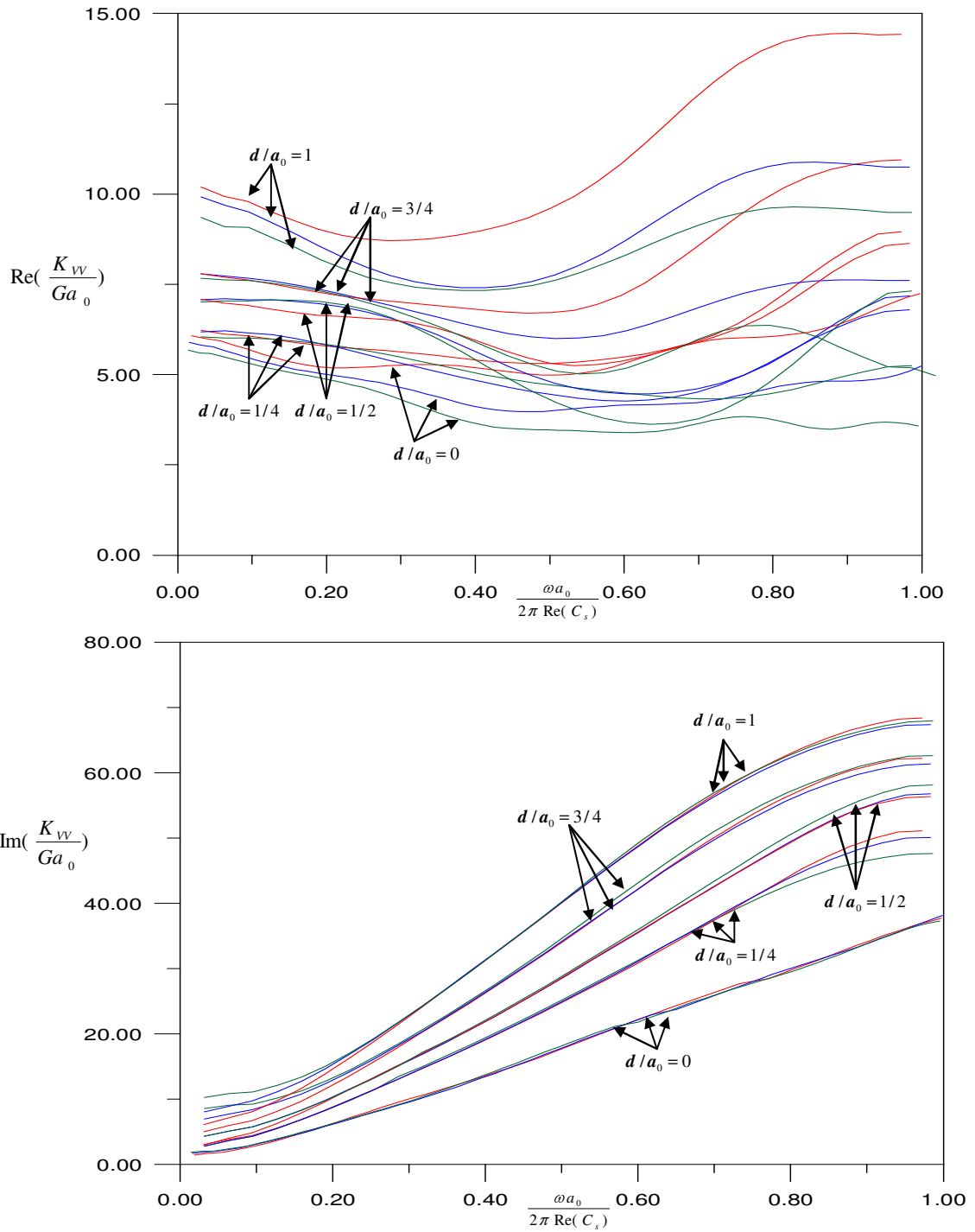


Fig. 4-17. Non-dimensionalized vertical impedance with different depths

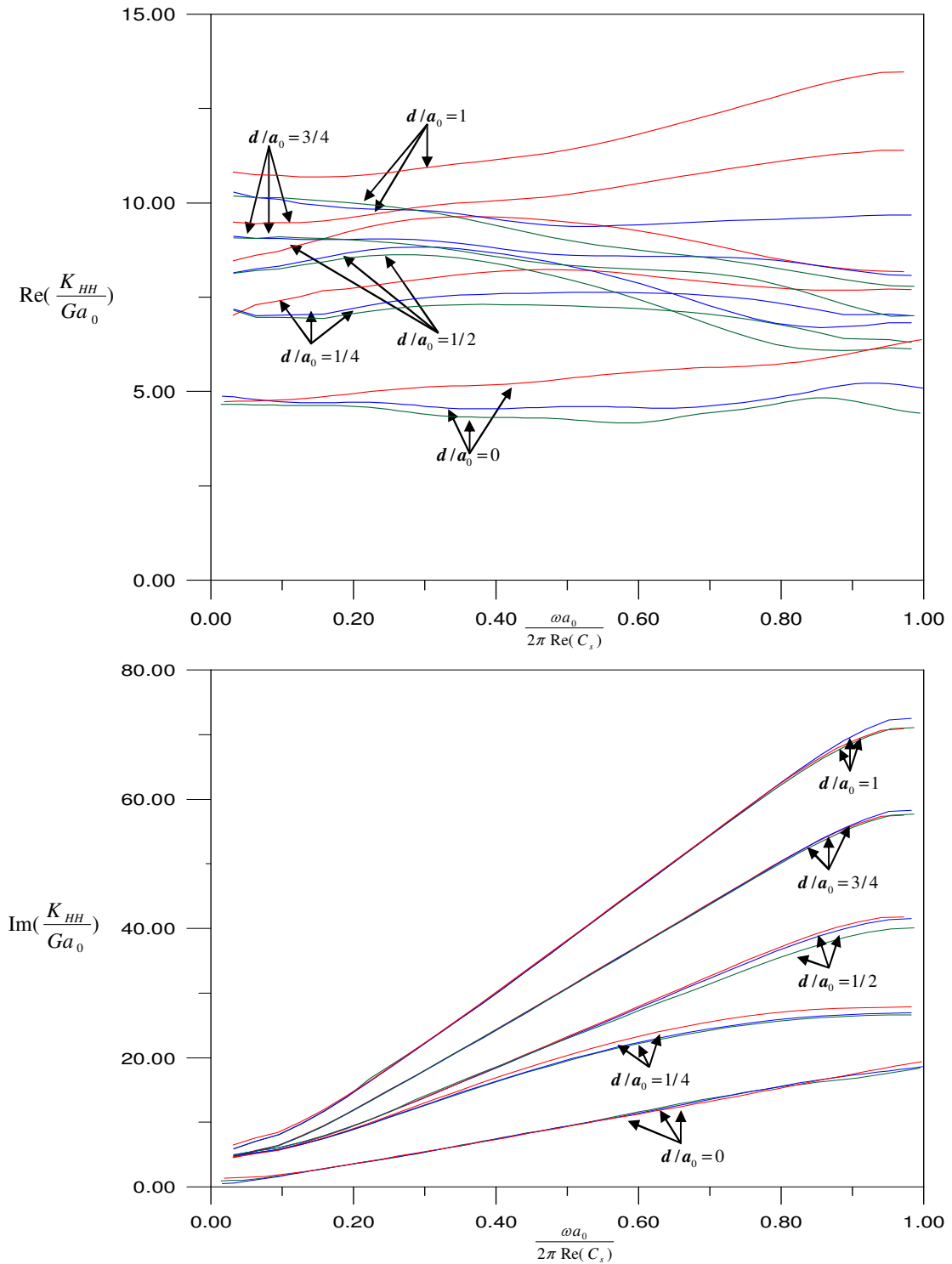


Fig. 4-18. Non-dimensionalized horizontal impedance with different depths

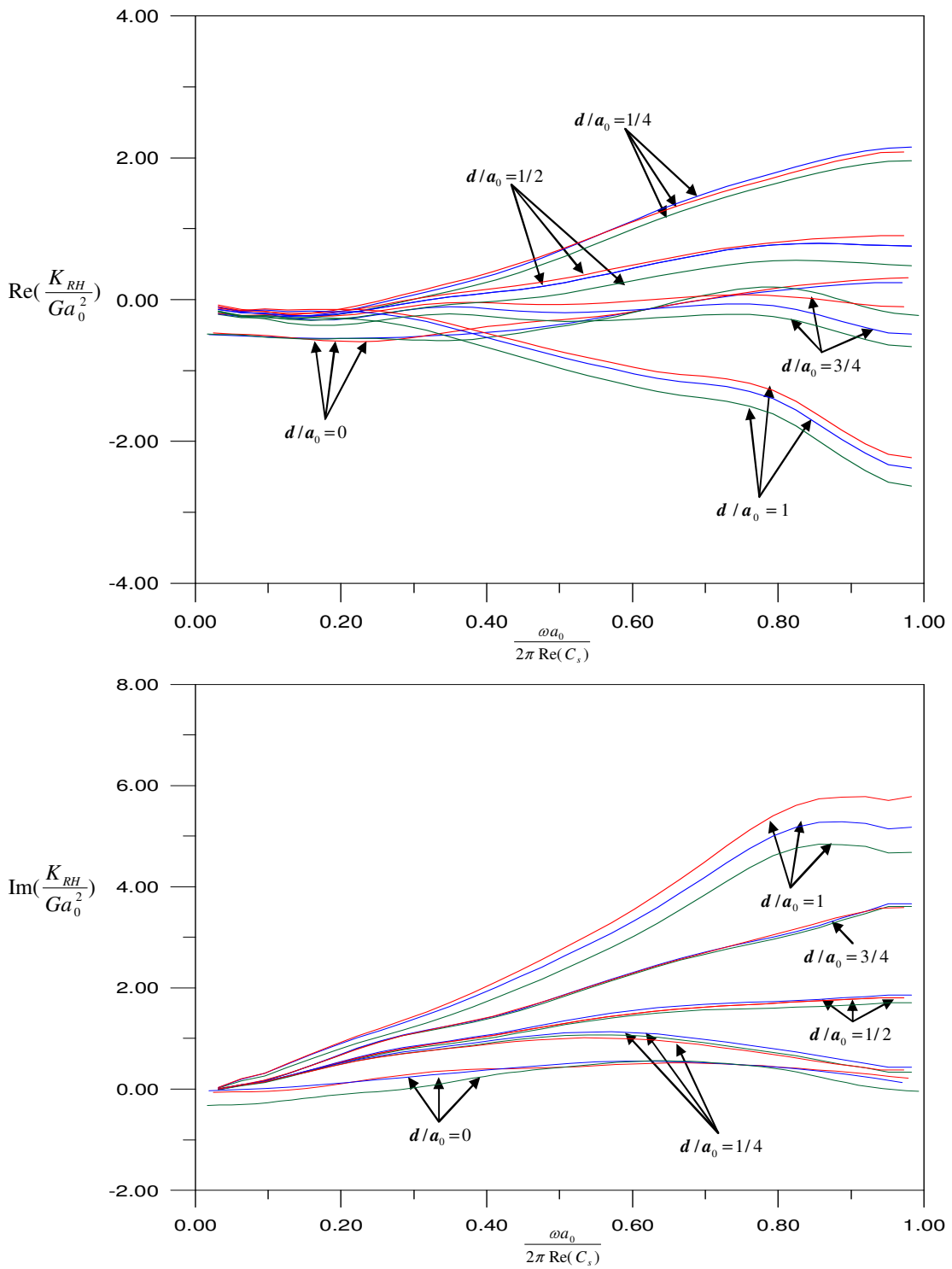


Fig. 4-19. Non-dimensionalized coupling impedance with different depths

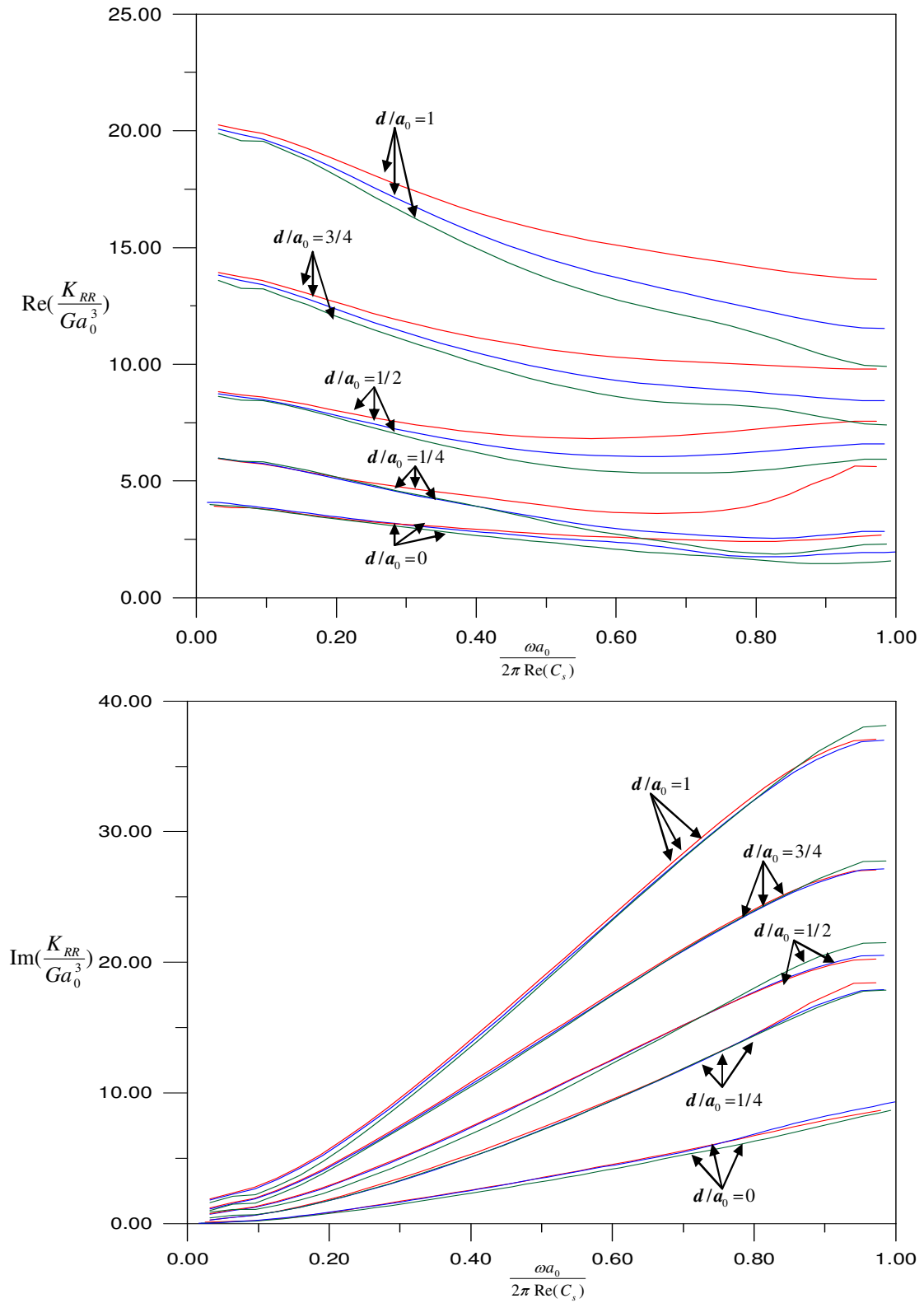


Fig. 4-20. Non-dimensionalized rocking impedance with different depths

Chapter 5

Conclusions and Further research

5.1 Conclusions

The study presented in this thesis focused on not only the investigation of calculating torsional, vertical, horizontal, coupling and rocking impedances in frequency domain for axial-symmetric foundations embedded in layered medium, but also on axial-symmetric foundations embedded in an elastic half-space medium approximated using analytical solutions in layer. From this study, conclusion can be made as follows :

1. The analytic solutions of impedance matrices for axial-symmetric foundations embedded in layered media has been derived and numerical results of torsional, vertical, horizontal, coupling and rocking impedances with different embedded depths has been presented.
2. We have employed the analytic solution for soil-structure interaction in layered media to develop a general-purpose program of the transcendental equations and numerical results of solving the complex root of the transcendental equations has been discussed.
3. The procedure to calculate impedance functions for foundation embedded in layered medium is explored to calculate that for the case of half-space medium by using enough thickness of layered medium. To approximate the situation of half-space medium, a computer program of calculating torsional, vertical, horizontal, coupling and rocking impedances with different embedded depths in half-space medium has been presented numerically.

4. The computational cost for generating impedances by the presented scheme is much inexpensive while compared to that by other traditional methods; e.g. Finite Element Method and Boundary Element Method.

5.2 Further research

After generating torsional, vertical, horizontal, coupling and rocking impedances numerically for foundation embedded in different depth, the following observations can be obtained :

1. The presented scheme can be easily employed to calculate impedances for foundation embedded in a multiple layer stratum.

2. From the above derivations, the scheme can be extended to calculate the impedances for flexible foundation with arbitrary shape.

3. The presented scheme can also be extended to approximately calculate all impedance functions for foundation in a multiple layered half-space medium, if the bottom layer of stratum is thick enough.

References

- [1] Tzong TJ, Penzien J. Hybrid modelling of a single-layer half-space system in soil-structure interaction. *Earthquake Eng Struct Dyn* 1986;14(4):517-530.
- [2] Lysmer J, Kuhlemeyer RL. Finite dynamic model for infinite media. *J Eng Mech Div* 1969;95(4):859-877.
- [3] White W, Valliapan S, Lee IK. Unified boundary for finite dynamic model. *J Eng Mech Div* 1977;95(5):949-964.
- [4] Werkel H. Dynamic finite element analysis of three-dimensional soil models with a transmitting element. *Earthquake Eng Struct Dyn* 1986;14(1):41-60.
- [5] Ahmad S, Banerjee pk. Multi-domain BEM for two-dimensional problems in elastodynamics. *Int J Num Meth in Eng* 1988;26(4):891-911.
- [6] Chow YK, Smith IM. Static and Periodic infinite solid elements. *Int J Num Meth in Eng* 1981;17(4):503-526.
- [7] Pak RY, Guzina BB. Seismic soil-structure interaction analysis by direct boundary element methods. *International Journal of Solids and Structures* 1999;36(31):4743-4766.
- [8] Liou GS. Analytic solutions for soil-structure interaction in layered media. *Earthquake Eng Struct Dyn* 1989;18(5):667-686.
- [9] Liou GS. Vibration of surface foundations of arbitrary shapes. *Earthquake Eng Struct Dyn* 1991;20(12):1115-1125.
- [10] Liou GS, Lee GC, Ketter LR. Analytic solution for dynamic loading on half-space. *ASCE J Eng Mech* 1991;117(7):1485-1495.
- [11] Liou GS, Lee GC. Impedance matrices for axial symmetric foundations on layered

- media. Struct Eng Earthquake Eng 1992;9(1):33-44.
- [12] Liou GS. Impedance for rigid square foundation on layered medium. Struct Eng Earthquake Eng 1993;10:47-57.
- [13] Aviles J, Perez-Rocha LE. A simplified procedure for torsional impedance functions of embedded foundations in a soil layer. Computers and Geotechnics 1996;19(2):97-115.
- [14] Tassoulas JL, Kausel E. On the effect of the rigid sidewall on the dynamic stiffness of embedded circular footings. Earthquake Eng Struct Dyn 1983;11(3):403-414.
- [15] Wolf JP, Preisig M. Dynamic stiffness of foundation embedded in layered halfspace based on wave propagation in cones. Earthquake Eng Struct Dyn 2003;32(7):1075-1098.
- [16] Wolf JP, Meek JW. Cone models for a soil layer on a flexible rock half-space. Earthquake Eng Struct Dyn 1993;22(3):185-193.
- [17] Jaya KP, Prasad AM. Embedded foundation in layered soil under dynamic excitations. Soil Dyn Earthquake Eng 2002;22(6):485-498.
- [18] Sezawa K. Further studies on rayleigh waves having some azimuthal distribution. Bulletin of Earthquake Research Institute 1929;6:1-18.
- [19] Conte, de Boor. Elementary Numerical Analysis; An Algorithmic Approach “ 3rd ed. McGraw-Hill Book Company, 1980.

Appendix A

The Bessel function matrix \bar{J} in Eq. (2-5)

$$\bar{J} = \begin{bmatrix} J'_n(kr) & 0 & 0 & 0 & \frac{n}{r} J_n(kr) & 0 \\ 0 & kJ_n(kr) & 0 & 0 & 0 & 0 \\ 0 & 0 & J'_n(kr) & 0 & 0 & \frac{n}{r} J_n(kr) \\ 0 & 0 & 0 & kJ_n(kr) & 0 & 0 \\ \frac{n}{r} J_n(kr) & 0 & 0 & 0 & J'_n(kr) & 0 \\ 0 & 0 & \frac{n}{r} J_n(kr) & 0 & 0 & J'_n(kr) \end{bmatrix} \quad (A1)$$

in which $J_n(kr)$ is the first kind of Bessel function with order n and $J'(kr) = \frac{dJ_n(kr)}{dr}$

The transfer matrices \mathbf{a}_j 's in Eq. (2-5) can be expressed as follows :

$$\mathbf{a}_j = \mathbf{E}_j \mathbf{e}(\mathbf{h}_j) \mathbf{E}_j^{-1} = \begin{bmatrix} \mathbf{a}_1 & 0 \\ 0 & \mathbf{a}_2 \end{bmatrix} \quad (A2)$$

in which

$$\mathbf{a}_1 = \begin{bmatrix} \frac{2k^2}{k_\beta^2}(\mathbf{CH}-\mathbf{CH}')+\mathbf{CH} & -\frac{k}{k_\beta^2}[(2k^2-k_\beta^2)\frac{\mathbf{SH}}{v}-2v'\mathbf{SH}] & \frac{-1}{Gk_\beta^2}(v'\mathbf{SH}-k^2\frac{\mathbf{SH}}{v}) & -\frac{k}{Gk_\beta^2}(\mathbf{CH}-\mathbf{CH}') \\ \frac{k}{k_\beta^2}[2v\mathbf{SH}-(2k^2-k_\beta^2)\frac{\mathbf{SH}}{v}] & \mathbf{CH}-\frac{2k^2}{k_\beta^2}(\mathbf{CH}-\mathbf{CH}') & \frac{k}{Gk_\beta^2}(\mathbf{CH}-\mathbf{CH}') & -\frac{1}{Gk_\beta^2}(v\mathbf{SH}-k^2\frac{\mathbf{SH}}{v}) \\ G\frac{4k^2}{k_\beta^2}v\mathbf{SH}-\frac{(2k^2-k_\beta^2)}{k_\beta^2}(\frac{\mathbf{SH}}{v}) & -\frac{2kG}{k_\beta^2}(2k^2-k_\beta^2)(\mathbf{CH}-\mathbf{CH}') & \frac{2k^2}{k_\beta^2}(\mathbf{CH}-\mathbf{CH}')+\mathbf{CH} & -\frac{k}{k_\beta^2}(2v\mathbf{SH}-(2k^2-k_\beta^2)\frac{\mathbf{SH}}{v}) \\ \frac{2kG}{k_\beta^2}(2k^2-k_\beta^2)(\mathbf{CH}-\mathbf{CH}') & G\frac{(2k^2-k_\beta^2)^2}{k_\beta^2}\frac{\mathbf{SH}}{v}+\frac{4k^2}{k_\beta^2}v'\mathbf{SH} & \frac{k}{k_\beta^2}[(2k^2-k_\beta^2)\frac{\mathbf{SH}}{v}-2v'\mathbf{SH}] & \mathbf{CH}-\frac{2k^2}{k_\beta^2}(\mathbf{CH}-\mathbf{CH}') \end{bmatrix} \quad (A3)$$

and

$$\mathbf{a}_2 = \begin{bmatrix} CH' & \frac{SH'}{G\nu'} \\ G\nu'SH' & CH' \end{bmatrix} \quad (\text{A4})$$

$$CH = \cosh \nu d_j \quad , \quad CH' = \cosh \nu' d_j \quad , \quad SH = \sinh \nu d_j \quad , \quad SH' = \sinh \nu' d_j \quad ,$$

$$K_\beta = \sqrt{\frac{\omega^2}{c_s^2}} \quad , \quad G \text{ is the shear modulus, } \nu' = \sqrt{k^2 - \left(\frac{\omega^2}{c_s^2}\right)} \quad , \quad \nu = \sqrt{k^2 - \left(\frac{\omega^2}{c_p^2}\right)} \quad ,$$

C_s is the shear wave velocity and C_p is the compressional wave velocity. Matrices \mathbf{J}_1

and \mathbf{J}_2 in Eq. (2-10) can be expressed as follows :

$$\mathbf{J}_1 = \begin{bmatrix} 0 & kJ_n(kr) & 0 \\ J_n'(kr) & 0 & \frac{n}{r}J_n(kr) \\ 0 & 0 & 0 \end{bmatrix} \quad (\text{A5})$$

$$\mathbf{J}_2 = \begin{bmatrix} \left(-\frac{J_n'(kr)}{r} + \frac{n^2}{r^2}J_n(kr)\right) & \left(\frac{n}{r}J_n'(kr) - \frac{n}{r^2}J_n(kr)\right) \\ 0 & 0 \\ \left(\frac{n}{r}J_n'(kr) - \frac{n}{r^2}J_n(kr)\right) & \left(-\frac{J_n'(kr)}{r} + \left(\frac{n^2}{r^2} - \frac{k^2}{2}\right)J_n(kr)\right) \end{bmatrix} \quad (\text{A6})$$

The matrix $\mathbf{F}_1 \mathbf{e}(z - \mathbf{h}_{j-1}) \mathbf{E}_j^{-1}$ and $\mathbf{F}_2 \mathbf{e}(z - \mathbf{h}_{j-1}) \mathbf{E}_j^{-1}$ in Eq (2-10) can be expressed as

follows :

$$\mathbf{F}_1 \mathbf{e}(z - \mathbf{h}_{j-1}) \mathbf{E}_j^{-1} =$$

$$\left[\begin{array}{cc} \frac{G}{k_\beta^2}(4k^2vSH - (2k^2 - k_\beta^2)\frac{SH'}{v'}) & -\frac{2kG}{k_\beta^2}(2k^2 - k_\beta^2)(CH - CH') \\ \frac{2kG}{k_\beta^2}(-(2v^2 + k_\beta^2)CH + (2k^2 - k_\beta^2)CH') & \frac{G}{k_\beta^2}((2k^2 - k_\beta^2)(2v^2 + k_\beta^2)\frac{SH'}{v'} - 4k^2v'SH') \\ 0 & 0 \end{array} \right] \quad (A7)$$

$$\left[\begin{array}{cccc} \frac{2k^2}{k_\beta^2}(CH - CH') + CH' & \frac{k}{k_\beta^2}((2k^2 - k_\beta^2)\frac{SH'}{v'} - 2vSH) & 0 & 0 \\ \frac{k}{k_\beta^2}(2v'SH' - (2v^2 + k_\beta^2)\frac{SH}{v}) & \frac{1}{k_\beta^2}((2v^2 + k_\beta^2)CH - 2k^2CH') & 0 & 0 \\ 0 & 0 & Gv'SH' & CH' \end{array} \right]$$

$$\mathbf{F}_2 \mathbf{e}(\mathbf{z} - \mathbf{h}_{j-1}) \mathbf{E}_j^{-1} = \left[\begin{array}{cccc} 2G(\frac{2k^2}{k_\beta^2}(CH - CH') + CH') & \frac{2kG}{k_\beta^2}(2v'SH' - (2k^2 - k_\beta^2)\frac{SH}{v}) & & \\ & 0 & 0 & \\ & \frac{2}{k_\beta^2}(k^2\frac{SH}{v} - v'SH') & -\frac{2k}{k_\beta^2}(CH - CH') & 0 \quad 0 \\ & 0 & 0 & 2GCH' \quad 2\frac{SH'}{v'} \end{array} \right] \quad (A8)$$

